FINAL REPORT

New Approach to Assess Running Fracture in Transmission Pipelines

To

US Department of Transportation

February 2007

Final Report

to

New Approach to Assess Running Fracture in Transmission Pipelines

Prepared for

US Department of Transportation PHMSA

Contract No. DTRS56-05-T-0003

Project No. G005189

by

B. N. Leis and T. P. Forte

February 2007

BATTELLE

505 King Avenue

Columbus, Ohio, 43201-2693

Neither Battelle, nor any person acting on their behalf:

Makes any warranty or representation, expressed or implied, with respect to the accuracy, completeness or usefulness of any information contained in this report or that the use of any information, apparatus, method, or process disclosed in this report may not infringe privately owned rights.

Assumes any liabilities with the respect to the use of, or for damages resulting from the use of any information, apparatus, method or process disclosed in this report.

REPORT DOCUMENTATION PAGE

Form Approved
OMB No. 0704-0188

Public reporting burden for this collection of information is estimated to average 1 hour per response, including the time for reviewing instructions, searching existing data sources, gathering and maintaining the data needed, and completing and reviewing this collection of information. Send comments regarding this burden estimate or any other aspect of this collection of information, including suggestions for reducing this burden to Department of Defense, Washington Headquarters Services, Directorate for Information Operations and Reports (0704-0188), 1215 Jefferson Davis Highway, Suite 1204, Arlington, VA 22202-4302. Respondents should be aware that notwithstanding any other provision of law, no person shall be subject to any penalty for failing to comply with a collection of information if it does not display a currently valid OMB control number. **PLEASE DO NOT RETURN YOUR FORM TO THE ABOVE ADDRESS.**

1. REPORT DATE *(DD-MM-YYYY)* 05/02/2007	**2. REPORT TYPE** Final	**3. DATES COVERED** *(From - To)* 08/12/2004 – 07/12/2006
4. TITLE AND SUBTITLE: **New Approach to Assess Running Fracture in Transmission Pipelines**		**5a. CONTRACT NUMBER** **5b. GRANT NUMBER** **5c. PROGRAM ELEMENT NUMBER**
6. AUTHOR(S) **B. N. Leis and T. P. Forte**		**5d. PROJECT NUMBER** 164 **5e. TASK NUMBER** **5f. WORK UNIT NUMBER** 132
7. PERFORMING ORGANIZATION NAME(S) AND ADDRESS(ES) AND ADDRESS(ES) **Battelle** **505 King Avenue** **Columbus, OH 43201**		**8. PERFORMING ORGANIZATION REPORT NUMBER** **G005189**
9. SPONSORING / MONITORING AGENCY NAME(S) AND ADDRESS(ES)		**10. SPONSOR/MONITOR'S ACRONYM(S)** **11. SPONSOR/MONITOR'S REPORT NUMBER(S)**

12. DISTRIBUTION / AVAILABILITY STATEMENT

13. SUPPLEMENTARY NOTES

14. ABSTRACT

This project formulated an alternative fracture curve and the reassessed approach used to deploy the two-curve concept that underlies the BTCM as the basis to formulate an engineering model for fracture propagation and arrest. This facilitates assessing the response as the crack-tip encounters differing circumstances in its travel along the pipeline or full-scale test section. Further, it facilitates identifying first-order factors that must be addressed and helps to understand the breakdown of similitude between the model and the reality of the full-scale test or operating pipeline. This formulation is unique as it tracks the fracture process along the pipeline, similar to the process employed in much more complex numerical schemes based on finite element analysis. Key conclusions include:

- **an engineering model was formulated based on the two-curve concept and shown valid for grades through X100 and toughness levels up to ~250 ft-lb (340 J) for both single-phase and two-phase decompression – this model incorporated an alternative "fracture curve" formulated for use in the two-curve concept, which admitted the dissipative effects of both the flow and fracture properties,**
- **a fracture-arrestor design model was developed based on this validated technology, and formatted for use in Windows-based software,**
- **the results indicate that energy dissipated in the creation of new crack surface is second-order in comparison to the effects of flow-induced dissipation,**
- **the results suggest the ideal laboratory specimen and test practice to characterize propagating fracture resistance would embed dissipative traits that involve both flow and fracture.**

15. SUBJECT TERMS

running ductile fracture, fracture propagation, fracture arrest, arrestor design, valid engineering model

16. SECURITY CLASSIFICATION OF: **Standard**			**17. LIMITATION OF ABSTRACT**	**18. NUMBER OF PAGES**	**19a. NAME OF RESPONSIBLE PERSON** **Brian Leis**
a. REPORT **Final**	**b. ABSTRACT**	**c. THIS PAGE** iii			**19b. TELEPHONE NUMBER** *(include area code)* **614.424.4421**

Standard Form 298 (Rev. 8-98)
Prescribed by ANSI Std. Z39.18

This page intentionally blank.

Table of Contents

	Page
Background	1
Introduction – Running Fracture and its Arrest	3
Report Organization	8
Approach and Deliverables	9
Objective and Scope	11
Results	12
Fracture Arrest Distance as Function of Pipeline Properties	12
Full-Scale Running Fracture Velocity and Arrest Database	12
Reformulation of a "Fracture Curve"	14
Conclusion	19
Training, Evaluation, and Validation of the Crack Velocity Model	19
Training the Crack Velocity Model	19
Trending and Preliminary Evaluation of Equation 2	20
Conclusion	24
Fracture Velocity as a Function of Stress, Toughness, and Gas Properties	26
Sensitivity Analysis – Setup	27
Conclusion	30
Analysis to Assess the Effect of Uncertainty in Toughness and Flow Response	30
Sensitivity Analysis – Toughness	30
Sensitivity Analysis – Flow Stress	30
Conclusion	30
Develop and Validate the Fracture Arrestor Design Basis	32
Develop and Calibrate Arrestor Design Model	32
Arrestor Design Software	33
Arrestor-Design Examples	34
Conclusion	38
Practical Aspects in Implementing Fracture Control and Arrestor Technology	38
Conclusion	40
Empirical Aspects Involving Flow and Fracture Response beyond Initiation	40
Historical Trends in Using the BTCM	41
Derivation of the Fracture Curve	43
Conclusion	48
Similitude Considerations – Empirical Aspects Involving Increased Toughness and Fracture Arrest Pressure	49
Similitude and Increasing Toughness	49
Similitude and Arrest Pressure – Flow Properties	53
Similitude and Arrest Pressure – Definition of P_a	55
Conclusion	56
Backfill Constant and its Empirical Definition	57
Effect of Backfill and its Empirical Role in the BTCM	57
Similitude and Definition of the Backfill Constant	58
Similitude and the Plausible Role of Flow Properties Embedded in the Backfill Constant	61
Conclusion	64
Reformulate the Propagation Velocity and Arrest Model Addressing Similitude	65

Similitude Issues and Gaps 65
Summary: Reformulation and Resolution of Similitude Issues and Gaps 66
The Plausible Role of Elastic Response 67
Background 67
Analysis 67
Conclusion 69
The Role of Flow-Induced Dissipation 69
Background 69
Analysis 70
Conclusion 71
Stopgap Fracture Arrest Model 71
The Stopgap Formulation 71
Approach 72
Steady State Propagation versus Reality 72
Model Validation in terms of Arrest versus Propagate 73
Conclusion 77
Energy-Based Framework for Dissipation 77
Background 77
Analysis 79
Conclusions 82
Practical Cases where Dissipation via Creation of Crack-Surface Can Dominate 83
Background 83
Analysis 83
Implications for Vintage Pipelines 86
Conclusion 87
Summary and Conclusions 88
Recommendations 91
References 93
Appendix A
Crack Arrestor Concepts and Designs A2
Background – Running Ductile Fracture and its Arrest A2
Background – History and Usage A2
Generic Arrestor Concepts A3
Generic Implementation Schemes A3
Desirable Attributes A5
References to Appendix A A7

List of Figures

	Page
Figure 1. BTCM and the definition of arrest condition	5
Figure 2. Test temperatures included in the database.	15
Figure 3. Range of diameter to wall thickness ratios included in the database.	15
Figure 4. Range of pressure stress to yield stress ratios included in the database.	16
Figure 5. Range of toughness and yield stress values included in the database.	16
Figure 6. Fracture velocity versus position for various initial stress levels.	22
Figure 7. Fracture velocity versus position for various flow stress levels.	22
Figure 8. Fracture velocity versus position for various Charpy toughness levels.	23
Figure 9. Fracture velocity versus position for various normalized strength levels.	23
Figure 10. Fracture velocity versus position for various normalized pipe geometry levels.	25
Figure 11. Fracture velocity versus position for various pressurizing media.	25
Figure 12. Two-curve scenarios for propagating and stable states, and the arrest condition	26
Figure 13. two-curve concept curves for a sample full-scale test (continued).	28
Figure 14. Experimental data and simulated effect of a +10/0/-10 percent on toughness	31
Figure 15. Experimental data and simulated effect of a +4/0/-4 percent on flow stress	31
Figure 16. results summary sheet of the arrestor design macro.	35
Figure 17. Example - arrestor analysis for lean natural gas (methane)	36
Figure 18. Example - arrestor analysis for 95 percent methane - 5 percent propane mix	36
Figure 19. Typical velocity-distance response approaching versus within the arrestor	37
Figure 20. Crack arrest distance versus CVP and yield stress for lean gas	39
Figure 21. Crack arrest distance versus CVP and yield stress for the rich gas	39
Figure 22. Predictions of FSE CVN arrest toughness based on four simplified models.	43
Figure 23. Database for X80, X100, and X120 full-scale tests[48]	44
Figure 24. Full-range stress-strain response of X42 and X70	46
Figure 25. Charpy energy versus true fracture toughness from a tensile test.	47
Figure 26. Charpy energy versus true fracture strain from a tensile test.	50
Figure 27. True fracture strain from a tensile test versus the ratio of yield to ultimate stress.	50
Figure 28. Energy components comprising energy via instrumented CVN testing	51
Figure 29. Evaluation of the simplified BTCM in conjunction with Equation 13	52
Figure 30. Stress-strain response for X-52 steel for axial and hoop orientations.	54
Figure 31. Stress-strain response for recent X-100 steel: axial and hoop orientations	54
Figure 32. Burst test results validating PAFFC for vintage and modern steels	55
Figure 33. Similitude breakdown associated with arrest pressure in the BTCM (typical)	56
Figure 34. Experimental data used to estimate the backfill constant in the BTCM	59
Figure 35. Full-scale results for soil, sand and without backfill and pressurized with air	60
Figure 36. Experimental data and the effect of variation in the backfill constant	61
Figure 37. Variation in strain-hardening exponent	63
Figure 38. Flow stress as a surrogate for true fracture stress	64
Figure 39. Trend as strength evolved in terms of actual yield stress	68
Figure 40. Predicted versus observed propagation response for one X100 test section	69
Figure 41. Typical illustration of simulated crack-velocity response within a test pipe	71
Figure 42. Predicted versus observed propagation response for another X100 test section	74
Figure 43. Arrest versus propagate comparison for terminal pipe joint	76

Figure 44. Illustration of dissipation as characterized by Equation 16 81
Figure 45. Trend as strength evolved in terms of toughness measured as CVP 84

List of Tables

Page

Table 1. Work scope for this project, including coverage by the cost-share project.....10
Table 2. Comparison of model predictions versus observed test outcomes 83

Acknowledgments

This report presents work that leverages co-funding from research done developing the fracture control plan for the Alliance Pipeline, and in the PRCI project PR-003-0049. Useful discussions with Mr. Mike Crump and Dr David Johnson then of CrossCountry Pipeline are gratefully acknowledged, as are discussions with the transmission pipeline fracture-control community.

Executive Summary

This project formulated an alternative fracture curve and the reassessed approach used to deploy the two-curve concept that underlies the BTCM as the basis to formulate an engineering model for fracture propagation and arrest. This facilitates assessing the response as the crack-tip encounters differing circumstances in its travel along the pipeline or full-scale test section. Further, it facilitates identifying first-order factors that must be addressed and helps to understand the breakdown of similitude between the model and the reality of the full-scale test or operating pipeline. This formulation is unique as it tracks the fracture process along the pipeline, similar to the process employed in much more complex numerical schemes based on finite element analysis.

This project's objectives in implementing the just-noted approach were to:

1. assess the viability of the premise that fracture arrest is due to energy dissipated in the creation of new crack surface, to better understand the ideal laboratory specimen and test practice to characterize propagating fracture resistance,
2. develop insight into 1) the mechanics and dynamics of the soil-structure interaction, 2) the gas dynamics during decompression, and, 3) the dynamic fracture process in the pipe by exploiting existing analytical formulations and semi-analytical schemes, as the basis to maximize productivity,
3. assess the premise that fracture arrest occurs through dissipation mechanisms in addition to crack-propagation resistance – and the premise that arrest as toughness increases as a process that transitions from a propagating crack to a running tensile instability, as the basis to understand the essential aspects of fracture propagation and arrest, and as appropriate
4. develop an engineering model for fracture propagation and arrest by exploiting existing analytical formulations and semi-analytical schemes like the BTCM.

Important conclusions from this work were presented in the conclusions subsection to each major aspect of this report. Readers interested in the details should consult each section. Suffice it here to list the critical conclusions, which here are synopsis of those listed in concluding the report as they target only the first objective listed above. These include:

- an engineering model was formulated based on the two-curve concept and shown valid by its application to the propagation behavior over the course of such full-scale testing, as well as for its discrimination between arrest and propagation – the validation considered grades through X100 and toughness levels up to ~250 ft-lb (340 J) for both single-phase and two-phase decompression,
- a fracture-arrestor design model was developed based on this validated technology, and formatted for use in Windows-based software,
- an alternative "fracture curve" was formulated for use in the two-curve concept that addressed the dissipative effects of both the flow and fracture properties in the validated engineering model,
- the results indicate that energy dissipated in the creation of new crack surface is second-order in comparison to the effects of flow-induced dissipation,

- the ideal laboratory specimen and test practice to characterize propagating fracture resistance should embed dissipative traits that contribute to flow and fracture – in a balance dictated by further analysis.

Critical conclusions regarding the second, third, and fourth objective on the list above are incorporated in closing the Summary and Conclusions section.

Many recommendations for improvements are compiled in the closing paragraphs of each section of the report. For the sake of brevity only the high-level high-impact topics follow:

1. Backfill and axial restraint have a significant impact on the propagation velocity and so the arrest conditions, but as yet these effects have been commingled with the effects of the strain-hardening exponent and considered a "backfill constant" – during the course of this work the historical archives for most of Battelle's full-scale tests were fortuitously located, including extensive and generally unpublished data on "backfill effects".

   There is great potential value in mining this data and in its analysis and incorporation in the two-curve formulation developed in this project, which avoids the cost of the testing and so has great value-added.

   There is equally great value-added by developing and evaluating alternative formulations for the "backfill constant", to uncouple backfill and the line pipe properties, which should consider the as yet untapped value of the recent work considering the plastic wave velocity.

   Much of what is attributed to backfill effects could develop via the effects of axial restraint, which act to limit the size of the plastic zone ahead of the crack, thereby leading to higher cracking velocity – again much added value can arise by uncoupling what is attributed to backfill but is more likely due to axial restraint.
2. The initial design of the full-scale tests spaced crack-detection wires a meter apart such that at the transition between pipe joints the spacing is typically two meters. This practice has persisted, which is unfortunate as it precludes identifying the true effect of the change in toughness and flow properties on the propagation velocity.

   The present work implies countering effects of these parameters, and local complexity due to the effects of momentum. More detailed analysis of this scenario is possible by mining the literature, and by further simulation – again with great value-added.
3. The alternative "fracture curve" was formulated for use in the two-curve concept focusing both the flow and fracture properties, but with limited insight into the concern addressed in Point 2 above.

   Following consideration of Point 2, care should be taken to incorporate the findings into the fracture curve – otherwise the added value is lost.
4. The results indicate that ideal laboratory specimen and test practice to characterize propagating fracture resistance should embed dissipative traits that contribute to flow and fracture – in a balance dictated by further analysis. As this is a significant departure from current directions, consideration should be given to alternative test practices.

   The insight provided by Equation2 implemented in the form of Equation 16 should be utilized as a guide to identify the appropriate test to characterize running fracture resistance – with great potential value but only for targeted applications.

5. The premise that arrest as toughness increases as a process that transitions from a propagating crack to a running tensile instability has great utility in understanding the fracture response of modern-design pipelines.

    Consideration should be given to the further development of this concept to ensure the safe serviceable operation of pending pipeline designs.

6. The engineering model as currently formatted and packaged in software can be used in the design of fracture arrestors, but in this form cannot applied to characterize fracture propagation or discriminate between propagation and arrest.

    Consideration should given to packaging the engineering model for use in software much like DYNAFRAC packages the BTCM. This would help to capture the value of this project.

7. Changes in the possible use of the pipeline infrastructure point to the use of the current system to transport LNG, or where waivers are granted to experience higher pressures.

    Consideration should be given to an evaluation of such impacts in regard to the potential for fracture propagation, as guidance to avoid future related problems.

8. A validated engineering model for the design of fracture arrestors was developed and packaged as software to facilitate the design of integral fracture propagation arrestors.

    As this technology is fully general and could be generalized for similar use with external arrestors, consideration should be given to such applications – with great potential value added given the platform already exists for integral arrestors.

Background

The challenge of efficiently and safely operating the natural gas and hazardous liquid transmission system in the US has existed and evolved since pipelines were recognized as the best way to transport hydrocarbons between supply basins, processing plants, and markets. This project was one of four concurrent activities completed under a consolidated program designed to help improve the integrity of the pipeline infrastructure in the U.S.

This project targeted integrity assessment associated with control of running fracture. This topic tends to be associated with advanced-design high pressure large-diameter gas transmission pipelines. However, as a consequence of FERC Order 636, which opened the pipeline infrastructure to common-carrier service, and with the potential for shipping liquefied natural gas (LNG) derived gas, which runs much colder than current operation that embeds heat-of-compression and often contains heavy ends, running fracture could reemerge as a threat for existing pipelines. While pipeline owners can "control" gas quality for the gas they ship, the means for such control and its practicality in continuous real-time are limited, opening the door to much worse circumstances than hereto experienced for some pipelines. While running fracture remains an unlikely occurrence, it is a possibility with every rupture on gas pipeline rupture or split on a hazardous liquid pipeline transporting super-cooled fluids, whose length controls the extent of exposure to life and property and therefore dictates the consequences of failures. While technology has been developed to address this threat, it does not directly address the design of fracture arrestors that could be used to control running fracture, and gaps remain in addressing some new advanced-design scenarios. This project considers the design of fracture arrestors and existing technology gaps to help ensure fracture arrest through Integrity Management Plans (IMPs) developed in response to the Government requirements for as stated in recent regulations[(1,2)*] and addressed in industry responses to those regulations[(e.g., 3,4)].

While developing the structure and requirements embedded in the recent regulatory changes involved significant effort on the part of the Government, the real challenge lies in successfully implementing those requirements to ensure the system integrity sough by the regulations. Auditors must be able to identify and concur that the requirements of the plan have been met. This is relatively easy for typical new pipeline designs that exist within the proven experience base for line-pipe steels, design, and modern construction practices coupled with quality control. However, for designs and steels beyond that experience base, or for existing systems that might transport products under more demanding circumstances than historically encountered, it is much more complex. Auditors must be able to track the efforts of the pipeline engineer throughout the fracture control plan for new designs or IMP for existing pipelines, and quantify and agree that the objectives of the plan have been met. Suitable tools must exist or be developed to effectively implement the plan, and track the related process, and show continuous improvement in safety. The present project is directed at such needs and actions specific to fracture control, for both existing pipelines and new advanced-design pipelines.

Many potential **threats** open the door to possible running fracture such as third-party damage, stress-corrosion cracking, the growth of seam defects due to pressure cycles, with rupture even

---

[*] Numbers in superscript parenthesis refer to the list of references at the end of this report.

possible due to external or internal corrosion depending on the nature of the steel and corrosion. The severity of these threats to the **condition or serviceability** of the pipeline depends on the pipeline's pressure and geometry, the line-pipe grade and toughness, and the properties of the transported product. The consequences depend on the circumstances along the right-of-way (RoW), the pressure and pipeline diameter, and other factors. As the threats that can lead to rupture involve both random and time-dependent drivers, managing running fracture involves both avoidance for the random threats and periodic **re-inspection** for the time dependent ones. Ideally, this process will include the ability to capture systemic changes that bring new threats into consideration, while being both simple and reliable in field applications. The focus here is on fracture arrest, and arrestor design, with consideration of avoidance of random threats and re-inspection intervals for time-dependent threats beyond the scope.

Introduction – Running Fracture and its Arrest

In the unlikely event of fracture initiation leading to a rupture, because of the compressibility of certain transported fluids the energy stored in high-pressure transmission pipelines can sustain the axial propagation of a rupture. As is now well known, where the decompression front propagates from initiation at a velocity greater than the fracture velocity, this wave-front outpaces the fracture with arrest occurring when the pressure decays to a level that no longer supports propagation. In addition to considerations such as loss of service and product, and the cost to replace potentially significant lengths of pipeline, other consequences of running fracture for some products and pipeline locations require certainty that propagation can be arrested within a short predictable distance.

The term running "brittle" fracture (RBF) was introduced to describe axial propagation with limited energy dissipation due to deformation or crack formation. In contrast, the term running "ductile" fracture (RDF) was used where significant plastic deformation develops, and the failure mechanisms were associated with locally ductile stretching leading to void nucleation, growth, and coalescence that create "crack surface" as the crack extends.

As propagation runs axially along a pipeline, the fracture tends to open in the wake of the crack. For RBF, the size or extent of the flap opening can be very limited. For some pipe materials, the fracture remains closed in the wake of the crack due to residual stresses induced in pipe making, as occurs for the early polyethylene pipe used in gas distribution mains. However, with RDF flaps form as the pipe opens and flattens in the wake of the propagating crack. The extent of the flaps and their opening reflect the energy associated with the crack's passage, the extent of the energy stored prior to its passage, and the ductility of the line-pipe material. Flap formation and the extent of this opening develop longitudinal and circumferential stresses ahead of the crack. Such stresses cause thinning of the wall and can induce significant ovality[(e.g., 5)1] of the pipe's cross-section. Concepts that underlie some RDF crack arrest formulations consider flap formation, on the presumption that the stresses due to the flaps and the related dynamic effects contribute to the crack's advance. Likewise, some RDF crack-arrestor concepts act to restrain flap formation, or rely on increased dissipation of the fracture energy, or enhance the apparent fracture resistance.

Approaches to characterize driving force and inherent fracture resistance can be found elsewhere in terms of fracture mechanics, gas dynamics, and thermodynamics[(e.g., 5)]. While of interest as a basis to categorize concepts to predict arrest and identify schemes to develop arrestors, such details are not essential here. Suffice it to note that crack arrest occurs by directly tipping the balance between driving force and fracture resistance toward arrest, or by redirecting axial propagation from along the pipe until the crack driving force subsides (i.e., the decompression front runs past the crack tip).

As the significance of RBF and the consequences of this fracture mode were understood in the 1960s, steels were developed with lower transition temperature and then viable toughness levels. It was found that RBF could be avoided by specifying steel whose transition temperature was

---

[1] Reference 5 is a summary of the state of the art in RDF, providing entrée to a broad literature base. It is used here as a surrogate for that literature.

safely less than that of lowest temperature in service or upset conditions, with provision for some reasonable margin of safety. Accordingly, the focus hereafter is crack arrest and arrestors for RDF. While the expectation was that problems with running fracture would be resolved when RBF was controlled, full-scale experiments done with steels designed to be ductile under dynamic cracking conditions in the late 1960s and into the early 1970s showed that ductile fracture propagation was still possible at hoop stress levels typical of service. Thus, the challenge was to develop line-pipe steels with sufficient dissipative capacity to arrest the axial propagation, or to provide arrestors designed to stop that propagation, and do so gradually leading to a so-called "soft arrest" where the pipeline remains intact and in the ground.

Theories of quasi-static fracture were still somewhat rudimentary in the 1970s when the possibility of RDF propagation in pipelines became apparent. Consequently, understanding RDF required observations and analyses of full-scale experiments considered to simulate pipeline response. These experiments involved a test section several hundred feet in length in which variables such as pressure, diameter, wall thickness, strength, and toughness, were systematically varied[e.g., see 6-8]. A lower-toughness "initiation joint" was placed symmetrically between pipe joints of increasing toughness, with the highest toughness greater than anticipated to cause arrest, or an arrestor was located in or on the last of the joints. The "test section" was connected at either end to reservoir pipe of comparable diameter but often heavier wall thickness – whose purpose was to store sufficient energy to run the fracture through the test section. The reservoirs were connected into a smaller-diameter pipe-loop that facilitated control (and measurement) of the desired fluid properties to ensure uniformity within the test section. The propagation velocity was measured using "timing wires" typically spaced one-meter apart. Crack-arrest toughness was defined in such experiments as the toughness of the pipe joint in which the propagating fracture arrested. However, as this toughness and the related mechanical properties could not be determined at the point of arrest, this outcome must be defined within the typical variability that develops within a joint of pipe.

With the pipe joints arranged in order of increasing toughness with a moderate incremental increase with each joint, the velocity of the running crack was not significantly affected by its propagation through the previous joint and in the transitions. Therefore, such full-scale testing was considered to develop "steady-state propagation" at decrementing velocity until arrest occurred. The toughness measured in the arrest joint defined the "arrest toughness" for the set of pipe properties (diameter, grade, wall thickness, toughness), fluid properties (composition, pressure, temperature), and backfill conditions (depth, soil-type, compaction, temperature) considered in each test. This full-scale testing approach has become the accepted as the standard by which to determine the toughness needed to arrest RDF.

Unfortunately, full-scale testing is very expensive and produces data specific to the test parameters. This already expensive scenario is made costly by the fact that the alternative of testing end-capped pipe segments – regardless of their length – without use of earth-anchors to preclude axial stretching produces non-conservative results as compared to a typical buried and earth-anchored" pipeline. To date, testing according to such practices has unproven utility even as a relative metric for specific applications. For this reason, viable full-scale testing remains very expensive while generating valid results with limited general utility. Thus, a need existed to quantify the behavior in such testing for use in pipeline design, or the design of arrestors to control RDF, and to assess the susceptibility of existing pipelines to RDF for specific operating conditions.

In response to this need and given the state of available technology Battelle formulated a semi-analytical approach to predict RDF arrest toughness focused on natural gas pipelines in the early 1970s[9]. This formulation considered gas decompression and dynamic crack-propagation as uncoupled processes. The fracture resistance and the driving force for continued steady-state propagation were related through the fracture and decompression velocities, which were coupled empirically through a parameter that was considered constant, referred to as the backfill constant. This approach initially used a graphical solution seeking tangency between the two curves that describe these processes, as illustrated schematically in Figure 1. Because this graphical solution involved a "gas curve" and a "fracture curve", the approach became known as the Battelle "two-curve model" (BTCM). This two-curve model included provision for two-phase decompression behavior, which was motivated by interest in the 1970s in transporting gas from formations that produced methane in combination with other natural-gas liquids (NGLs).

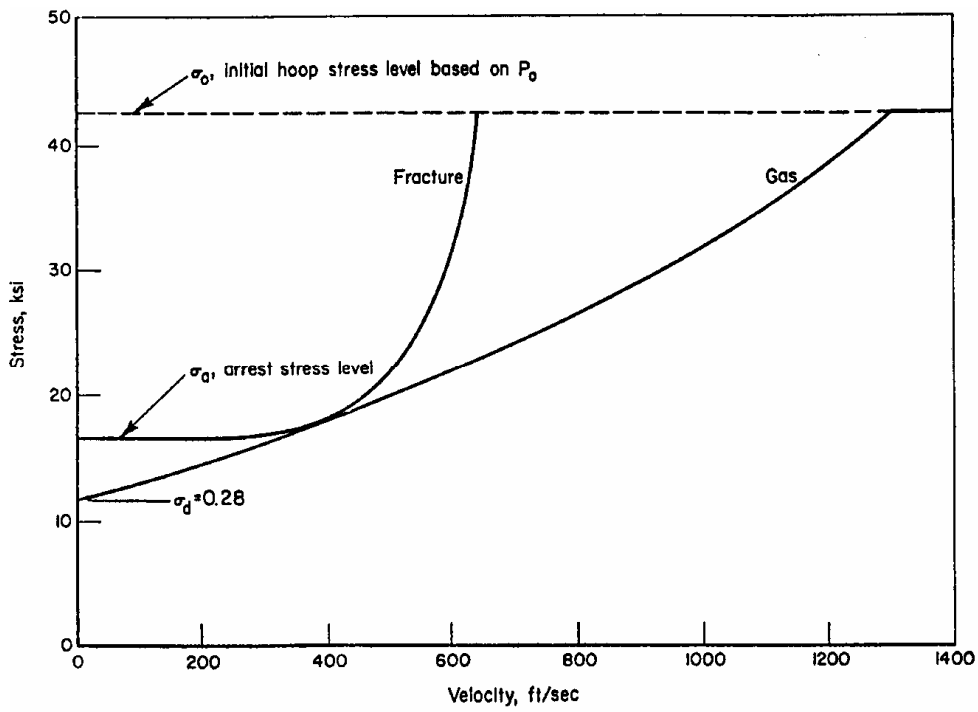

Figure 1. BTCM and the definition of arrest condition

Because full-scale tests for such "rich gases" required mixing to avoid stratification and/or plugs of dense-phase gas, most full-scale tests avoided this complexity by testing with fluids that showed single-phase decompression, such as air, nitrogen, or methane. However, as the first rich-gas tests were being completed it became clear that rich gases required much higher arrest-toughness than was required for single-phase decompression[(e.g., 10-12)]. The complexity in such rich-gas tests coupled with the rudimentary mixing capabilities and limited sampling to ensure the desired mix was achieved and homogeneous during testing opens to question the viability of some of the early tests. This complexity coupled with the related costs encountered in rich-gas tests meant that the majority of full-scale tests were done considering the simpler single-phase scenario.

As time passed, parametric analyses were done for a typical large-diameter pipeline design via the BTCM the results of which were trended leading to a single-phase model developed as a

curve-fit to the trends. While this "simplified" model was evolving, work in the US, Europe, and Japan continued the full-scale testing adapting the practices developed in the US – which for the reasons noted above largely targeted single-phase decompression scenarios. The fracture properties of the steels used in the vast majority of such experiments were characterized only in terms of the Charpy vee-notch (CVN) test[13], the method popular for this purpose when the possibility of dynamic fracture was recognized. As the full-scale fracture-arrest database grew for single-phase decompression, work began to empirically trend these results leading to curve-fit models for arrest toughness. Including the Battelle single-phase equation, a total of six so-called "simplified models" were eventually developed for single-phase applications[14-19].

The early full-scale experiments typically involved large diameter sections, typically 24 or 36 inches, made of line-pipe steels with strengths typically X65 or less and toughness typically less than 100 J. This scenario was consistent with steel making capabilities into the early 70s and then available line pipe. The results of this early full-scale testing indicated that CVN energy provided a suitable measure of fracture resistance for the various steels and models used to characterize dynamic fracture over the range of pipeline situations represented in these experiments. In part, this suitability traces to the fact that the data embedded in the "calibration" of the curve-fitted simplified models, and the BTCM, were being used to assess their viability.

As line-pipe became available in high-strength-low alloy (HSLA) steels, and thereafter control-rolled steels, the full-scale testing expanded to include these line-pipes. Into the early 90s, such testing included commercially available line-pipe in Grades up to X80 with toughness occasionally approaching 250 ft-lb, with some X90 also tested along with an experimental X100 steel. While reliable "predictions" of arrest toughness were made when the analyses of the 70s and early 80s was used within the scope of its calibration, as full-scale test results became available for the stronger, tougher steels it was apparent that all such models led to non-conservative predictions for these newer steels[20], which since has been broadly shown to involve a similar error for all such models[21].

The logical response to problems with empirical models used beyond the limits of their calibrating database is that fundamental differences in the controlling processes are developing – such that similitude no longer exists in the failure process between the more recent steels and those embedded in the calibration database – for the BTCM as well as the simplified models. While consideration of similitude requirements offered logical resolution to the erroneous predictions, opinion then was that arrest occurred dissipation due to propagation creating new crack surface. In this context the CVN specimen was considered too small to develop significant propagation and therefore inappropriate to quantify steady-state RDF. Accordingly, attention then focused on trial and error alternatives to the CVN test as the means to improve arrest-toughness predictions.

Early alternatives focused on a larger test specimen to characterize propagation resistance, based on adaptations of the drop-weight tear test (DWTT)[22] specimen. Work was done to minimize the contribution of other dissipation processes, to ensure propagation resistance was quantified. Various notching practices argued to reduce or isolate dissipation due to deformation and initiation were considered[e.g., see 23]. Initially such concepts were considered promising, so the work continued. However, work done in Japan using novel experimental practices reported in the mid 1980s showed the fracture velocity in such specimens was well short of that for full-scale conditions, such that they failed to reflect RDF in pipelines[23].

Subsequent work began to address similitude requirements[24], with the expectation that arrest in tougher steels involved dissipation that slowed the crack due to deformation at the crack-tip and in the adjacent lateral stretch zone – leading to continuous "re-initiation" as the crack propagated down the pipeline. That work accounted for differences in the components of energy dissipation for higher-toughness steels as compared to those embedded in calibrating arrest models like the BTCM. Application of this similitude adjustment as presented in References 21and 24 underlay the first accurate "blind" predictions of fracture-arrest toughness for high-toughness steels in a high-pressure rich-gas scenario[25,26]. Success via consideration of similitude suggest that similar benefits might accrue through a broader assessment of the requirements for similitude – to identify and offset other shortcomings due to differences in early steels used to calibrate the BTCM as compared to modern higher-strength higher-toughness steels.

This project considers differences in current higher-strength higher toughness steels building on the two-curve concept that underlies the BTCM and assessing the implications of its calibration in reference to Grade 448 (X65) or below, at toughness of 100 J and less. It also considers the breakdown of similitude in formulating the BTCM that involve the flow response through the strain hardening exponent and true fracture strain, and the fracture resistance represented as dissipation due to deformation, fracture initiation, and fracture propagation. Fracture initiation enters the formulation of the BTCM through consideration of the fracture arrest pressure, which carries back to the log-secant-based NG-18 equations[27,28]. Fracture propagation for the BTCM embeds both the deformation response and fracture resistance.

Report Organization

This report develops technology to assess the arrest-toughness from two distinctly different perspectives. One involves design of fracture arrestors that might be used in retrofitting existing pipelines to contain RDF due for example to changes in operation or transported product. The key in arrestor design is reducing the fracture velocity over the length of the arrestor sufficiently to ensure arrest occurs within that length. The second involves support of fracture control plans in applications involving advanced-design pipelines to be constructed using modern higher-strength higher-toughness steels. The key in fracture control is providing sufficient toughness to arrest a running fracture should one initiate, and do so within a predictably short length.

Because technology to assess propagation distance and arrest-toughness is central to both perspectives, the initial sections of the report address topics involving fracture propagation behavior as a function of propagation distance, and the properties of the pipeline and transported fluid. An alternative to the fracture curve of the BTCM is formulated, and thereafter applied to screen the suitability of this formulation. The formulation is then used to assess the effects of uncertainty in the mechanical and fracture properties of line pipe – to determine its impact on predicting arrest. The design of fracture arrestors is considered next, after which similitude issues are dealt with in terms of strength, flow, and fracture properties of the line-pipe steel. Problems in the historic use of the BTCM are examined as the basis to identify "hard to predict" scenarios and to define potential similitude issues. Several sections then follow evaluating the breakdown of similitude traced to both the flow and fracture properties of modern steels versus those addressed in formulating the BTCM. The extent of errors traced to similitude issues is then evaluated and similitude issues resolved to the extent possible. Once a viable model is established its validity is assessed. The stopgap model formulated in reference to similitude is evaluated subject to the current full-scale test database – to the extent it is defined in the open literature. This stopgap formulation is then applied to determine if scenarios exist within the US pipeline infrastructure where long running ductile fracture poses a problem. Finally, the implications for a rational path forward are outlined. The report closes with a summary, conclusions, and recommendations.

Approach and Deliverables

Work on fracture arrest has historically built on the premise that propagation slows leading to arrest because of the energy dissipated through the creation of new crack surface, which is characterized by the line-pipe steel's crack-propagation resistance[e.g., see 5]. This view was clearly viable for the early pipeline steels. This is evident in the observation that even the physically small CVN specimen showed in excess of 70-percent of the total energy dissipated due to propagation[24] for steels typical of those used to calibrate the BTCM.

The premise that arresting fracture propagation involves dissipation through the creation of new crack surface underlies the significant continued investment in identifying a laboratory specimen to characterize RDF. The effort to identify such a specimen began with questions of the utility of the CVN specimen in the 1970s[e.g., 29,30]. This led to adaptation of the DWTT specimen[22] and continued with attempts to modify the crack-starter notch to minimize dissipation other than that due to cracking[e.g., 23,30,31]. The shift away from such approaches to use of the crack-tip opening angle (CTOA) began for pipelines in the early 1980s. While the early definition and laboratory measurement of CTOA considered both deformation and fracture[e.g., 32-36], work continued into the new millennium attempting to isolate propagation energy from the total energy[37-40]. The advent of CTOA also led to extensive numerical modeling directed at better characterizing crack driving force and measures resistance. This work also has been built on the premise that fracture arrest involves dissipation through the creation of new crack surface. This modeling began in the mid 1980s[41-48] and also has continued to develop in the new millennium[e.g., 40].

Work based on the premise that fracture arrest is due to dissipation due to creation of new crack surface is central to most recent developments. However, in spite of significant effort worldwide and major investments the order of many millions of dollars over ~25 years this approach has not led to simple methods or engineering tools to assess RDF. Rather, the trend is to increasingly complex constructs to assess arrest behavior, which have been dotted by some major shifts as approaches built on this premise were found to miss the mark. Examples include redefinition of the laboratory metric for CTOA in 1995[36] and subsequent re-calibration of the driving force for crack propagation in 2000[46]. Use of CTOA in blind fracture arrest predictions for the Alliance Pipeline indicted arrest could require values of CTOA well in excess of that from then available steels[49]. In contrast, the full-scale testing demonstrated arrest in line pipe produced without a corresponding price-penalty at toughness levels routinely exceeded for over a decade[25,26].

As the path to a model for RDF after ~25years is toward increasingly complex methods based on the "propagation-energy premise", perhaps an alternative premise is timely. The is reinforced by the observation that none of the specimens evolved to quantify propagation resistance was found to correlate with either the arrest toughness or fracture velocities measured in the Alliance full-scale testing[50]. In contrast, CVN energy abandoned in the pursuit of propagation energy was found to directly correlate with both the arrest toughness and fracture velocity for this full-scale testing[50]. These observations, and the fact that arrest in that full-scale testing showed energy dissipation other than in crack propagation, led to the conclusion[51] "the next step-improvement (in assessing arrest) will not come by finding a specimen that isolates fracture resistance".

Because arrest of running fracture involves:

- the mechanics and dynamics of the soil-structure interaction,
- the gas dynamics during decompression, and,

- the dynamic fracture process in the pipe,

each of which is nonlinear and so by itself can be very complex, their coupled interaction is even more complicated. This is not to say they cannot be modeled numerically or otherwise, but it does imply that these factors must be uncoupled and understood before a model the couples their individual contributions can be successful and proven in general. This uncoupling will require extensive, expensive full-scale testing unique to the past. Because such testing has no immediate return on the investment, prior to such radical action it is appropriate to establish the need for and value of such investments. To this end, the value of past investments and model development must be fully exploiting, as must insight available via existing analytical formulations [(e.g., 52-56)] and semi-analytical schemes like the BTCM.

The present project begins this process of based on the premise that fracture arrest occurs through dissipation mechanisms in addition to crack-propagation resistance – and the premise that arrest as toughness increases as a process that transitions from a propagating crack to a running tensile instability. These views differ substantially from the historical view that RDF can be characterized simply in terms of dissipation through the creation of new surface leading to crack propagation. The viability of these views are tested through the work of this project, which begins by characterizing the extent to which propagation within a joint of pipe alters the fracture velocity, and thereby contributes to fracture arrest, as compared to the effect of incremental toughness experienced when the running fracture propagates into an adjacent pipe joint.

By contract, including the cost-share companion projects, the work scope for this project is presented in Table 1. Results developed for each of these topics are presented subsequently in sections that typically target each of these topics – although the section titles differ somewhat.

Table 1. Work scope for this project, including coverage by the cost-share projects

Task	Deliverable / Milestone
CS1	arrest distance quantified as function of pipeline properties
CS2	arrest distance function validated by full-scale database
CS3	fracture velocity trended with stress, toughness, and gas properties
CS4	fracture arrestor design basis developed and validated
CS5	trends summarized for practical applications of arrestor technology
1	empirical aspects involving fracture initiation evaluated
2	empirical aspects involving flow response of pipe steel evaluated
3	Empirical aspects involving backfill constant evaluated
4	arrest model embedding revised empirical aspects reformulated
5	full-scale test data to quantify role of grade and flow response trended
6	assess role of elastic response as grade increases
7	dissipation due to plastic deformation remote to crack assessed
8	dissipation due to plastic stretching prior to tensile instability assessed
9	stopgap fracture arrest model formulated
10	first-principles model for active sources of dissipation formulated
11	cases where crack surface dissipation dominates identified

Objective and Scope

The objective was to develop the above-noted alternative premise for fracture arrest by exploiting the value represented by existing analytical formulations and semi-analytical schemes like the BTCM. This was done by formulating a model for fracture arrest that tracks the fracture process as it encounters differing circumstances in its travel along the pipeline or full-scale test section. This approach helps to identify first-order factors that must be accounted for to satisfy similitude between the arrest model and the reality of the full-scale test or operating pipeline.

The work scope noted in Table 1 targeted extension of the two-curve concept that underlies the BTCM, considering similitude between the aspects embedded in this model and its calibration in terms of steels and pipeline scenarios circa 1975 versus the situations considered for its use since then. This scope for existing pipelines targets the design of fracture arrestors to address changes in operation or transported product, for example transporting LNG-derived gas. Because this gas runs much colder than current service, which embeds heat-of-compression, and often contains heavy ends, running fracture could reemerge as a threat for existing pipelines. In contrast, the scope for new pipelines targets technology viable for high-toughness higher-strength steels.

The focus for the advanced-design pipelines involves the existing full-scale testing that covers commercial grades primarily through X80as well as the limited testing done for X100 and X120 that is openly available in the literature. For the X100, the line-pipe evaluated reflects pipe production nearing commercially available products, while that for X120 might be considered less commercially developed.

Five deliverables with near-term value to the pipeline industry evolve by integrating the results of the tasks outlined in Table 1. The first deliverable is identification of differences between the flow and fracture characteristics of the calibration database for the BTCM, and the corresponding traits of the line-pipe steels that have developed since. Such differences were identified by empirically trending these properties. This deliverable provides insight in designing fracture arrestors as well as in fully exploiting the potential of the existing technologies. The second deliverable is a model and algorithm for the design of fracture arrestors, which is specific to so-called integral arrestors as opposed to other types of arrestors as elaborated in Appendix A. This deliverable was met through an artificial-intelligence-based approach wherein a small sample of the full-scale test database was used to train a model whose mathematical form followed from first principles. This deliverable replaces the “fracture curve” currently in use in the BTCM. The third deliverable is technology developed to establish similitude between the calibration database and the steels for which there is a need to predict arrest-toughness. This technology was evolved via use of both analyses and trending of laboratory and full-scale experiments that target gaps identified in developing the first deliverable. This deliverable guides formulation of the fourth deliverable, a stopgap fracture arrest model. The fifth deliverable is consideration of first-principles in combination with the work completed based on the two alternative premises noted above, which includes all forms of dissipation contributing to fracture arrest. The last two deliverables evolved via the same approach adopted in meeting the third deliverable.

Results

Fracture Arrest Distance as Function of Pipeline Properties

The objective of this task was to use analytical and theoretical considerations to identify key parameters and the mathematical format of the relationship between fracture propagation versus distance along the pipeline or pipe joint, the properties of the pipeline or pipe joint (geometry, grade, toughness) – and thereafter quantify these key parameters in the framework of an artificial intelligence (AI) formulation. Key parameters were quantified using a "training dataset" derived from the full-scale test database. The goal was to integrate this knowledge to quantify fracture velocity and decay in fracture velocity as a function of stress, toughness, and parameters that characterize the geometry of the line pipe and the properties of the transported gas or fluid.

The dataset used to "train" the AI model consisted of experimental data derived from full-scale tests conducted on simulated pipelines. As the approach adopted has not been pursued in past, the first step was to assemble openly published trends that document fracture velocity over the course of such tests. A database was compiled representing fracture velocity, as well as fracture arrest defined in terms of the rapid decay in velocity during the arrest. While a logical basis to understand and formulate models for fracture propagation and arrest, previously such data have not been compiled, as no such database was located in the open literature. This database reflects the behavior from the initiation event through propagation and arrest, and so is quite different from datasets typically published. Such databases, as in Appendix E of Reference 5, normally focus on test parameters and the toughness of the arresting pipe joint. As available, the fracture velocity data were supplemented by mechanical property data derived from tests on conducted on samples cut from the pipes used in the full-scale tests.

The following subsection provides an overview of the database developed for use in "training" and evaluating the model(s) to be developed. Thereafter, the next subsection presents the analytical model and its training using a small portion of this database, with the next section evaluating this model to screen for undesirable bias that would necessitate reformulation.

Full-Scale Running Fracture Velocity and Arrest Database

Because the analytical model for predicting propagation velocity to replace the fracture curve of the BTCM was derived in consideration of the crack propagation behavior in full-scale tests, this section begins with a review of such testing as an introduction to the data they generate.

As introduced earlier, a typical full-scale fracture propagation test involves a test section comprising a series of pipe segments with symmetrically increasing toughness centered about an initiation pipe. This test section is connected into a loop that is used to mix and control/monitor the properties of the test media. Once the setup is completed, pressurized, and stabilized, a crack is initiated in the central initiation joint. The two cracks then propagate from the tips of that crack in opposing directions – hopefully with minimal interaction – until both tips arrest. Prior to the test, the anticipated arrest toughness is estimated and pipe joints selected to provide incremental toughness leading to arrest. In contrast, the initiation joint is selected with properties anticipated to accelerate quickly leading to fracture running with sufficient velocity to propagate into the adjacent pipe segments.

The position of the running crack is monitored during the test section using timing or trip wires that are placed at a fixed interval along the simulated pipeline. Historically these have been spaced about one-meter apart, which where girth welds occur leads typically to a two-meter gap. In addition, pressure is measured at fixed locations along the pipe, with other transducers deployed depending on the purposes of the test. The time that each trip-wire is broken is recorded and the average velocity determined by the elapsed time required for the crack to traverse the distance between adjacent trip-wires. Such data are used to estimate the propagation velocity of the crack as functions of the pipe diameter, wall thickness, material, as well as the backfill, and the type of gas used to pressurize the simulated pipeline. Obviously, accurate and precise measurement of the interval between the trip wires is critical to minimize scatter in the crack velocity.

Data useful in characterizing fracture propagation velocity were derived from References 57 to 66, with fracture velocity developed as a function of location along the test section for the test range of testing conditions evaluated. The database developed reflects open literature results, as well as unpublished or privileged-circulation data that is made available on the provision they will not be publicly divulged in any detail.

The database from which a training dataset could be culled initially included the result of 25 full-scale tests in which 684 crack position and velocity measurements were recorded over 134 different pipe segments. Pressurizing media included natural gas and air, which for analytical purposes were treated as pure methane and pure nitrogen, respectively. The pipe diameters ranged from 24 inches through 56 inches, with wall thickness ranging from 0.313 to 1.2 inches. When used, the backfill materials included "soil" and "sand", with depths ranging from 18 to 40 inches. In some cases, the width of the side-fill was recorded as well, which ranged from 18 to 60 inches. Based on the number of recorded position-velocity data pairs, the dominant test conditions were natural gas with 40 inches of "soil" backfill. Approximately half as many data pairs were available for pipes pressurized with air and covered with 30 inches of "sand" backfill. Approximately half again as many data pairs were available for tests with air and no backfill. Testing was done at temperatures that ranged from 46 to 80ºF, at pressures leading to wall stresses in the test pipes up to 90-percent of the specified minimum yield stress (SMYS).

Over the course of this project additional data became available and were incorporated into this database, leading to more than 1000 crack position versus time data-pairs. As time passed and the testing practices were more completely documented it became apparent that some fundamentally different circumstances were represented by otherwise similar terms used by different organizations or investigators. Of these, the use of anchor-blocks to axially restrain the pipeline was found to be inconsistent was the application of backfill. Aboveground testing typically does not use axial anchors even though some such pipelines experience varying degrees of axial restraint. In contrast, the simulation of buried or "backfilled" pipelines typically use anchor blocks, as such pipelines tend to be "earth-anchored". The role of axial restraint is potentially quite significant independent of any "backfill" effects, as the end-capped loading acts to restrain the opening of the flaps, which for many is central to the driving force for RDF. This makes testing absent anchor-blocks non-conservative in contrast to anchored scenarios. The term backfill also was loosely used. Some "backfill" tests reflect on-grade testing under loose overburden piled to a specified depth, with different widths of overburden being used. Other testing done with backfill used a ditched test section that was filled but not tamped or compacted, while other ditched sections used moderate tamping to compact the backfill. Some scenarios

made use of "soil" that had apparent cohesive strength, while others made use of sand as the fill material. In general little other detail concerning the fill material or the backfill practice was reported save for an indication of the depth.

Figures 2 through 5 present the distributions of test parameters covered by the range of data that was compiled. Temperature is addressed in Figure 2, while the range of pipe diameters and wall thickness is addressed in Figure 3. Note that each data point in this figure can represent more than one test pipe. The legend in Figure 3 overlays contours of diameter to thickness ratio, with about half of the D/t ratios for the database lying between 80 and 100. Figure 4 illustrates the range of pressure-induced stress divided by the actual yield stress (AYS) for this database, which is presented there as a function of AYS. The figure shows that the range of AYS goes from 57 to 104 ksi for pipes in the test section, with the range of test pressure to ASY occasionally at levels much greater than typical of pipeline service. Results for initiation pipes are shown therein as solid symbols, whereas those for test pipes are shown as open symbols. Again, each data point in this figure can represent more than one test pipe. Finally, Figure 5 shows the range of Charpy toughness levels included in the database, and their distribution relative to the AYS for each segment. As expected the lowest toughness levels correspond to the initiation segments. As for the other figures in this discussion each data point in this figure can represent more than one test pipe.

Reformulation of a "Fracture Curve"

The analytical model for predicting the propagation velocity was derived considering basic fracture concepts and observations made regarding crack propagation behavior in the full-scale tests. Notable in regard to observations in propagation behavior is the observation that the early testing tended to produce smoother more continuous trends in crack velocity. In contrast, the more recent testing of tougher and stronger grades tends to produce what appears as somewhat unstable propagation, with sharp increasing and decreasing changes in velocity evident. The results indicate changes in velocity begin to occur on occasion prior to physical entry into the next joint. This very likely reflects the fact that the crack tip travels in the wake of the plastic zone that forms ahead of the crack – such that the flow-induced properties of this next joint control the crack's response. This observation clearly implies the velocity of the propagating crack tip is dictated by the velocity of the propagating plastic wave that formed upon fracture initiation. Continued axial propagation in this context is driven by the pressure in the pipe ahead of the crack, and by the inertia of the pipe flaps in the wake of the crack. Significant implications for this process arise in the context of plastic wave propagation, whose benefits have yet to be fully exploited.

The above considerations led to a parametric predictive model for running fracture velocity, with the observation that step-like changes are possible in the velocity as the crack propagates within each pipe joint or as from one segment into the next. This approach was selected to facilitate understanding the role of dissipation over the course of fracture propagation, to identify controlling parameters and isolate the significance to propagation resistance.

The AI model initially formulated specifically to simulate arrest as part of one of the cost-share projects[67] satisfied similitude requirements in terms of historically apparent first-order factors by expressing crack-tip velocity as a function of differences in crack-tip position, the line-pipe geometry and pressure leading to wall stress, and CVN plateau toughness (CVP). This model was referenced to the pressure in the pipeline prior to fracture initiation chosen because it was

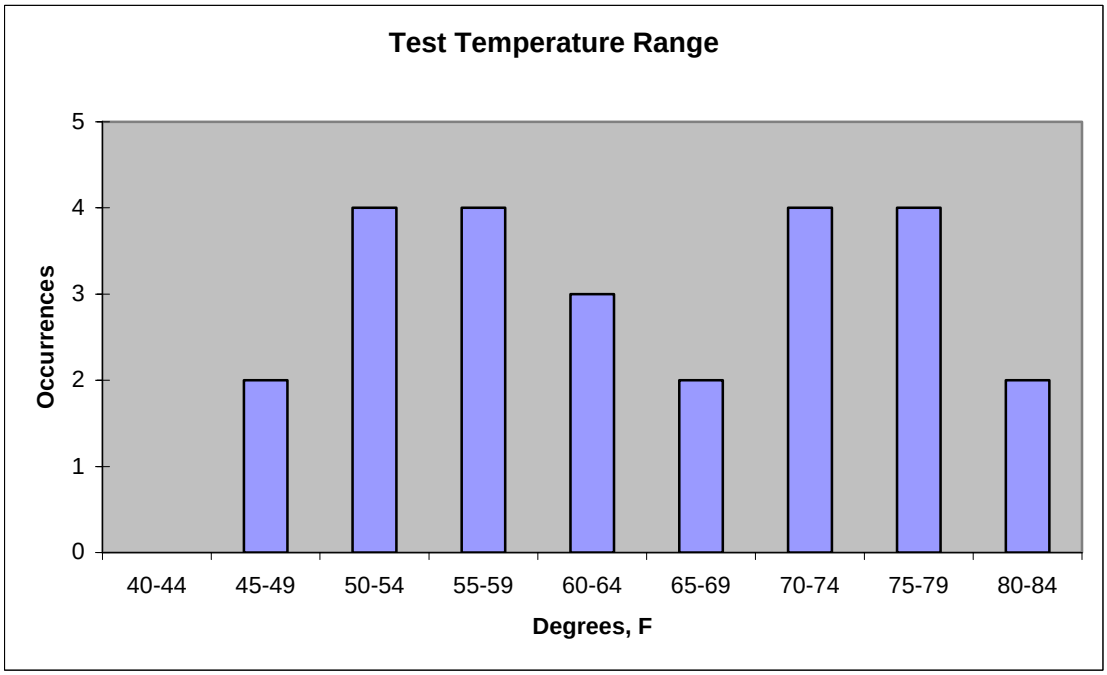

Figure 2. Test temperatures included in the database.

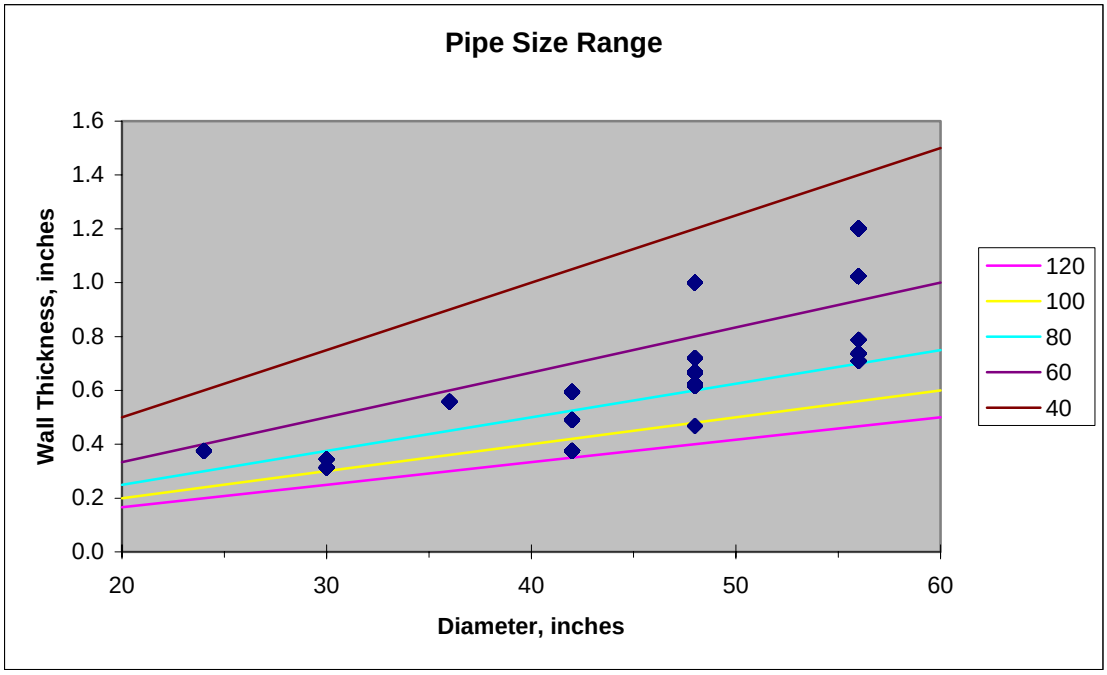

Figure 3. Range of diameter to wall thickness ratios included in the database.

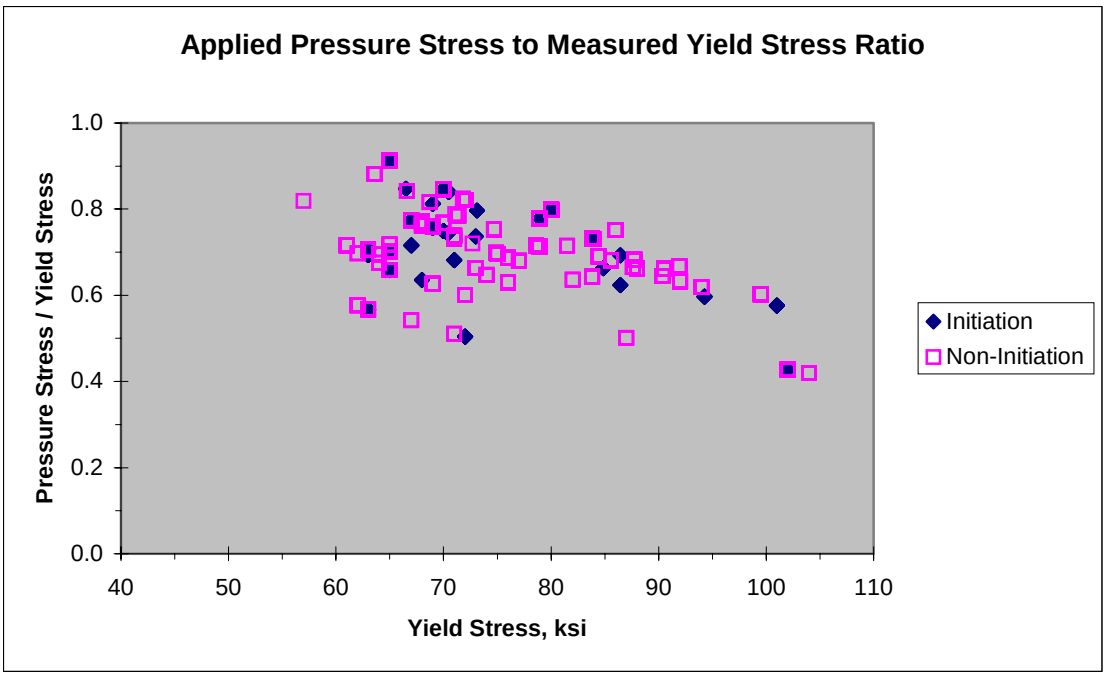

Figure 4. Range of pressure stress to yield stress ratios included in the database.

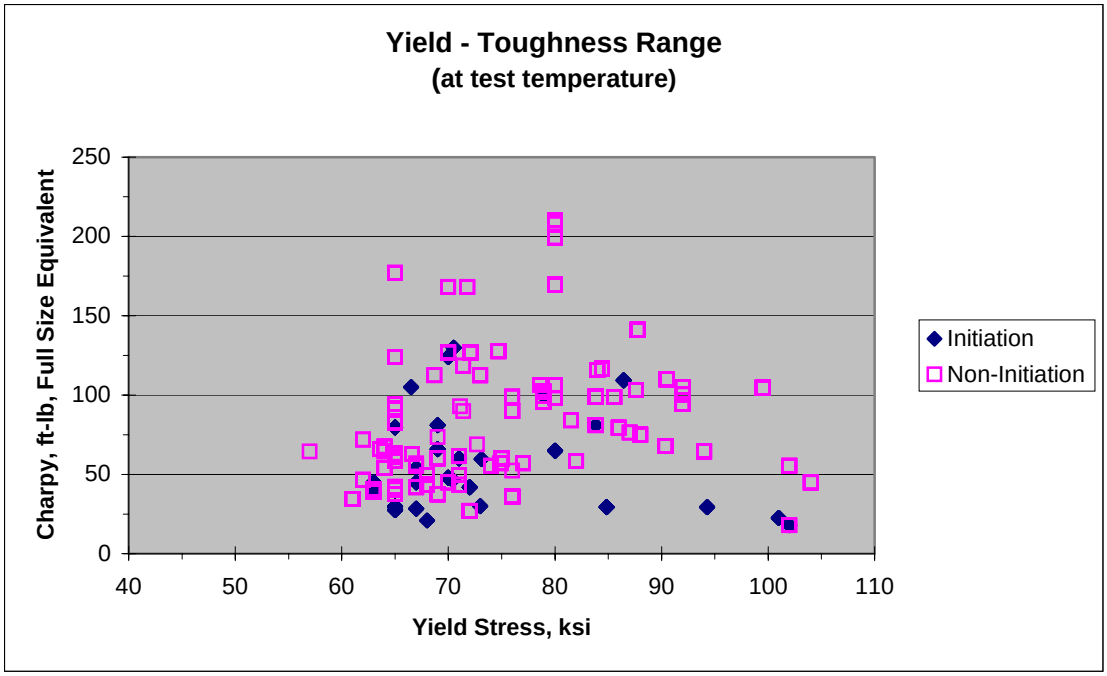

Figure 5. Range of toughness and yield stress values included in the database.

simpler in scope and easier to use, as it portrayed the pipeline's response without reference to the effects of decompression. No attempt was made in this initial formulation to isolate and embed the decay in crack velocity over the length of the individual pipe joints that comprise the test section.

As this work progressed it was recognized that the results of the prior analyses could be much better characterized with using fracture velocity expressed as:

$$V = a_0 \cdot \left(\sigma_{dynamic}\right)^{a_1} \cdot \left(\sigma_{flow}\right)^{a_2} \cdot \left({C_v}/{A} \right)^{a_3} \cdot e^{a_4 x} \qquad (1)$$

wherein:

V = crack velocity,
$\sigma_{dynamic}$ = dynamic stress induced by the instantaneous pressure,
σ_{flow} = flow stress, variously defined,
C_v = CVN impact energy at the test temperature, which is the CVP energy for fully ductile response,
A = cross-section area of the Charpy impact test specimen,
e = base of the natural logarithms,
x = location of the crack tip, and
a_i = regression parameters,

which was implemented in differential form.

In contrast to the format used for the cost-share work, this equation can be implemented to assess the response of individual pipe joints or a string of pipe joints as occurs in a pipeline or a full-scale test. In this context the effects of incremental changes in toughness can be isolated, as can the decay in velocity within each pipe joint in the test section. Such a model formulation provides insight into the factors contributing to arrest. Validation of such a model requires correctly simulating the cracking behavior throughout the full-scale test – rather than simply specifying arrest versus propagate – as occurs for other models such as the BTCM.

Equation 2 also includes consideration of flow stress, whose inclusion followed consideration of the definition of the plastic wave velocity[2] and the power-law stress-plastic-strain response of typical of many steels, including line-pipe steels. These considerations indicate that the flow stress and the Charpy toughness expressed as an energy density should be grouped as (flow stress / CVN energy). Equally, given that the effects of line-pipe geometry often can be minimized when normalized by $(Rt)^{0.5}$, with the location of the crack tip also normalized relative to the size of the pipe. With these considerations and using the notation:

R = pipe outside radius
t = pipe wall thickness.

[2] For discussion of this concept, see Reference 74, with a very recently published view with potential utility to late to address here evident in Reference 75.

Equation 1 becomes:

$$V = a_0 \cdot \left(\sigma_{dynamic}\right)^{a_1} \cdot \left(\frac{\sigma_{flow}^2}{C_v / A}\right)^{a_2} \cdot e^{a_3 x / \sqrt{R\,t}} \qquad (2)$$

which as noted above was implemented in differential form.

The "fracture curve" of Equation 2 was implemented in conjunction with the "gas curve" of the BTCM. Thus, the "two-curve" concept of the BTCM was retained, along with the "backfill constant" (see Reference 5 for more detail, or Reference 9. Using the gas curve and the backfill constant from the BTCM provides access to the local pressure in the vicinity of the crack tip. Thus, the dynamic stress, $\sigma_{dynamic}$, in Equation 2 was determined from the instantaneous pressure of the escaping fluid. While the fracture curve of the BTCM has been replaced in this approach, the gas curve has been retained. This follows from the observation that the "gas decompression curve" of the BTCM has proven viable through full-scale testing, as was apparent even for the high pressure very rich gas anticipated for the Alliance Pipeline[25,26]. It follows that an approach comparable to that introduced schematically in Figure 1 has been employed – although due to the nature of Equation 2 as implemented this two-curve concept must be solved much differently.

While use of the pressure-induced stress in the pipeline prior to fracture initiation in lieu of the dynamic stress simplifies both the model formulation and its application, the dynamic stress provided much more consistent results over a much wider range of parameters. This use of the dynamic stress, $\sigma_{dynamic}$ brings complication as it requires tracking decompression over the course of each full-scale test evaluated. In turn this requires the temperature of the test fluid in addition to pressure and composition, for which results are not always reported – particularly for the earlier tests.

The historically defined value of the flow stress adopted reflects that used in quasi-static empirically calibrated models assessing crack stability[27,28]. While logically this would be defined for such models as the stress in the limit as the crack size approached zero, the empirical fit was made across a broad range of defect sizes. In this context, flow stress has been variously defined, with values taken as 1.1 times the yield stress, as well as the yield stress plus 10 ksi (69 MPa). Subsequently, recent work considering plastic-collapse analyses points to the use of the ultimate tensile stress (UTS), or a value nearly equal to the UTS in lieu of historic flow-stress definitions[e.g., 68,69]. As this has been validated based on burst tests of defect-free pipe, the UTS has since been broadly adopted as the reference stress for plastic-collapse analyses of defect acceptance for both corrosion and cracks in pipelines[e.g., 68-73]. Even so, for reasons noted in the discussion of the backfill factor, the flow stress was taken as yield plus10 ksi (69 MPa).

The crack velocity was logically considered to vary exponentially over the distance traveled by the propagating crack. For the present formulation, the coefficient in the exponential term could accommodate: (*i*) a decrease in the crack velocity as energy is dissipated, (*ii*) a constant velocity if the crack is in a steady-state condition, or (*iii)* an increase in velocity after the crack has entered a pipe segment having a lesser resistance to propagation than the preceding segment.

The model was formulated to consider two definitions of the reference-zero for crack position, x, to determine if it affected the quality of the predictions. The first definition used the center of the initiating notch – in which case the crack's position approximates the distance traveled by

each crack tip away from the initiation. The second definition used the start of each test-pipe referenced to the location of the girth weld nearest the initiation – in which case the crack's position reflects the distance traveled within the test pipe. Regardless of the outcome, the model can be implemented to address a single joint of pipe, or a string of pipe joints.

Conclusion

An analytical model to predict the propagation velocity was derived considering basic fracture concepts and observations made regarding crack propagation behavior in the full-scale tests. Significantly, the early testing tended to produce smoother more continuous trends in crack velocity, whereas more recent testing of tougher and stronger grades tends to produce what appears to be occasionally unstable propagation, with sharp increasing and decreasing changes in velocity evident. A second key observation was that changes in velocity are evident well before physical entry of the crack into the next pipe joint. This suggests that the crack tip travels in the wake of the plastic zone that forms ahead of the crack – such that the flow-induced properties of this next joint control the crack's response. In turn, this implies that the velocity of the crack tip is dictated by the velocity of the propagating plastic wave that formed upon fracture initiation. Continued axial propagation in this context is driven by the pressure in the pipe ahead of the crack, and by the inertia of the pipe flaps in the wake of the crack. It follows that plastic wave propagation could control what has been called propagating fracture – in which case plastic flow and flow-induced dissipation control RDF as much as if not more than dissipation associated with the creation of new crack surface.

The parametric predictive model developed for running fracture velocity can deal with the step-like changes noted in the velocity as the crack propagates within each pipe joint or as from one segment into the next. It likewise will facilitate understanding the role of dissipation over the course of fracture propagation, to identify controlling parameters and isolate the significance to propagation resistance. Finally, significant implications develop for RDF in the context of plastic wave propagation, the benefits of which have yet to be fully exploited.

Training, Evaluation, and Validation of the Crack Velocity Model

Training the Crack Velocity Model

The coefficients in the fracture velocity model in Equation 2 were defined via regression analysis using a portion of the full-scale database to train the model. This training database included tests that fit the following criteria:

Pressurizing media: lean natural gas,
Backfill: soil (typically 1-meter depth),
Starting location for the crack: leading edge of test-pipe segment (a girth weld),
Minimum crack extension: unconstrained, with a minimum of zero.

Using these criteria leads to a model that reflects realistic operating conditions in regard to the first two provisions, with the benefit that the response in each test-pipe segment could be evaluated to identify changes in crack velocity due only to the formation of new crack surface via the remaining provisions. This approach facilitates use of Equation 2 to develop insight into the significance of dissipation via propagation and the existence of "steady-state" propagation in comparison to the absolute effect of toughness on crack arrest. Further, it facilitates isolating the

effects of fluid properties and other line-pipe properties by comparison of results developed against this simple pipeline scenario.

Of the two definitions considered for the reference-zero for crack position, *x*, evaluated the second definition referenced to the start of each test-pipe, or equally the first girth weld encountered for each test pipe was adopted. Regardless of which definition was taken, the model still can be implemented to address a single joint of pipe, or a string of pipe joints.

Several different values of the minimum amount of crack extension were evaluated realizing that non-steady-state conditions exist as the crack passes from one test pipe to the next; crossing a girth weld as it does. While some minimum amount of crack extension was anticipated as this would minimizes the transient aspects following fracture initiation or the transition into another test pipe, the regression analysis indicated the best fit developed when the minimum propagation length was set at zero.

The final coefficients determined by training in this manner were:

$$a_0 = -6.863406051$$
$$a_1 = 1.859335743$$
$$a_2 = 0.572825469$$
$$a_3 = -0.000815089 \qquad (3)$$

with very similar interim sets evolving over the course of the project. With these coefficients it becomes possible to simulate the fracture velocity and decay in fracture velocity for each segment of pipe in a full-scale test, which once validated can be used to recreate fracture-control scenarios in pipelines.

Trending and Preliminary Evaluation of Equation 2

Evaluation of the model began with comparison of fracture velocity predictions made using the trained AI model for the database of full-scale running fracture tests as it was compiled initially. This was done via trend comparisons of fracture velocity as a function of position during fracture propagation which for this preliminary screening sought bias in the results as a function of wall stress, toughness, and parameters that characterize the geometry of the line pipe and the properties of the transported gas or fluid. This preliminary screening targeted scenarios that reflect full-scale testing through the mid 1990s, sprinkled with several results for higher strength and higher toughness line-pipe. This database was selectively expanded as time passed and requests for specific data were honored. This process tended to focus on scenarios identified as problematic for the BTCM, to ensure “hard-to-predict” results were included.

Figures 6 through 11 contrast measured crack velocity as a function of propagation distance for the screening database, with a view to identify possible bias in the quality of predicted crack velocity for each of the parameters included in Equation 2. These specific figures use the crack origin the full length of the test section in the full-scale fracture-propagation experiment as their reference location. These results are then presented for each specific pipe in the test section, with the reference zero for plotting being the start of each pipe joint to better evaluation trends specific to the variables examined by the joint in the full-scale testing. These figures include results for lean natural gas, air, as well as rich natural gas, covering the full range of grades to X100, toughness to in excess of 250 ft-lb (full-size equivalent), diameters from 24 to 56 inches,

temperatures from ~45ºF to ~90ºF, and pressures associated with up to 90-percent of SMYS. On this basis, the results cover a very broad range of acoustic velocity, and its influence on decompression.

As the purpose of this preliminary evaluation was to screen for obvious deficiencies in Equation 2, no attempt was made to isolate results for specific pipe joints – although this was done on occasion. Given this purpose, multiple predictions were grouped and screened for relative differences in predicted trends within each grouping, and across the groups. As many results can be found on some figures, direct comparison of predicted and actual results can be difficult. In spite of this, consideration of these images on a large screen showed that many predictions closely match the observed response. It was also apparent that the trends within data groups and across them were similar. While circumstances that drive acceleration in the full-scale test cannot be isolated, it is clear that instabilities in cracking are evident as acceleration and deceleration, with the predictions being similar to the observed trends. As expected, more detailed evaluation shows the predictions and the data trends indicate the crack velocity decreases quite gradually as the crack travels through a pipe joint, except where the interface between pipe joints is crossed or the arrest toughness is encountered. Arrest appears to occur quickly, as can be discerned with study on a larger screen, often occurring within a few pipe diameters. Similar study showed the expected decrease in crack velocity is predicted as the crack propagates into successively more resistant pipe joints. As introduced earlier, more resistant in this context reflects inherently "tougher" steel or other factors considered to influence arrest, such as heavier wall thickness or higher strength level. Further opportunities to evaluate such trends in detail follow later throughout the report, with the validation process considering each data-pair on these figures – plus those added over the course of the project.

Finally in regard to overall trends Figures 6 to 11 indicate the trends predicted by the model tend to be shifted toward larger values along the x-axis, which in these figures reflects the location of the crack tip within a pipe joint. Some groups of predictions show this tendency more than others. Nevertheless, as trained, this screening shows model slightly over-predicts the propagation distance. This is a conservative trend as the model indicates that the cracks will grow further than in reality, leading potentially to larger arrest toughness as compared to reality. For practical applications where the increment in properties reflects the length of one pipe joint (40 feet or ~11 meters), this error is small.

Figures 6 and 7 evaluate Equation 2 coupled with the gas curve of the BTCM in terms of AYS and flow stress, respectively. Figure 6 illustrates the influence of the initial pressure-induced stress as a percentage of AYS. To facilitate this evaluation by reducing the number of trends presented in each figure the results have been grouped into four groups of AYS, covering ranges from 40 to 55, 55 to 70, 70 to 85, and 85 to 100 ksi. Unfortunately, as much of the database lies within the middle two categories, many results are included on these plots. In spite of this, the trends summarized above are evident, with the effectiveness of the model not showing strong bias over the range of AYS considered. Of these trends, perhaps the easiest viewed prediction comes for one pipe joint presented in the last group – with similar success apparent for many other cases as well. Figure 7 illustrates the influence of the flow stress, which by the definition of flow stress embeds the trends in Figure 6 (because the flow stress is defined relative to the yield stress, which for this comparison specifically considers yield plus 10 ksi). On this basis it is not surprising that the results in Figure 7 are comparable to Figure 6. Again, to facilitate this evaluation by reducing the number of trends presented in any one plot the results have been

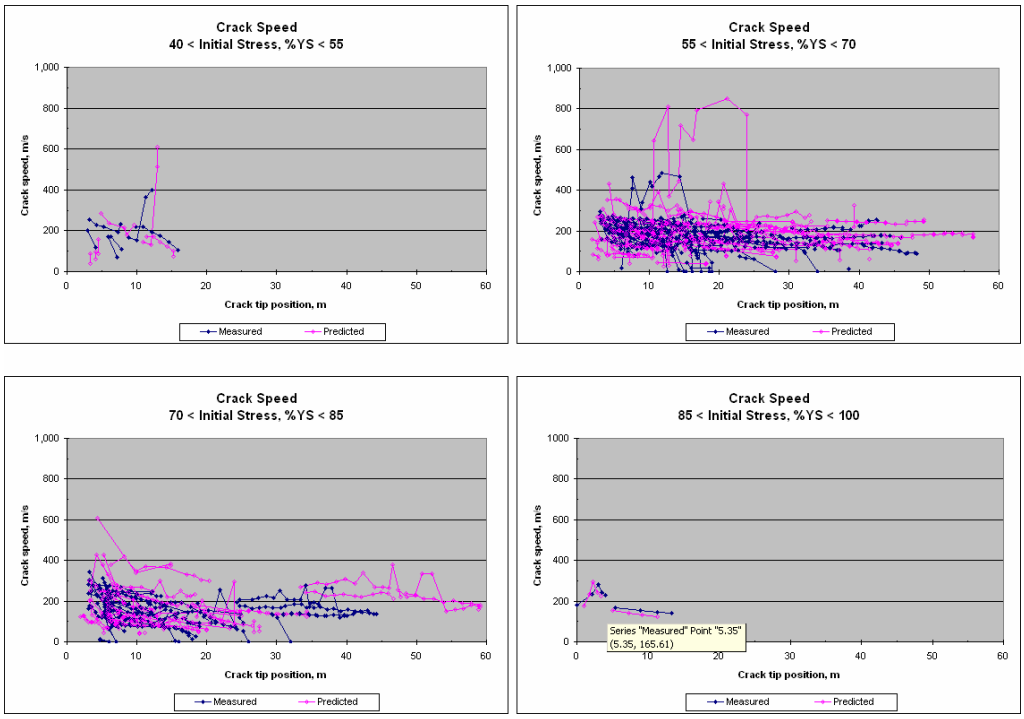

Figure 6. Measured and predicted fracture velocity versus position for various initial stress levels.

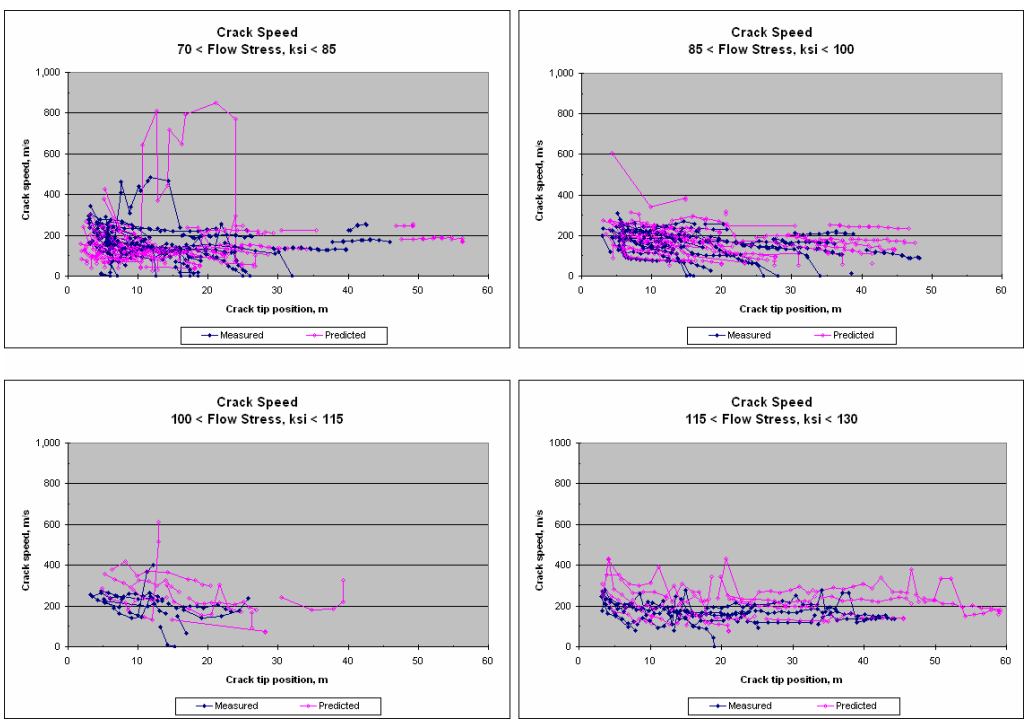

Figure 7. Measured and predicted fracture velocity versus position for various flow stress levels.

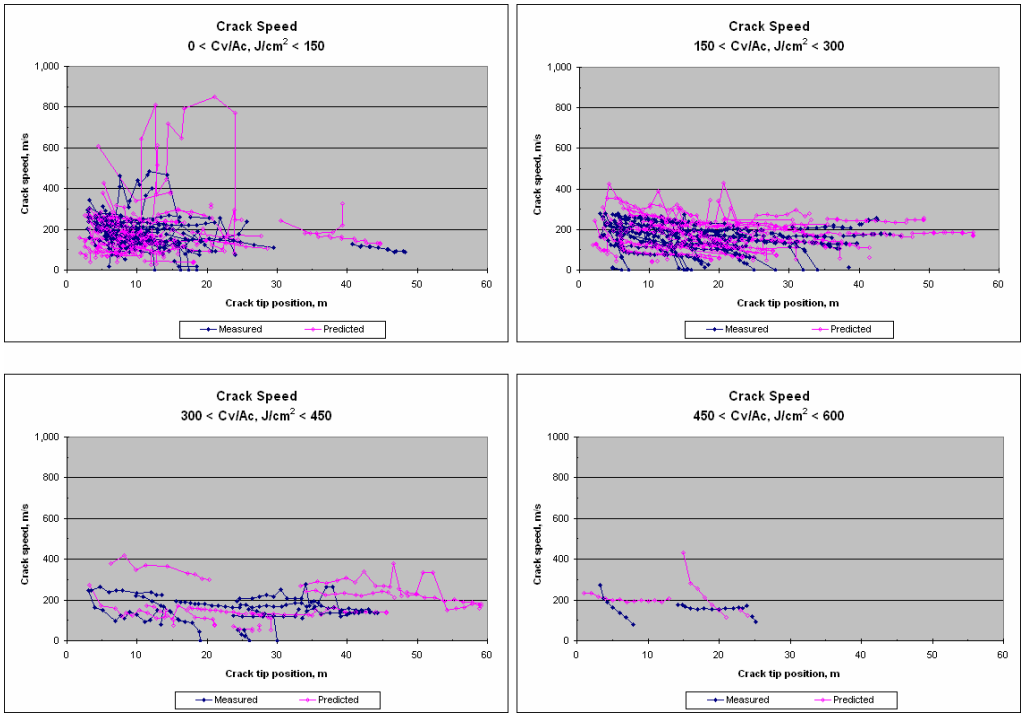

Figure 8. Measured and predicted fracture velocity versus position for various Charpy toughness levels.

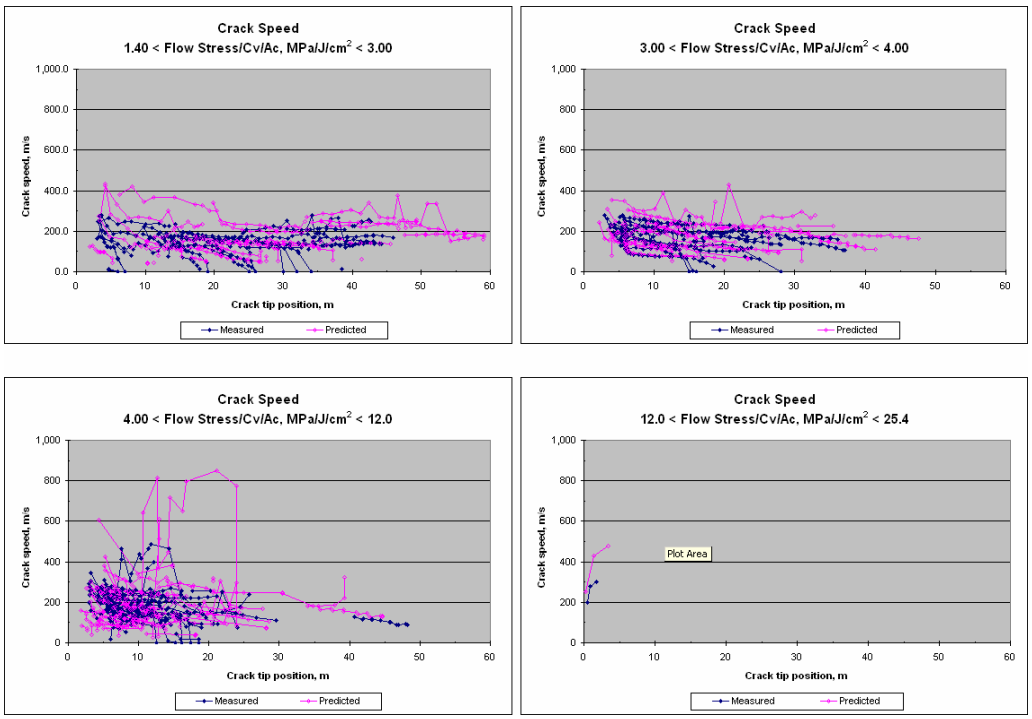

Figure 9. Measured and predicted fracture velocity versus position for various normalized strength levels.

grouped into four flow-stress groups, from 70 to 85, 85 to 100, 100 to 115, and 115 to 130 ksi. As for AYS, the quality of the predictions does not show a bias with flow stress, which indicates the viability of the model in regard to this parameter.

Figures 8 and 9 evaluate the model in terms of toughness-related parameters, with Figure 8 evaluating the influence on CVN as an energy density, and Figure 9 evaluating the parameter grouping flow stress divided by CVN/A as it occurs in Equation 2. Figure 8 illustrates the influence of CVN grouped in four ranges from 0 to 150, 150 to 300, 300 to 450, and 450 to 600 J/cm^2. The trends summarized above are again evident, with the effectiveness of the model being independent of toughness expressed by CVN energy, with the results being similar across the full dataset. Figure 9 illustrates the influence of the flow stress coupled with CVN/a, which by the definition of flow stress must embed the trends in Figure 6. On this basis it is not surprising that the results in Figure 7 are comparable to Figure 6. As above, the quality of the predictions does not show a bias with toughness or toughness grouped with flow stress as in Equation 2, which indicates the viability of the model in regard to these parameters.

Figures 10 and 11 evaluate the viability of Equation 2 in terms of the line pipe properties and the pressurizing media, respectively. Figure 10 considers results for predicted crack location normalized by the square root of the product of the outside radius and the wall thickness. This parameter combination is embedded in the term that characterizes the decay of crack velocity under conditions influenced only by dissipation due to creating new crack surface. To facilitate this evaluation by reducing the number of trends presented within a given plot the results have been grouped into four groups of pipe geometry represented as $(Rt)^{0.5}$, including values from 2 to 2.99, 3 to 3.99, 4 to 4.99, and 5 to 5.99 inches. Again much of the database lies within the middle two categories such that many results are covered by these two plots. In spite of this, the trends noted above are evident, with the quality of the predictions free of bias relative to the line-pipe geometry, which indicates the viability of the model in regard to the range of line pipe diameter and wall thickness of interest. Figure 11 illustrates the influence of the pressurizing media. As expected, the agreement between the model and experimental is best when it is applied to the test data for natural gas as these data were used to calibrate the model. The quality of the predictions is slightly reduced for testing with air, which may occur because some air tests having been conducted above ground or with backfill conditions other than those represented by the values of backfill constant available for the BTCM. As such, there is an apparent effect of the backfill on the quality of the predictions that might be traced to its absence from the training database. Alternatively, because the backfill constant as developed in the BTCM embeds more than the effect of backfill, it is plausible this accounts for this behavior. The earlier observation that the early rich gas tests were done possibly without adequate feedback on mixing to avoid stratification or richer-phase plugs also could be a factor, as in one case such a test is consistently miss-predicted.

Conclusion

The new AI-based model structure developed in the prior section as an alternative to the "fracture curve" used in the BTCM was trained using a portion of a database compiled for present purposes to characterize fracture propagation as observed in full-scale testing. Screening the utility of this model trained in regard to a portion of this database indicates it can simulate the fracture propagation response in full-scale testing without bias in regard to line pipe properties, with slightly less success evident in regard to properties of the test media and the backfill conditions. Suffice it to note that most predictions closely match the observed response, where

Figure 10. Measured and predicted fracture velocity versus position for various normalized pipe

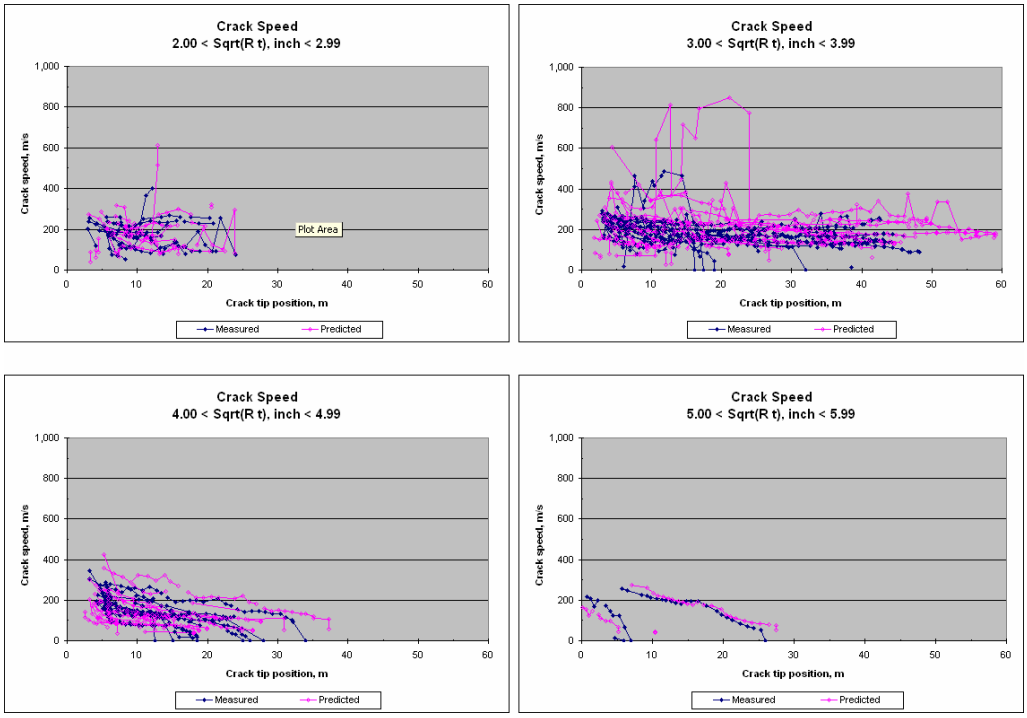

geometry levels.

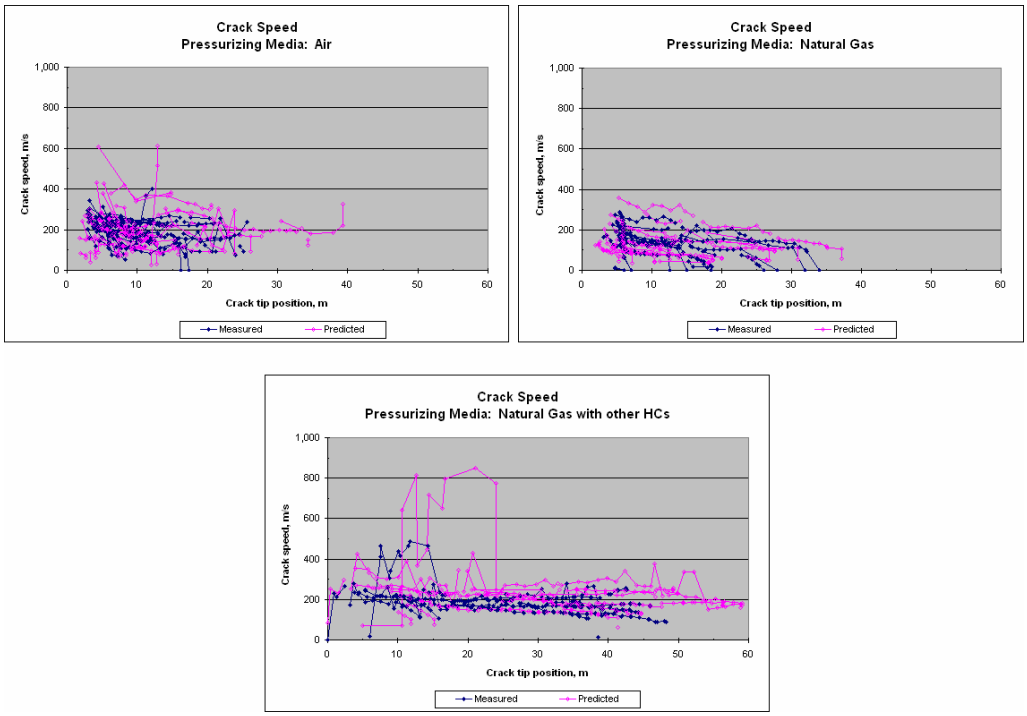

Figure 11. Measured and predicted fracture velocity versus position for various pressurizing media.

others match somewhat less closely. Unique events in the full-scale tests such as the acceleration of the cracking are evident in the predictions, as were cases where sharp deceleration occurred. Because the predictions were slightly conservative as compared to the full-scale test results the constants embedded for this preliminary screening need some refinement. However, because there is no clear bias in the quality of the predictions the form of the model as shown in Equation 2 is viable as a basis to move forward.

Fracture Velocity as a Function of Stress, Toughness, and Gas Properties

This section continues consideration of Equation 2 through analysis comparing full-scale results characterizing fracture velocity to assess the effect of uncertainty in line-pipe properties on the predicted outcome in terms of fracture propagation and arrest. Recognizing the greatest uncertainty in full-scale testing involves the mechanical and fracture resistance properties within each test pipe, the focus here is on the effects of variability in flow stress and toughness. The illustrations in this evaluation consider the same model coefficients used in the prior section.

This section assesses the range of predicted propagation velocity as a function of the plausible variations in the Charpy energy or flow stress within the test pipe using the two-curve concept introduced earlier in Figure 1. Determining whether or not a fracture propagates or arrests in this context involving two curves – one representing the fracture velocity as defined in Equation 2 and the second representing the velocity of the decompression wave front that is used as defined for the BTCM. As the distance propagated is equal to the integral of velocity over time since

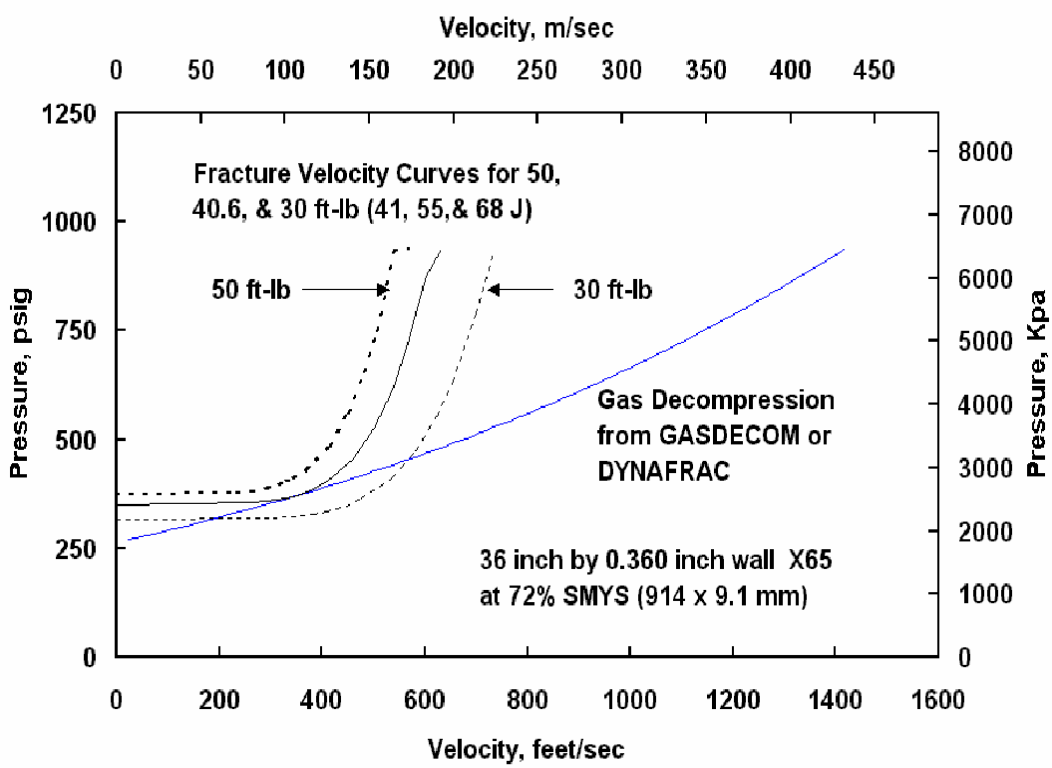

Figure 12. Two-curve scenarios for propagating and stable states, and the arrest condition

fracture initiation, the trends in Figure 1 are inherently associated with the location of the crack tip relative to the origin of the fracture, which as noted can be referenced to that location or the start of each pipe joint.

As presented in Figure 1, the point of tangency between the two curves defines the instant that arrest becomes possible for the running crack, as it reflects equality between the velocity of the decompression wave front and the fracture for local pressure conditions. Figure 12 illustrates this arrest condition along with two other possibilities – with one beyond the arrest condition,

and the second not yet satisfying the arrest condition. When the Charpy energy is in excess of that required for arrest, the "fracture curve" in the language of Figure 1 is entirely to the left of or above the "gas curve". For this scenario, a crack cannot propagate a significant distance because at any pressure level, the decompression wave front will outrun the crack tip; thereby reducing the hoop stress which provides the driving force for propagating the crack. In contrast, when the Charpy energy is below that required for arrest, the "crack curve" is to the right of or below the "gas curve" at any given pressure. For this scenario the crack tip will outrun the decompression wave front and the hoop stress will remain large enough to propagate the crack indefinitely. In summary, the graphical interpretation of the two-curve concept indicates continued propagation when the crack curve is to the left of or below the gas curve. For the crack curve with inadequate Charpy energy for arrest shown in Figure 12, the propagation region is bounded by the two points where each crack curve intersects the gas curve. This suggests that there are two viable solution conditions possible when the model is applied to a pipe have too little crack growth resistance to arrest the crack.

Sensitivity Analysis – Setup

The just noted possible solution states for the two-curve concept are used next as the basis to assess the sensitivity of the propagating fracture and the crack velocity to typical variability in line-pipe properties. Each sensitivity analysis considers a plus/minus percentage variation on flow stress or toughness that approximates plus/minus one-standard deviation for that parameter. For variability in flow stress, one-standard deviation is approximated by a four-percent swing in its value, although the actual variability can depend on the vintage, chemistry, processing of the line-pipe steel, and other factors[e.g., 76]. For variability in CVN energy one-standard deviation is approximated by ten-percent[77] swing in its value, although again the actual variability can depend on the vintage, chemistry, processing of the line-pipe steel, and other factors.

The simulated effects of variability will be used in the next section to identify the margin of safety needed in practical use of the crack velocity model as the basis to design fracture arrestors, or develop fracture control plans. These results will be equally useful later in comparing fracture arrest predictions to the actual arrest toughness, as they define the otherwise hidden effect of statistical variability embedded in the full-scale test results.

Figure 13 presents the graphical solution for the two-curve concept for typical pipe joints that are otherwise identical except for inherent toughness. Whether or not cracking propagates through these joints under the identical full-scale test conditions shown in the figures depends on the inherent toughness of the line-pipe steel. Each part of this figure shows three curves. The central curve corresponds to the measured Charpy energy for the test pipe, while the curves above and below correspond to a plus and minus one-standard deviation variation on measured Charpy energy. A parallel set of similar curves has been developed for the same level of variability in flow stress, although these are not repeated here.

The symbols in the figures correspond to the intersection points of the "crack curve" and the "gas curve" of the two-curve concept. The legend of the figure identifies the upper and lower intersection points of the crack and gas curves. The + and – symbols reflect the effects of the plus and minus one-standard deviation variation for the varied parameter. The absence of a + or – indicates no variation, which reflects for present purposes the mean of the population. The open symbols indicate where the crack curves intersect the gas curve.

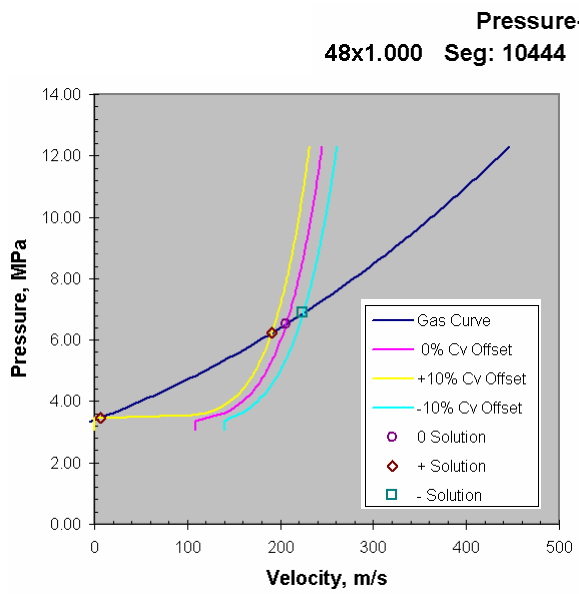

a). Segment 1.

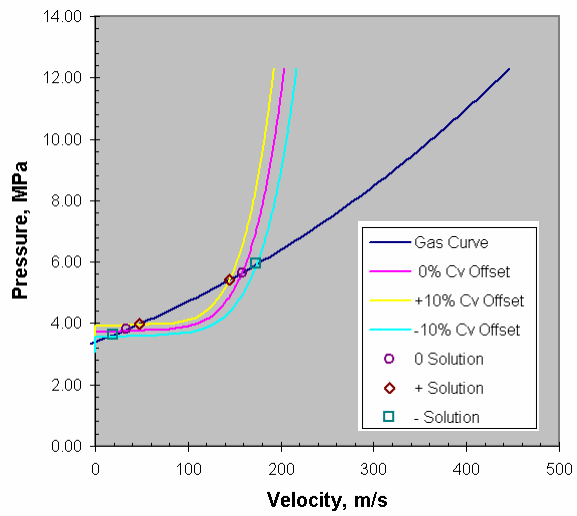

b). Segment 2.

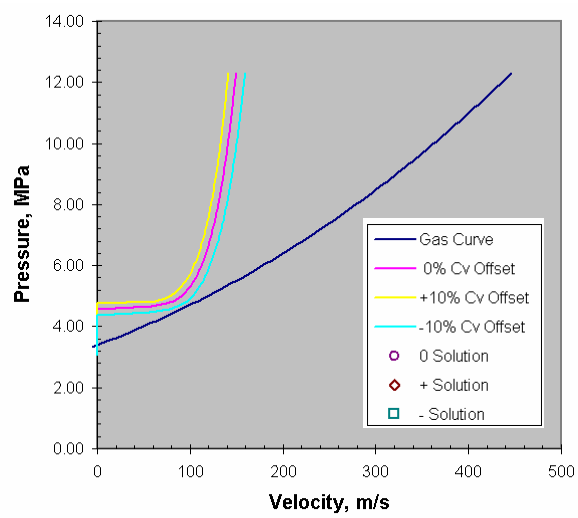

c). Segment 3.

Figure 13. two-curve concept curves for a sample full-scale test

The intersection points in Figure 13 are included on the velocity versus distance plot for this test as lines that bound the regions of crack propagation and stable response as shown in Figures 14 and 15, which respectively assess variability in CVN and flow stress. The legend of the figure identifies the experimental data versus that for the model prediction. It also identifies the trends labeled "UL" and "LL" that correspond to the intersection points in Figure 13. The horizontal lines and the connecting segments bound the propagate/stable regions on the assumption that the properties of the pipe and soil remain constant along each pipe segment that comprised the full-scale test section. Typically, the properties of the pipe segments in a running fracture test are designed to allow the crack to propagate into the first or second joint, with increasing resistance to propagation until a joint capable of arrest is encountered. This is evident in the convergence of the UL and LL curves along the length of the test section. Note that the plotted points for the UL and LL values correspond to the positions where the velocity was measured, which typically occurred at one-meter spacing. On this basis; the physical transition between pipe segments is represented for typical full-scale testing by the spacing between the trip-wires. It follows that the quite short distance between two pipe joints, which involves the distance across the heat-affected zones either side of each girth weld, is represented in full-scale testing by the distance between the trip-wires that typically are one meter apart in either side of this girth weld. Thus, where a step change might be inferred in crack velocity in stepping across a girth weld, this transition is instead evident across the quite large distance between the adjacent trip-wires.

Typically the crack velocity is observed and predicted to accelerate sharply over a short distance beyond the initiation point (i.e., the "zero" reference in plots like Figures 6 – 11, and 14 and 15). At this time the velocity is well above the steady state bounds derived in reference to the present two-curve formulation, the BTCM, or other such formulations. As outflow through the rupture develops and decompression ensues, the crack begins to slow and respond within the velocity propagation boundaries estimated by the two-curve concept adapted from the BTCM. Arrest is predicted when the crack slows sufficiently for the decompression wave front to pass by the propagating crack tip. Differences in crack velocity are evident along the length of each test pipe segment, with both acceleration and deceleration apparent. When the initial velocity is underestimated, the prediction logically lags the experiment, whereas when overestimated the prediction runs the fracture ahead of that observed. However, regardless of leading or lagging the actual result, the model faithfully tracks local velocity variations. It follows that success in these predictions is more determined by the initial estimate of velocity than it is by Equation 2.

In some cases details concerning the soil backfill or the temperature of the pressurizing fluid were sparse, which was the case for the experiment considered in this example. The backfill has a first-order influence on fracture velocity and its decay, whereas temperature has a strong effect on the acoustic velocity and resulting decompression behavior. Given this influence it is surprising these parameters are unreported for many tests. Equally surprising is the observation that both temperature and acoustic velocity tend to be excluded in most of the simplified models for arrest toughness introduced earlier in this report.

Finally, for Figures 14 and 15 the cracking runs through one test pipe before it slows as it runs through a second test pipe, and then arrests quickly within the third test pipe, which is apparent from the trends in the predicted bounds shown in these figures.

Conclusion

Equation 2 was used in conjunction with the gas curve of the BTCM to assess the sensitivity of the propagation velocity to practical variability in flow stress and toughness. Variability the order of one-standard deviation was considered for both flow stress and toughness. The trends indicated that uncertainty in flow stress had relatively less practical importance than did toughness. The practical implications of this variability are considered in the next section.

Analysis to Assess the Effect of Uncertainty in Toughness and Flow Response

This section assesses the trends predicted by the two-curve concept as a function of flow stress and toughness for otherwise identical scenarios in terms of the line-pipe geometry and the properties of the transported gas or fluid.

Sensitivity Analysis – Toughness

Predicted differences in crack velocity as a function of variability in CVN toughness are evident in Figure 14 through trends depicting results for the mean (actual) toughness and plus/minus 10-percent on it over the length of the test section. Toughness swings over this plus/minus one-standard deviation swing correspond to significant differences in fracture velocity. Depending on the incremental toughness used in the test design between adjacent pipe joints, this variability could lead to continued propagation through a joint anticipated to arrest the fracture.

The results developed suggest that a scatter-band be applied the order of plus/minus 10-percent when comparing predicted to actual arrest toughness and that a margin of safety the same order be applied to the minimum toughness for arrest for both fracture control plans and integral fracture arrestors whose design relies on inherent toughness.

Sensitivity Analysis – Flow Stress

Figure 15 presents results analogous to Figure 14 considering variability associated with the mechanical properties that comprise the flow stress, which includes the yield stress and the UTS, as simulated using the two-curve concept outlined earlier. As evident in the figure, varying the properties of the steel to the same normalized extent as for the CVN energy has somewhat less influence on the whether an arrest or propagation is predicted for a particular pipeline. For the variability within a typical joint of line pipe, this level of uncertainty could lead to continued propagation through a joint anticipated to arrest fracture, although this is much less likely than for the typical variability associated with CVN energy. Such results suggest a scatter-band be applied the order of plus/minus 4-percent in analyses comparisons of predicted to actual arrest toughness and that a margin of safety the same order be considered in analyses to determine the minimum toughness for arrest for both fracture control plans and integral fracture arrestors whose design relies on inherent toughness.

Conclusion

Trends predicted by Equation 2 in conjunction with the gas curve of the BTCM were used to assess the sensitivity of the propagation velocity to practical variability in flow stress and toughness. Variability the order of one-standard deviation on CVN energy was shown to cause a significant change in crack propagation velocity, indicating such variability could lead to continued propagation through a pipe joint whose toughness was considered adequate for arrest.

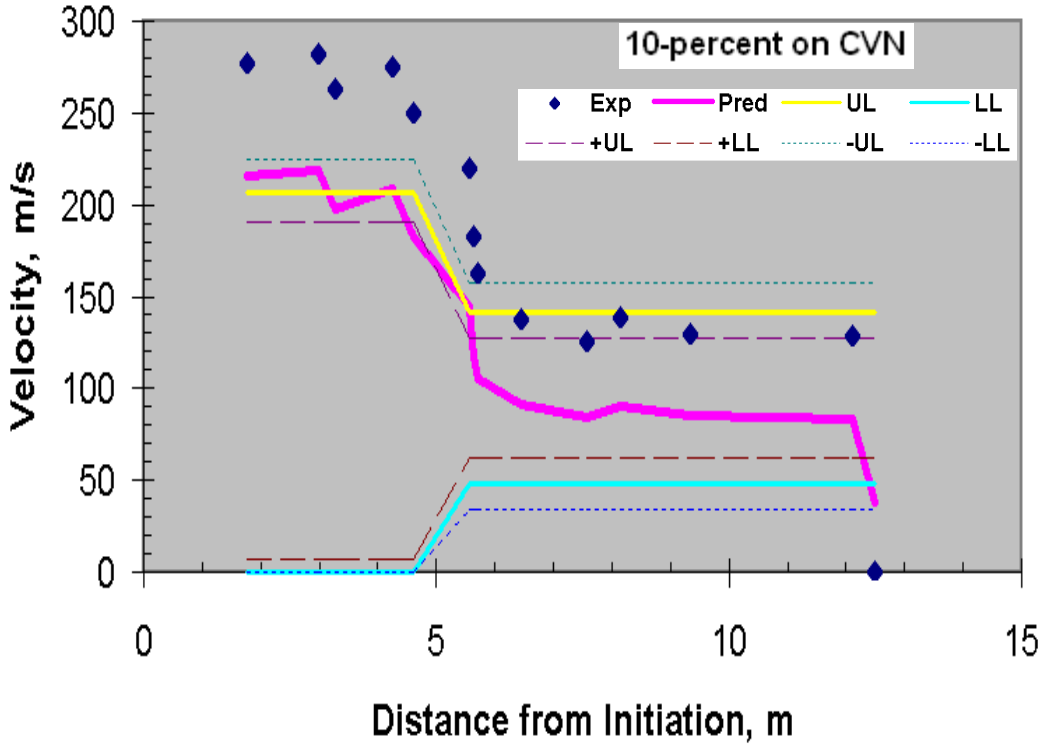

Figure 14. Experimental data and simulated effect of a +10/0/-10 percent on toughness

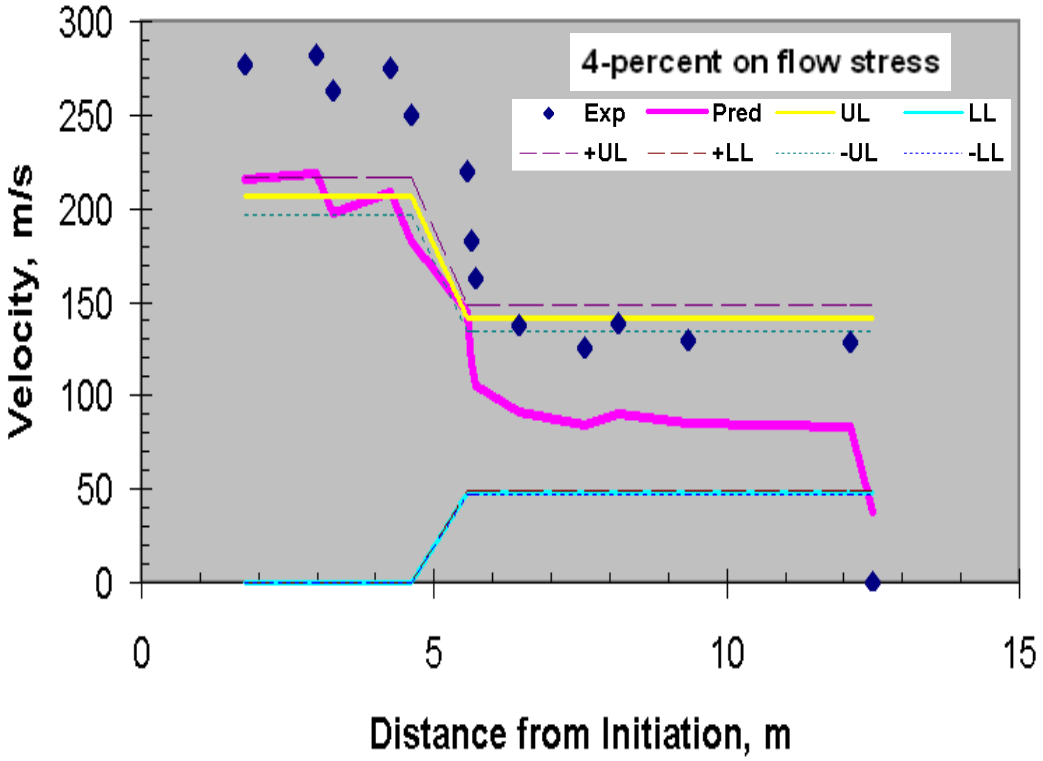

Figure 15. Experimental data and simulated effect of a +4/0/-4 percent on flow stress

On this basis it was suggested that a scatter-band be applied the order of plus/minus 10-percent when comparing predicted to actual arrest toughness. Likewise it was suggested that a margin of safety the same order be applied to the minimum toughness when predicting crack-arrest toughness. Similar variability was evaluated in regard to the effects of flow-stress. When the two-curve concept is used to calculate arrest toughness or for other such applications it is suggested that the effects of a four-percent variation in flow stress be considered.

Develop and Validate the Fracture Arrestor Design Basis

Development and validation of a design basis for fracture arrestors rests on the observation that fracture velocity as characterized by Equation 2 shows an abrupt decrease in velocity when the propagating crack encounters sufficient toughness for arrest. The trends in Figures 6 through 11 indicate arrest occurs well within a few diameters under such circumstances, which in most instances is predominantly due to ring-off and tearing shear rather than fracture arrest. This is clearly evident in Figures 14 and 15, where both the predicted and observed trends show the transition from quite high velocities to full arrest is complete within a meter. On this basis, Equation 2 can be used to determine the toughness necessary for arrest, and equally used to determine the distance traversed in arrest, which defines the length of the arrestor subject to the properties of the fluid and the line pipe considered in use of this equation.

The development process references the prior calibration of Equation 2, but would also provide for its unique calibration subject to circumstances other than those captured in this calibration. As use of the differential form of Equation 2 will be complex for some, it has been cast it into an algorithm as a function of stress, toughness, and the parameters that characterize the geometry of the line pipe and the properties of the transported gas or fluid. Thereafter this algorithm has been packaged in Windows-based software for use in designing integral arrestors in applications to new pipeline designs. This formulation is sufficiently general to be recast to address other forms of external arrestors should the desire for this application develop in regard to retrofitting exiting pipelines. As the technology embedded in Equation 2 was shown to be unbiased in regard to fluid and pipeline properties, and conservative in its calibration, there is no need to further consider validation. However, in light of the effects of variability in properties evident in Figures 14 and 15, discussion of a margin of safety concludes the consideration of arrestor design issues.

Develop and Calibrate Arrestor Design Model

The crack velocity model was formulated as above, and the database and model structured such that any data subset could be used for calibration, such that the model can be re-calibrated to match unique circumstances in the event some unusual design scenario is encountered.

As evident from Equation 2, the model considers the toughness and grade of the arrestor line-pipe specifically in terms of its flow stress, as well as its diameter and wall thickness, and the properties of the transported fluid. Pressure is represented in terms of the instantaneous stress, which is determined from the initial static pressure-induced stress as the algorithm integrates as a function of position along the arrestor's length – which is done transparently via the arrestor-design software.

Arrestor Design Software

Equation 2 as implemented in its differential form is integrated numerically to estimate the propagation and arrest distance for a running fracture, which is done via the above-noted software, which has been compiled in executable format and so should be for useable on most any operating system. This software is currently executed from within a macro from in Excel.

The analysis simulates two segments, with the first being the pipeline and the second the crack arrestor. The software determines whether a propagating crack would be arrested before it reaches the end of the arrestor, in which case the user must alter the arrestor's properties to ensure arrest. The software is structured to offer a built-in sensitivity analysis matrix so that multiple values of the input parameters can be evaluated each time the software is executed, thereby making it possible for the user to iterate to a suitable design more efficiently.

To execute the macro, the user enters the parameters of the simulation, namely:

Name and composition of the gas (the gas composition is stored in a separate Excel spreadsheet that can be used as library to retain compositions from previous analyses)
Gas pressure
Metal temperature, equal to the gas temperature
Pipe diameter
Backfill constant and exponent
Properties for the crack initiation and candidate arrest segments:
Length
Wall thickness
Charpy impact energy (FSE result)
Yield strength

As shown in Figure 16a, the above parameters are entered into Excel using the worksheet labeled "Design Info". The columns to the right of the input field definitions are used to list the parameters for the sensitivity studies. Parameters common to both the pipeline and arrestor are entered at the top of the sheet – with the parameters specific to each segment entered below these entries.

The software tracks and reports its progress to the user on this sheet as well. The remainder of the input sheet can be used for notes or supporting analyses and calculations. Figure 16a also shows tabs for the other worksheets used by the macro; these will be described shortly.

Figure 16b presents the results summary worksheet, from the tab labeled "Results". This sheet can be used to plot the results of the sensitivity study using the charting features embedded in Excel. The results of each of the individual analyses that comprise the sensitivity study can be saved or deleted as directed by the user. When saved, each is given a unique filename constructed from the input parameters. The following is an example output file name, which has a comma delimited format:

Gas#2,Pi=1350,T=55,D=48d0,BF=0d470,Li=40,ti=0d625,CVi=60,YSi=65,La=40,ta=0d625,CVa=100,YSa=80.xls

In this file name, the "gas name" is the first parameter, followed by the "pressure", "metal (gas) temperature", "diameter" (all decimals are replaced by "d"), and the "backfill constant". These

parameters are followed by the "arrestor length", "wall thickness", "FSE CVP energy", and "yield stress" of the pipe (suffix i) and integral arrestor (suffix a), respectively. US customary units are used in the filenames. Two Excel sheet name tabs containing the word "plot" are evident in Figure 16a. These two sheets contain: 1) raw data and a pressure-velocity plot from the Battelle two-curve method and 2) raw data and velocity-distance plots for the pipeline and arrestor. These sheets and other data are copied to the output sheet and saved if requested by the user. The last tab, labeled "Run Parameters" contains a template for a PowerPoint file that can be used to view plots from multiple output files more conveniently than currently available with Excel alone. Note that this feature requires the user to have PowerPoint and also requires specific macro reference libraries to be installed with Excel. Additional illustrations of the model are presented in the following examples.

Arrestor-Design Examples

Two example arrestor designs are considered in the context of the gas curve and the fracture curve that underlie the two-curve concept are presented in Figures 17 and 18, respectively. This two-curve concept is retained in using Equation 2, the difference being that Equation 2 represents fracture velocity in lieu of the fracture curve of the BTCM as developed in the 1970s.

Each of Figures 17 and 18 shows the pressure-velocity curves developed for the pipeline and the arrestor. The example pipeline has a diameter of 48-inches and a wall thickness of 0.625-inch, and operates 1250 psi transporting gas at 55ºF, with typical backfill conditions represented by a backfill constant of 0.47. The gas curves shown in Figures 17 and 18 reflect this pipeline transporting, respectively, either lean natural gas (taken as pure methane) or a mixed "rich" gas (taken as 95 percent methane and 5 percent propane). The addition of the propane produces a plateau in the gas curve and shifts it to the left. As a result, higher toughness will be required to arrest a running crack driven by the propane-containing gas as compared to a crack driven by methane, as becomes evident shortly.

Both example pipelines have a yield stress of 65 ksi and are made of line pipe that is fully ductile with a FSE equivalent Charpy energy of 35 ft-lb at the service temperature. For each example pipeline the arrestor will be made of Grade X70 line pipe (yield stress = 70 ksi). For the first of these examples the arrestor has a specified minimum FSE Charpy plateau energy for the service temperature of 62 ft-lb, while for Figure 18 the corresponding energy was 90 ft-lb. This increase in the specified Charpy energy from 62 to 90 ft-lb for the second arrestor anticipates the likely effect of propane on the arrest toughness.

It follows from the above design background that these examples share the same pressure-velocity curve as evident in Figures 17 and 18; with only the portion of the curve corresponding to pressure greater than the minimum pressure of the gas curve being shown. Arrest is predicted using the Battelle two-curve concept when the curve for the arrestor is tangent to the gas curve. As such, the curves for the arrestor satisfy the arrest condition. In contrast, the curves fracture propagation is predicted for the pipeline in both cases, because the curve for the pipeline crosses the respective gas curve in these figures.

Using information extracted from the crack and gas pressure versus velocity curves, it is possible to compute an estimate of the distance a crack will travel before arresting or traveling completely along the length of a segment. Figure 19 shows a typical velocity versus distance response for

	A	B	C	D	E	F	G	H	I	J	K	L	M	N	O
1	ARRESTOR DESIGN														
2	Input Parameters		Count	1	2	3	4	5	6	7	8	9	10	11	12
3	Operating Conditions	Gas Name	3	Gas #2											
4		Pressure, psi	1	1,350											
5		Temperature, F	1	55.0											
6		Diameter, inches	1	48											
7		Backfill Coefficient	1	0.470											
8	Initiation Segment	Length, ft	1	40											
9		Wall Thickness, inch	1	0.625											
10		Charpy V-notch toughness (full size specimens), ft-lb	1	60.0											
11		Yield Stress, ksi	1	65.0											
12	Arrest Segment	Length, ft	1	40											
13		Wall Thickness, inch	1	0.625											
14		Charpy V-notch toughness (full size specimens), ft-lb	24	90	100	110									
15		Yield Stress, ksi	1	80.0											
16		Total Number of Analysis Runs =	3												
17		Percent of Runs Completed =	66.7	%											
18		Elapsed time =	15	seconds											
19															
20	Notes:														
21	1	V = A0 * (Sd)^A1 * (FS/sqrt(CvR))^A2 * exp(A3 * x)													
22	2	Backfill coefficient of 0.47 corresponds to 1m cover on top of pipe.													
23	3	Minimum crack length used in regression analysis = 2 meters.													
24	4	No duplicates allowed in any row.													
25	5	An analysis will be conducted for each value in a row until a blank is encountered in that row.													
26	6	Elastic modlus is not a variable.													
27	7	Flow stress is not a matrix variables, FS = YS + 10,000 psi.													

Design Info / Results / PV-Plot / V-x Plot / Run Parameters

Ready

a) input sheet

	A	B	C	D	E	F	G	H	I	J	K	L	M	N	O
1	ARRESTOR DESIGN														
2	Input Parameters													Results	
3	Operating Conditions					Initiation Segment				Arrest Segment					
4	Gas Name	Pressure, psi	Temperature, F	Diameter, inches	Backfill Coefficient	Length, ft	Wall Thickness, inch	CvN (FS), ft-lb	Yield Stress, ksi	Length, ft	Wall Thickness, inch	CvN (FS), ft-lb	Yield Stress, ksi	Arrest Distance, ft	Comments
5	Gas #2	1350	55	48	0.47	40	0.625	60	65	40	0.625	90	80	0.02	SUCCESSFUL ARREST PREDICTED!
6	Gas #2	1350	55	48	0.47	40	0.625	60	65	40	0.625	100	80	0.02	SUCCESSFUL ARREST PREDICTED!
7	Gas #2	1350	55	48	0.47	40	0.625	60	65	40	0.625	110	80	0.02	SUCCESSFUL ARREST PREDICTED!
8															
9															
10															
11															
12															
13															

Design Info / Results / PV-Plot / V-x Plot / Run Parameters

Ready

b) results summary sheet (image compressed laterally in this figure)

Figure 16. results summary sheet of the arrestor design macro.

the arrestor. The velocity drops precipitously when the crack first enters the segment because of the higher toughness relative to the pipeline. Beyond that point, the velocity decreases at a much slower rate. If the rate of decrease is too slow – or the velocity when the crack enters the arrestor is too high – the crack will not arrest within the length of the arrestor, which for the sake of

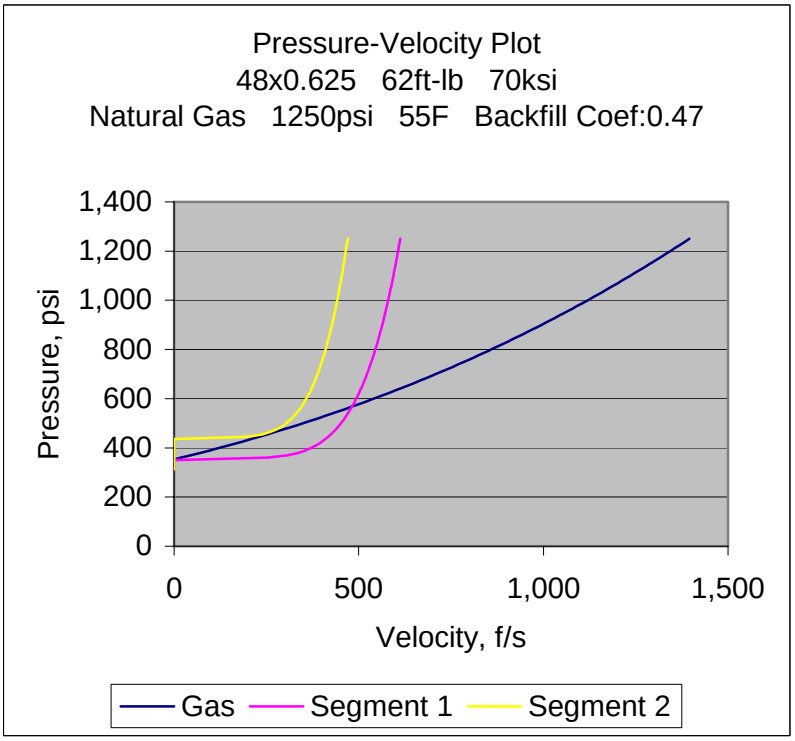

Figure 17. Example - arrestor analysis for lean natural gas (methane)

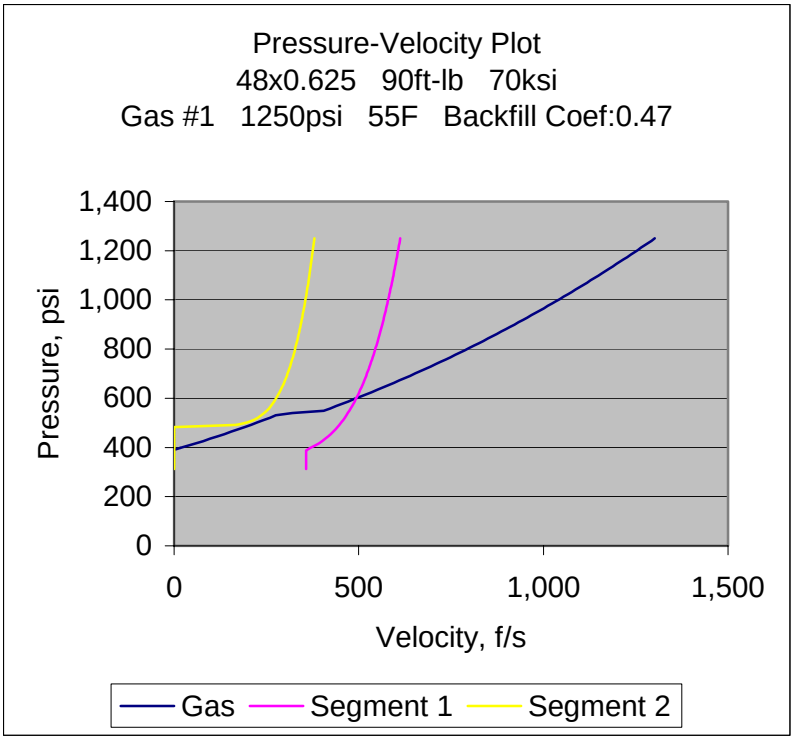

Figure 18. Example - arrestor analysis for 95 percent methane - 5 percent propane mix

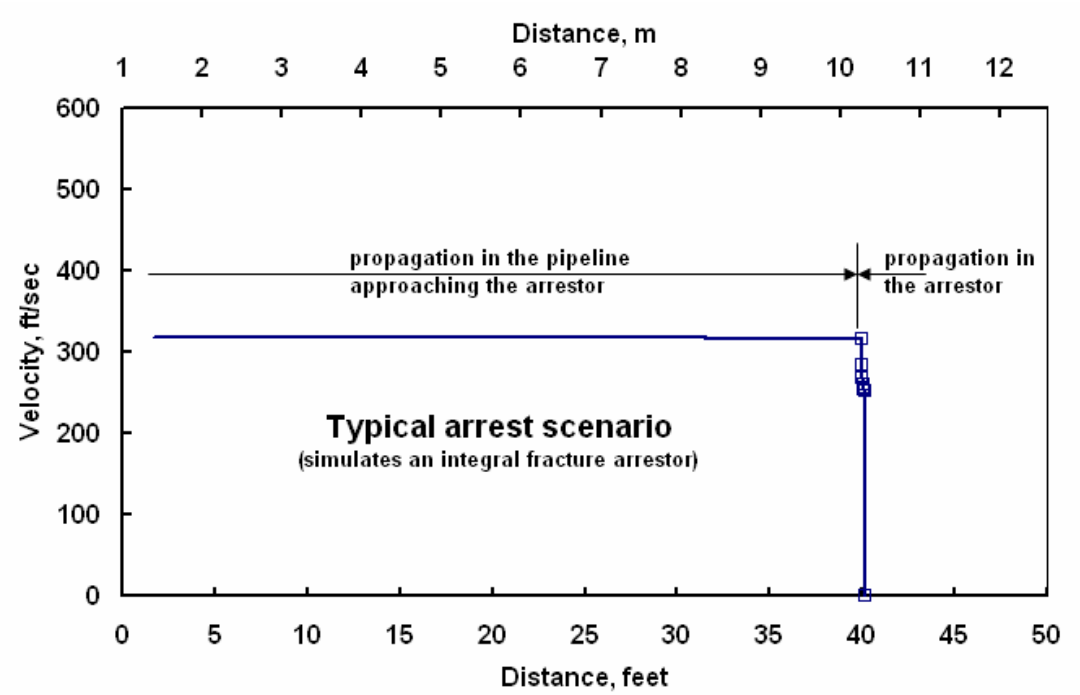

Figure 19. Typical velocity-distance response approaching versus within the arrestor

simplicity has been taken as the length the order of a typical pipe joint (i.e., ~40 feet). This has been done realizing Figures 14 and 15 indicate that the full-scale test results and the model both show full arrest to zero velocity beyond the sharp drop in fracture velocity typical of the onset of arrest occurs slowly. That is full arrest to zero velocity occurs through a "tail" evident in these figures in the shallow velocity-distance slope as velocity approaches zero. Such behavior typically reflects the ring-off following arrest, which occurs by a process different than that embedded in Equation 2. As this process is not addressed by Equation 2, it is suggested the arrestor length be increased beyond the design length by one pipe diameter.

Alternatively, as this tail reflects the possibility for running fracture to reinitiate if the crack runs through the arrestor, full arrest must can achieved within the desired length, including provision for ring-off, by targeting arrest in a shorter distance via alternative arrestor designs. Figures 20 and 21show results for a range of arrestor designs achieved via differing combinations of toughness and grade for the pipelines just considered, transporting either the lean gas or rich mix, respectively. Each figure considers a grade above and below the two arrestor designs evaluated above, with each grade represented by a trend in these figures. Each grade has been evaluated over a range of CVP levels including that for the above designs, with the value of CVP being shown on the x-axis. The y-axis in these figures presents the distance the crack propagates into the arrestor before it fully arrests, as determined parametrically for the many line-pipe property combinations using the arrestor-design macro.

Figures 20 and 21 clearly show the distance required for arrest can be reduced to very short lengths by appropriate selection of grade and toughness. Note by comparing these figures that a very large increase in toughness is required to arrest the crack when the propane is present. Note too that arrest as discussed herein considers axial crack extension that gives rise to a symmetric reduction in wall thickness on either flank of the crack. As the crack slows the axial extension is often terminated in a spiral "ring-off" that involves lower-velocity propagating shear rather than

a tensile instability. It is likely the "tail" evident in the test data reflects this spiral ring-off, which as noted above can be accounted for by adding a diameter's length to the arrestor.

Conclusion

Equation 2 formulated to replace the "fracture curve" of the BTCM has been coupled with the "gas curve" of the BTCM and built into an algorithm that facilitates the design of crack arrestors through use of an Excel macro. Realizing that other aspects of this project could bring changes to the technology embedded in this algorithm, it was structured to use coefficients other than those of Equation 3.

The arrestor design model was validated by successful of predicted crack velocity and propagation response throughout the test sections of full-scale fracture propagation tests that terminated in arrest. The results showed that beyond the onset of arrest the propagation velocity decreases sharply as a function of the toughness available for arrest. This makes it possible to design arrestors with relatively short length, although provision must be made for "ring-off", which occurs typically as a spiral low-velocity shear fracture that runs around the pipeline.

Practical Aspects in Implementing Fracture Control and Arrestor Technology

As was evident in Figures14 and 15, uncertainty on the value of the mechanical and fracture properties specified for use in fracture control of new pipelines or for arrestors designed to manage existing pipelines can significantly affect the fracture velocity. For example, reference to Figure 14 indicates that a difference of about one standard deviation in toughness based on multiple sampling within a one joint of vintage line pipe leads to about a 20 m/s swing in fracture velocity. Because running fractures propagate at high velocity and have significant inertia due to flap formation in their wake, the fracture will continue to run supported by the lowest toughness experienced along its path. While the model represented by Equation 2 and the calibration constants in Equations 3 tends to be conservative, as noted earlier this reflects the choice of a conservative initial velocity more so than the inherent nature of the model and its calibration. As such, prudence dictates inclusion of a margin of safety on arrest toughness that reflects the application and the line-pipe steel involved.

Applications targeting a fracture control plan for a pipeline constructed of modern high-strength high-toughness steel do not face the degree of uncertainty that underlies Figures 14 and 15 if the controls used in steel-making offset this variability. As such, for these applications specification of an all-heat-average coupled with limits on variability should be viable when using the fracture arrestor model to specify line pipe with inherent fracture control capabilities. Suffice it to note that suggests a conservative estimate of initial fracture velocity should be used to determine the running fracture scenarios that must be contained.

However, when dealing with vintage line pipe, the properties scatter within one joint can be quite large, and the distribution of properties along the pipeline can be uncertain. Prudence suggests evaluating the propagation velocity in the pipeline in regard to a high estimate of initial fracture velocity to determine what must be addressed in the event that analysis indicates the service pressure and temperature coupled with the transported fluid will promote running fracture. In turn, the design of the arrestor to mitigate the risk of running fracture should use a margin of safety on the specified minimum arrestor toughness the order of 10-percent.

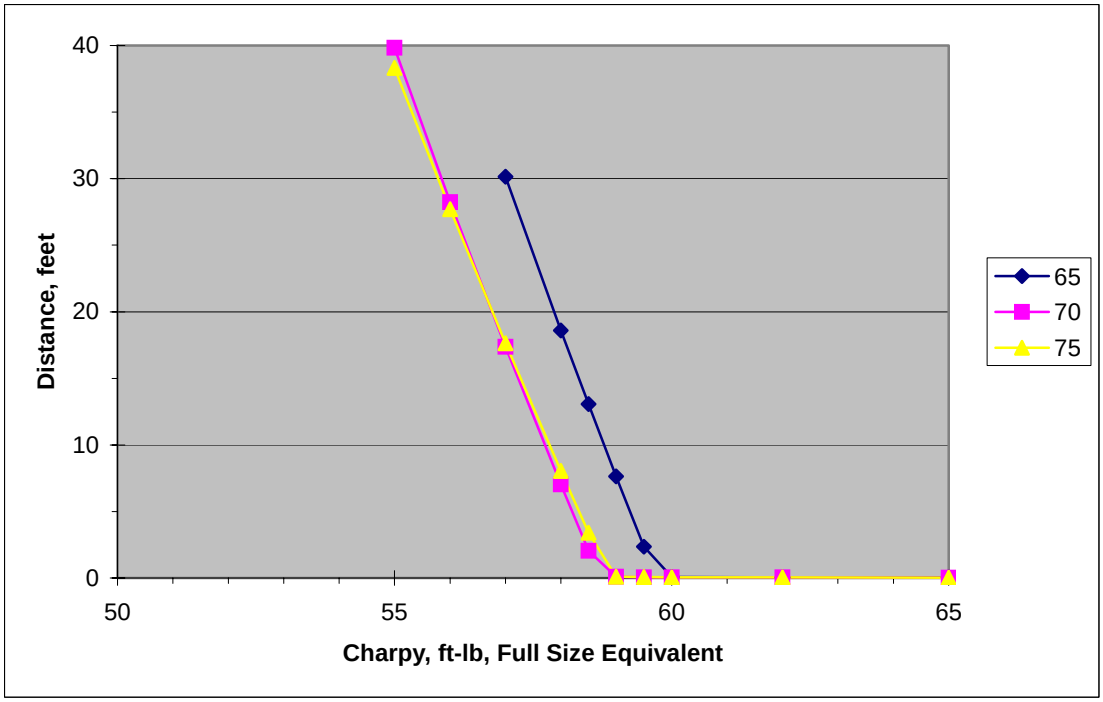

Figure 20. Crack arrest distance versus CVP and yield stress for lean gas

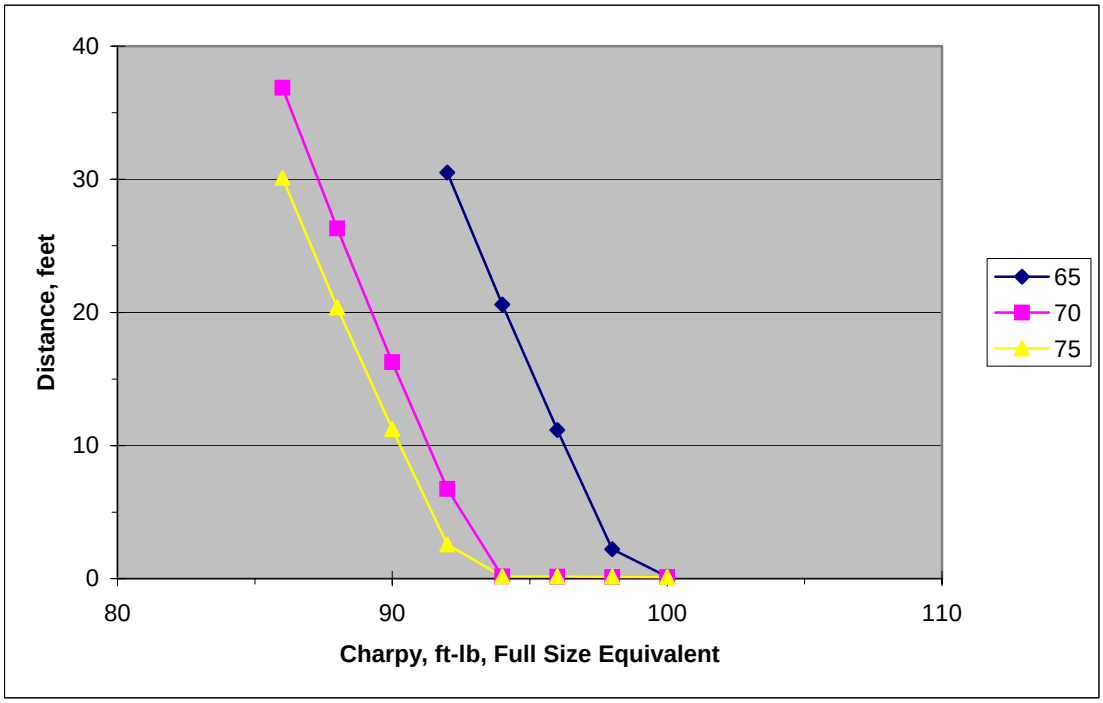

Figure 21. Crack arrest distance versus CVP and yield stress for the rich gas

Where uncertainty exists in regard to gas control and quality that could lead to the possible presence of hydrocarbon liquids (HCLs) and transport of dense phase gases, care must be taken to consider the scope of both the HCLs that might be present as well as their relative mole fractions. This concern is amplified by comparing the trends in Figures 17 and 18. These results indicate almost a 50-percent increase in fracture resistance is needed to address this rich-gas scenario, with the incremental difference depending on the nature of the rich gas. It is particularly a concern where existing pipelines are fed by LNG for two reasons. First, as shipped LNG often contains heavy ends (HCLs). Second, as LNG is expanded from its shipping temperature of -162ºC, it remains quite cold opening the door to RBF given the quite high transition temperatures known for some vintage line-pipe steels[(e.g., see 78)].

It follows that the use of Equation 2 as embedded in the arrestor design software or for other applications requires consideration of variability and service conditions that cannot be simply addressed otherwise.

Conclusion

The capability to successfully predict crack velocity and propagation response throughout the test sections of full-scale fracture propagation tests developed in the previous section was used to simulate arrest for a wide variety of practical scenarios. Trends developed in these analyses were then used to characterize factors controlling arrest.

The results show the crack velocity prior to arrest experiences two characteristically different types of response. Upon entering a new joint of pipe the crack shows an almost immediate change in velocity, the extent to which depends on the incremental toughness. Tougher joints cause a sharp decrease in velocity while less tough joints cause a corresponding increase in velocity. Beyond this almost immediate response, there is a gradual change in velocity the extent to which again depends on toughness – but with relatively less effect on crack velocity than that experienced in the transition between pipe joints. As anticipated, tougher joints cause a gradual decrease in velocity while less tough joints cause a gradual increase in velocity.

The results indicate that arrest is an abrupt event that follows otherwise gradual decay in crack velocity until the onset of arrest. Beyond the onset for arrest, the propagation velocity decreases sharply as a function of the toughness available for arrest. While the full-scale tests occasionally show a tail associated with “ring-off”, which occurs typically as a spiral low-velocity shear fracture that runs around the pipeline, this shear cracking differs from the propagating ductile fracture and so this closure to arrest was not captured by Equation 2 or the coefficients in Equation 3.

Empirical Aspects Involving Flow and Fracture Response beyond Initiation

This section begins consideration of the dynamic fracture process on the earlier states premise that fracture arrest occurs through dissipation mechanisms in addition to crack-propagation resistance developing through the creation of new crack surface. Support for this alternative premise – introduced as one element of the approach for this project – develops in regard to the behavior of the crack velocity that is evident for example in Figures 14 and 15. These results show that a small increase in toughness experienced as the crack-tip transitions from one test pipe into the next causes almost immediate arrest – whereas propagation through the prior test pipe did not appreciably alter the crack-tips velocity. Support for this alternative premise also

develop in terms of Figures 20 and 21, which indicate that ***once arrest begins*** an increase in toughness can significantly reduce the distance for full arrest. However, ***prior to the onset of arrest*** comparable increments in toughness have only marginal effect on the crack-tip velocity. The limited effect of toughness on crack velocity within a pipe joint can be inferred from the last term in Equation 2, where the exponent as calibrated has a very weak negative value of just 0.00082.

Significantly, trending using Equation 2 fails to show an influence of joint toughness on this exponent, indicating the sharp decrease in crack-tip velocity leading to full arrest is driven by factors related to toughness – rather than by toughness acting alone via dissipation due to creation of new crack surface. These tendencies, which are evident in the experimental data as well as by evaluating the simulated crack propagation and arrest behavior, indicate that the running fracture process differs substantially from the historical view that characterizes it simply in terms of dissipation involving the creation of new crack surface due to propagation.

It follows that the search for a specimen to characterize the resistance to running fracture must focus on aspects beyond crack-propagation resistance. It also follows that a composite measure of arrest behavior is needed that recognizes the sharp decrease in crack-tip velocity leading to full arrest is driven by factors related to toughness – rather than by toughness acting alone via dissipation due to creation of new crack surface. To fully address future scenarios that involve still tougher steels and their unique flow and fracture properties, this composite measure must address the need to view this dynamic propagation as a running tensile instability rather than a cracking process.

Because this more general scenario is still consistent with the view that arrest occurs when the decompression wave front outruns the propagating instability, the two-curve concept central to the BTCM remains valid, and so is retained. However, based on problems experienced in the use of the BTCM as toughness increased there is a need to ensure similitude exists in its application. Accordingly, this section targets Task 1 and 2 of the work-scope, which begin consideration of the significant differences in the grade and toughness of the line-pipe steels for which fracture control and arrestor technology might be applied to today versus that underlying the two-curve concept adopted for use thus far in this report. Empirical trends will be evaluated and on that basis similitude sought between the flow and fracture properties embedded in the BTCM developed circa the early 1970s versus those of today or what might evolve in the future. This lays the foundation for the stopgap model for fracture propagation and arrest. Because the "two-curve concept" is retained, laying this foundation begins with more detailed consideration of the BTCM and its shortcomings, beginning first with some historical trends and the viability of the two-curve concept in light of those tendencies.

Historical Trends in Using the BTCM

Historical use of the BTCM has shown problems developed as the steel toughness increased, which was noted first in the 1980s. Figure 22 illustrates this concern in reference to the four of the six previously discussed "simplified" fracture-arrest models, which apply specifically to single-phase decompression scenarios. Each part of this figure compares the arrest-toughness predictions for the same full-scale test database, which covers grades predominantly from X52 through X80, in diameters from (~406 to 1422 mm), to toughness levels greater than ~270 J. All four parts of this figure show that as the toughness of the steels increased the predicted toughness levels fell below that observed for arrest in full-scale propagating fracture testing. All parts of

Figure 22 show this error, which is evident as the trends bend away from the one-to-one line – starting at ~100 J. While scatter is evident, a similar pattern develops for all models – each of which uses CVN energy as its measure of fracture resistance.

Historical use of the BTCM also has implied a grade-dependent error, evidence for which began appearing in the late 1990s as results for testing with modern X80, X100, and X120 were published. One example of such trends is apparent in Figure 23, which summarizes results for these three grades[48]. It is apparent from this figure that the arrest toughness predictions via the BTCM as calibrated in the 1970s must be multiplied by a factor of 1.4 to 1.7 to correspond with these trends. It is further apparent that there are no arrest data for the X120, for which the propagation results lie above the trend for X100. Because the actual arrest toughness for these results is comparable to that of Figure 22 (note that the axes on these figures are reversed), a portion of this disparity could be traced to higher toughness. As Figure 23 shows, the data tend to band with grade, with the extent of this disparity increasing as grade increases. Thus, one can argue that the predictions via the BTCM err increasing as the grade increases.

In reference to the circled data-points in Figure 23, note that an arrest and propagate result lie at comparable levels, with the arrest occurring at toughness levels well beyond that observed for several of the propagate results – for the same sequence of full-scale tests. These tendencies suggest that toughness by itself is loosing its ability to discriminate between fracture arrest and propagation. Such results support the view that as toughness is increased the propagation process is moving away from fracture, and tending toward a propagating tensile instability. This same tendency is observed for quasi-static cracking, where fracture controls failure at lower toughness levels, with a transition to collapse control limited by the UTS as toughness increases[e.g., 81]. Under quasi-static conditions this transition begins at toughness the order of 30 ft-lb, with collapse control occurring regardless of the line-pipe properties and defect size beyond ~125 ft-lb. Recognizing that the yield stress increases as the strain rate increases[82], a similar transition to collapse control is anticipated for RDF – but at a somewhat higher toughness level. This analogy and the trends in Figure 23 both support the earlier premise that as toughness increases a transition to propagating tensile instability can be anticipated. This transition could affect a breakdown in similitude between the steels of the era of the BTCM versus those in use today.

The above comparisons involve only single-phase decompression, which avoids the complexity associated with decompression models and eliminates this complexity as a cause for such trends. On this basis there is reason to evaluate causes for this disparity in terms of the breakdown in similitude between the cracking response of the steels that underlie the formulation of the BTCM versus those considered in its use as strength and toughness increased beyond the early 1970s.

Whether the gas decompression formulation that underlies the BTCM "gas curve" – the second curve in the two-curve concept – is equally prone to error due to differing fracture control concerns since the early 1970s can be assessed via work done in the intervening years. For example, measurements targeting decompression response made in the Alliance full-scale tests indicate the isentropic formulation coupled with the Benedict-Web-Rubin-Starling (BWRS) equation of state embedded in the BTCM very effectively characterized the observed response[25,26]. Measurements in work targeting a more general gas-decompression formulation[79] likewise demonstrated that the "GASDECOM" algorithm developed to represent decompression for use in the BTCM was quite robust, producing results virtually identical to the more recent formulations. On this basis, the gas decompression curve in the BTCM does not

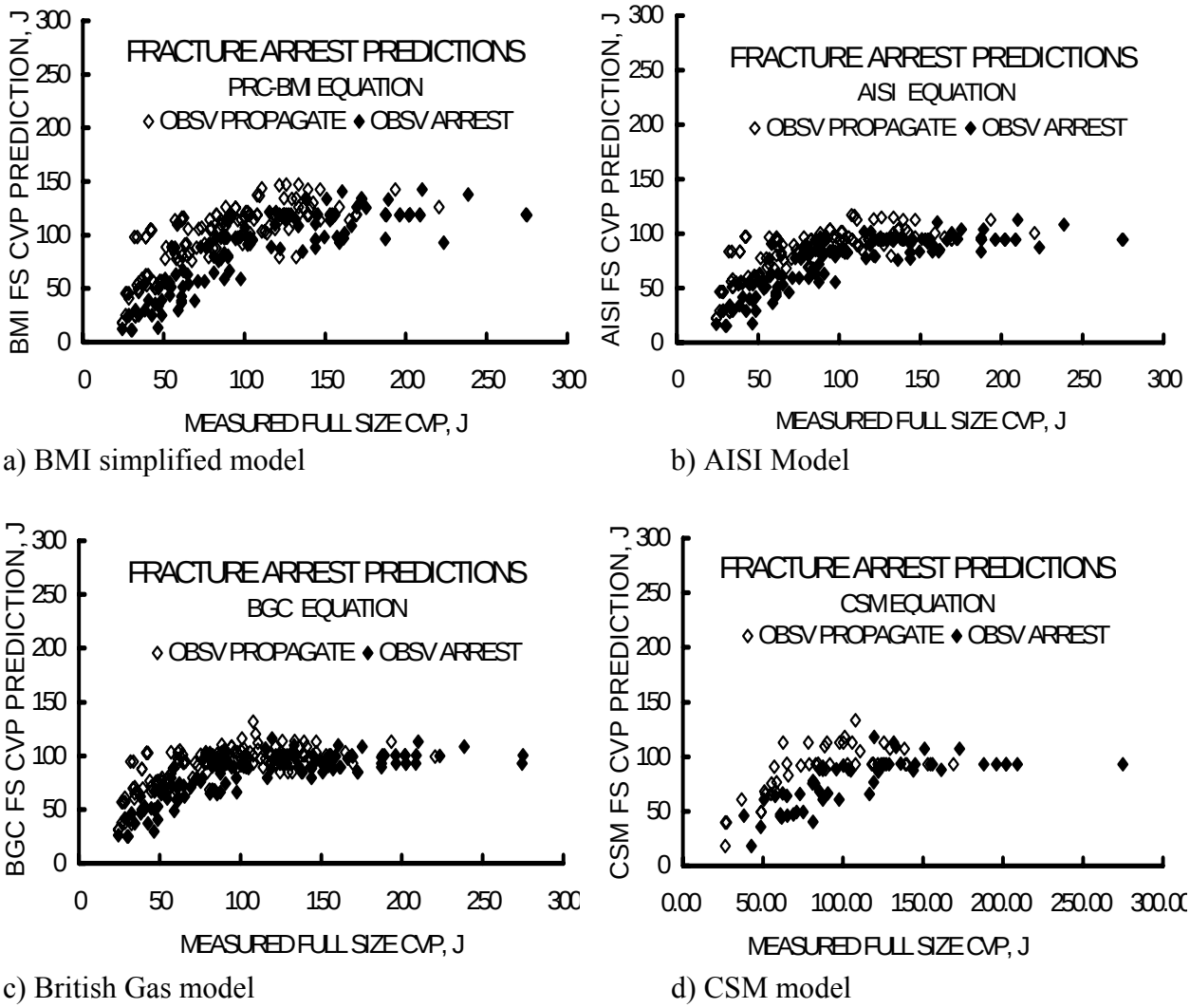

a) BMI simplified model b) AISI Model

c) British Gas model d) CSM model

Figure 22. Predictions of FSE CVN arrest toughness based on four simplified models.

appear to be a factor in the difficulties evident in Figures 22 and 23, and so is adequate at least currently.

In light of these historical tendencies, the ensuing subsections explore the fracture curve in the BTCM and the linking role of the backfill constant as the basis to understand why the above disparities develop.

Derivation of the Fracture Curve

The BTCM evaluates the decompression wave velocity and the fracture propagation velocity, and brings these together through an empirical artifice known as the backfill constant. This constant facilitates coupling the decompression velocity and the crack velocity. This subsection derives the BTCM crack curve, which includes an arrest-pressure model. A subsequent section considers the backfill constant.

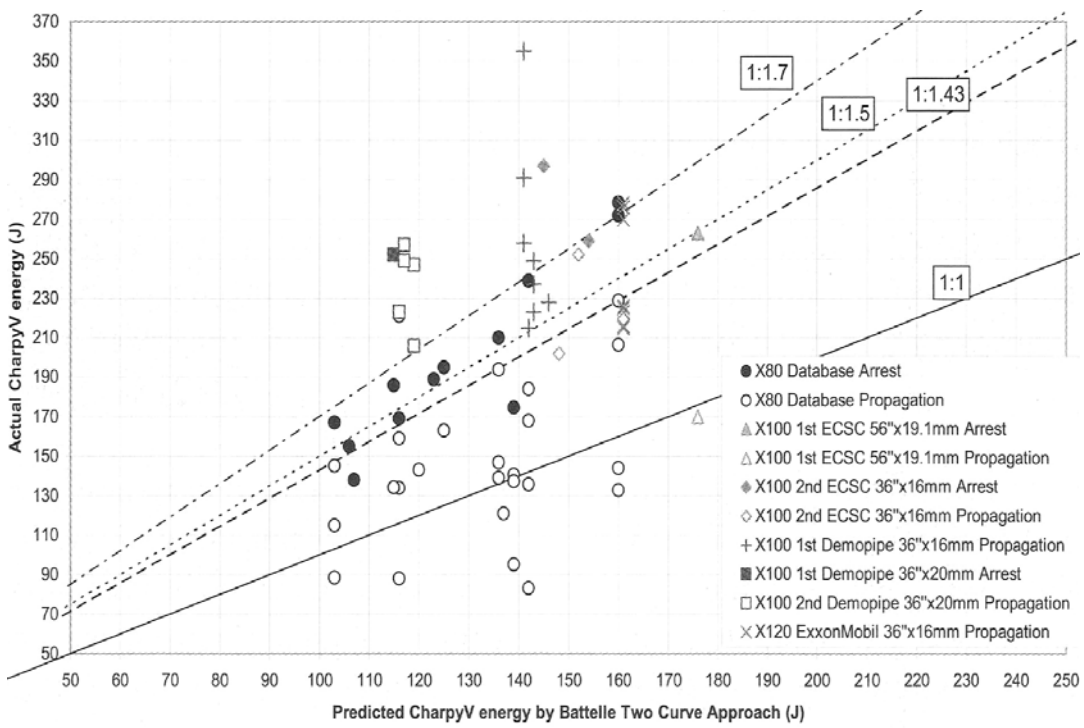

Figure 23. Database for X80, X100, and X120 full-scale tests[48]

<u>The Crack Curve and</u>
<u>the Interplay between Flow and Fracture Properties</u>

The formulation of the mathematical model for the pressure versus crack velocity in the BTCM assumed the crack velocity depended on the velocity of the plastic wave that propagates along the pipe ahead of the crack. This plastic zone is small in comparison to the dimensions of the pipeline, such that it follows in the wake of elastic wave(s) slightly ahead of the tip of the crack. Because the plastic wave moves with the tip of the crack, the plastic wave velocity can be a surrogate for the crack propagation velocity. Departing somewhat from the original derivation by Maxey[9], the plastic wave velocity can be expressed in analogy to the elastic wave velocity as follows[74]:

$$V_{el} = \sqrt{\frac{E_{bulk}}{\rho}} \qquad \text{and} \qquad V_{pl} = \sqrt{\frac{E_{pl}}{\rho}} \tag{4}$$

where:

V_{el} = elastic wave velocity
E_{bulk} = elastic bulk modulus
ρ = density of the line-pipe steel
V_{pl} = plastic wave velocity
E_{pl} = instantaneous plastic modulus.

Recognizing that ductile response is addressed and within the propagating plastic zone the elastic strain is negligible compared to the inelastic strain, the flow response characterized by E_{pl} in Equation 5 can be reasonably considered fully plastic. As is common for many line pipe steels

from vintage grades through modern commercial line pipe[80], this inelastic response can be adequately represented by simple power-law constitutive behavior in the form:

$$\sigma = K\varepsilon^n \tag{5}$$

where:

σ = true stress
K = strength coefficient
ε = true strain, that for ductile fracture is dominated by the plastic response
n = strain-hardening exponent.

The quality of the fit typically provided by Equation 5 is illustrated in Figure 24, considering vintage X42 in contrast to modern X70 line-pipe steel. It is apparent from this figure that Equation 5 is more than adequate for this purpose, which is usual for line-pipe steels.

By definition the instantaneous plastic modulus, E_{pl},

$$E_{pl} = \frac{d\sigma}{d\varepsilon}, \tag{6a}$$

such that:

$$E_{pl} = \frac{d\sigma}{d\varepsilon} = nK\varepsilon^{n-1} = \frac{n\ \sigma}{\varepsilon} \tag{6b}$$

where as indicated for Equation 5 the stress and strain variables in Equation 6 represent true fracture stress and true fracture strain.

The next step in reformatting Equation 4 to relate the local crack-tip pressure to the plastic wave velocity (equally the crack propagation velocity) follows from the reasonable assumption that the fracture resistance, R, can be characterized as a function of the energy dissipated in a CVN test. Some have historically suggested the Charpy energy should be replaced in this role as it fails to characterize "crack-propagation resistance". In contrast, the introduction to this section noted full arrest is driven by factors related to toughness – rather than by toughness acting alone via dissipation due to creation of new crack surface. Because the CVN test broadly couples a mix of dissipation due to deformation, initiation, and propagation it could serve this function – provided similitude requirements are addressed across the range of toughness levels considered.

Equation 7 expresses fracture resistance, R, as a function of the energy dissipated in a CVN test in the form of an energy-density:

$$R = B\frac{C_v}{A_c} \tag{7}$$

where:

R = material's resistance to propagating fracture, in-lbs/in^2 or J/mm^2
B = conversion factor, equal to 12 in/ft for English units and 1 MPa / J for metric units
C_v = Charpy impact energy, ft-lb or J
A_c = fracture area of the CVN specimen – for a full-thickness (standard thickness) CVN specimen, the thickness is 0.394 inches (10 mm) and the depth (fracture length) is 0.315 inches (8 mm), giving an area of 0.124 inch^2 (80 mm^2).

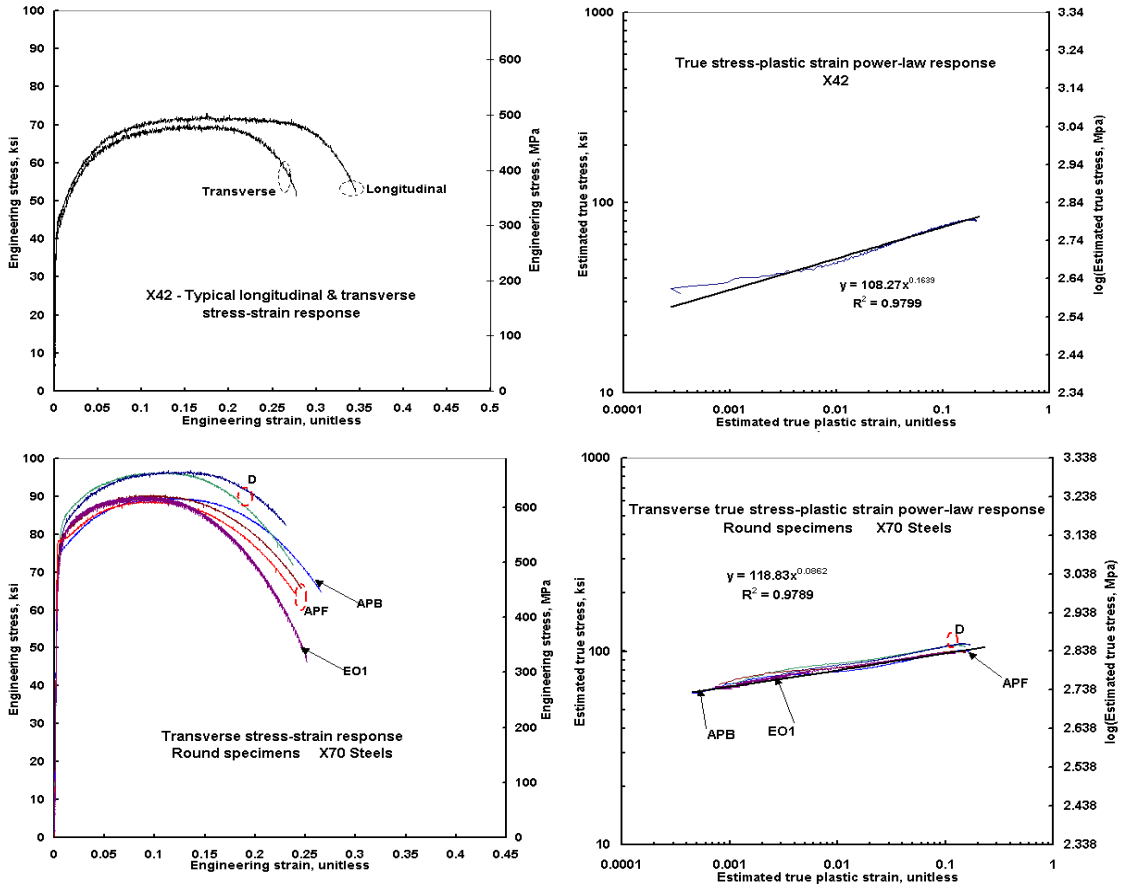

Figure 24. Full-range stress-strain response of X42 and X70

As shown in Figure 25 reproduced from Reference 24, nine steels ranging from vintage to modern grades indicate that under ductile fracture conditions the FSE CVN plateau (FSE CVP) energy is well correlated with the area under the stress-strain curve, which is sometimes called the true fracture toughness. In turn the true fracture toughness for ductile metals is reasonably given as the product of the UTS and the true fracture strain, but could be approximated using flow stress in lieu of the UTS, as was done by Maxey in the BTCM formulation. Using these relationships in place of C_V in Equation 7 leads to:

$$R \propto \overline{\sigma}\,\varepsilon_f \tag{8}$$

where in addition to the above defined parameters:

R = material's resistance to propagating fracture, in-lbs/in^2 or J/mm^2

ε_f = true strain at fracture.

Combining Equations 4, 6b, and 8 in reference to the point of fracture leads to the following expression for the plastic wave velocity:

$$V_{pl} \propto \sqrt{\frac{1}{n\rho}\left(\frac{\sigma_f\,\overline{\sigma}}{R}\right)} \tag{9}$$

where:

σ_f = true fracture stress,

or by introducing a constant that includes the steel's physical and mechanical response:

$$V_{pl} \propto C \frac{\overline{\sigma}}{\sqrt{R}} \tag{10}$$

where:

C = an empirical constant to be calibrated shortly.

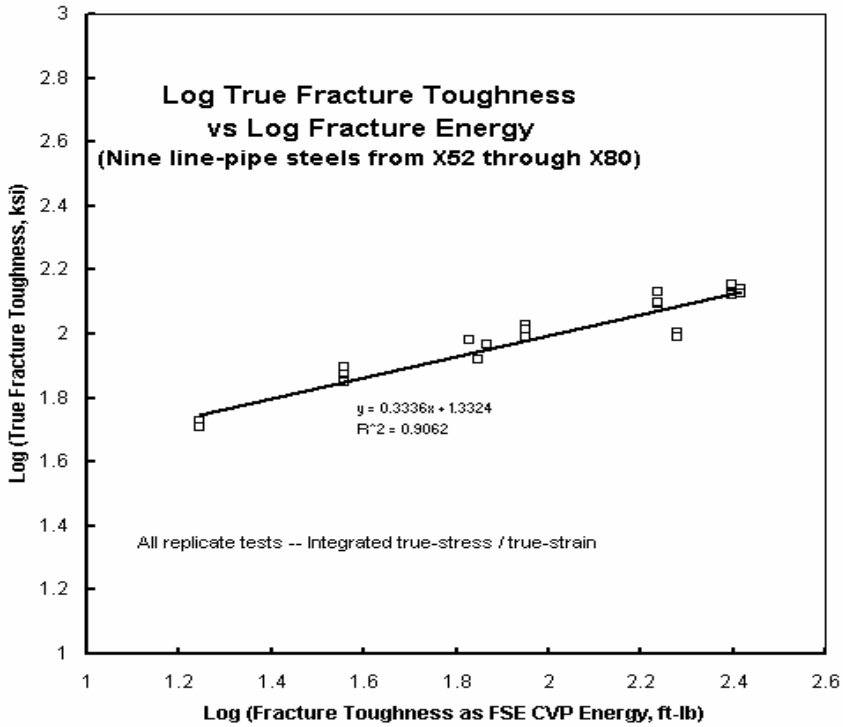

Figure 25. Correlation between the fracture energy from instrumented Charpy impact tests and the true fracture toughness from a tensile test.

The density, ρ, from Equation 9 was embedded in the proportionality constant C in Equation 10, which was consistent with known trends. The proportionality constant also embedded the strain-hardening exponent, *n,* from Equation 9, which was somewhat unusual because this exponent varies across the range of pipeline steels of interest, and even varies within the plate or skelp used in pipe-making. Apparently, this was done because this parameter was not typically known or measured for line-pipe steels. Likewise, while the true stress at fracture or the UTS would be better used in Equations 9 and 10, the flow stress was used apparently because again these parameters were not broadly reported – particularly for the early steels.

As Equation 10 applies at the point of the fracture where the local pressure decays through decompression, the crack velocity was expressed in the form:

$$V_c = C \frac{\overline{\sigma}}{\sqrt{R}} \left[\frac{P_d}{P_a} - 1 \right]^m \tag{11}$$

where in addition to the previously defined parameters:

V_c = crack velocity, fps, ≈ V_{pl} = plastic wave velocity, fps
P_d = dynamic pressure, psi
P_a = arrest pressure, psi
m = empirical fitting constant, discussed later in the section considering backfill, and
C = empirical fitting constant, discussed later in the section considering backfill.

The dynamic pressure, P_d in Equation 11 is the pressure applied to the pipe at the moving crack tip determined from the gas decompression curve.

Arrest Pressure Model

Referring to Figure 1, the arrest pressure is the intercept on that vertical axis pressure versus velocity curve for the crack. As such, it represents a stationary crack tip.

The BTCM determined this pressure for a stationary arrested crack via linear elastic fracture mechanics (LEFM) empirically calibrated through "burst" tests of line pipe with an initial crack that were pressurized until a leak or rupture occurred. This static "arrest" pressure had the form:

$$P_a = \frac{t}{r}\sigma_{arrest} = \frac{t}{r}\frac{2\bar{\sigma}}{\pi M_T} sec^{-1}\left[\frac{\pi R E}{8\bar{\sigma}^2 c_{eff}}\right] \tag{12}$$

where in addition to previously defined parameters:

σ_{arrest} = arrest stress level, ksi or MPa.
t = wall thickness, inches or mm, and,
r = outside radius of the pipe, inches or mm,
M_T = Folias correction at the effective crack length
$= [\ 1 + 1.255(c_{eff}^2/rt) - 0.0135(c_{eff}^2/rt)^2\ ]^{1/2}$
E = elastic modulus of steel, ksi or MPa
c_{eff} = effective crack length.

For a long running fracture the crack length approaches infinity relative to the other dimensions of the analysis, specifically the pipe diameter and wall thickness. Hence in the limit, as the crack length approaches infinity the arrest pressure in Equation 12 approaches zero while the crack velocity given by Equation 11 approaches infinity. More practically, as it was reasonable to consider that steady state develops for long cracks in lieu of these bounds, with the effective crack length taken as $c_{eff} = 3\sqrt{(R\ t)}$ because it best fit the experimental data. For pipes with D/t ratios from 30 to120 this effective crack length ranges from ~20 to ~40 percent of the diameter of the line pipe. For this effective crack length, the bulging factor is $M_T = 3.33$. The material's fracture resistance, R, is derived from CVN results as indicated in Equation 7.

Conclusion

Historical use of the BTCM has shown problems in its use that appear to reflect a breakdown in similitude as toughness increases, and possibly also as strength increases. The breakdown in similitude was anticipated and so planned for in terms of analysis and resolution to the extent possible, as addressed within the next several sections of the report.

Similitude Considerations – Empirical Aspects Involving Increased Toughness and Fracture Arrest Pressure

Consideration of the trend in Figure 22 and the results in Figure 23 suggests a breakdown in similitude between the fracture response of the steels from the 1970s, as embedded in the fracture curve of the BTCM, versus the response of modern line-pipe steels. If the earlier noted premise that running fracture is tending toward a propagating tensile instability as toughness increases noted at the outset of this section has merit, then correlations like that shown in Figure 25 suggest the true fracture ductility, ε_f, should correlate strongly with increasing toughness. Laboratory toughness test practices found with such a correlation have potential utility in models that developed to characterize this propagating tensile instability.

Similitude and Increasing Toughness

Figure 26 shows a strong correlation between ε_f and increasing toughness when toughness is represented by FSE CVP. This correlation develops across a range of steel grades from X52 through X80, which embrace both vintage and modern X52 and the more recent higher-strength grades. The y-axis in this figure is the true-fracture ductility, which is plotted versus CVP on the x-axis. While there is some scatter, the trend is clear and shows a strong dependence of ε_f on CVP. This result implies that as toughness has increased the strain at the tip of a propagating crack has increased significantly, bringing with it increased crack-tip stretch prior to failure, and therefore the potential for significant blunting of this crack-tip prior to failure. While the process leading to this blunting is dynamic, the time required to blunt the crack and develop tearing at its tip advancing the crack provides time for stretching to develop both ahead of the crack and laterally. Grey[83] has suggested use of this lateral stretch zone as the basis to characterize full-scale fracture behavior, and arrest resistance.

While Figure 26 shows a clear trend between ε_f and increasing values of CVP, the results in Figure 27 indicate that developing similitude between various classes of line-pipe steel might be somewhat complicated. This figure shows that the tradeoff between strength and ductility for the traditional solid-solution strengthened steels is not transferable to the newer controlled-rolled steels, which according to these trends has continued to evolve since the 1970s. But as each of these classes of steel is embedded in trend of Figure 26, such results indicate trends should be evident over these grades and toughness levels sufficient to establish similitude between the steels of the 1970s and those developed subsequently.

To this end, results for instrumented CVN specimens have been analyzed with a view to isolate contributions to the energy dissipated in this test due to initiation, propagation, and fracture, using definitions developed and reported in Reference 84. This results in the relationships shown in Figure 28. It is apparent from this figure that the propagation energy sharply falls at toughness levels associated with the onset of problems with the BTCM evident earlier in Figure 22. This figure shows that this decease is associated with an increase in energy dissipated via deformation, which leads to stretching across the crack faces following significant blunting and stretching local to the notch tip prior to the onset of ductile tearing through the net

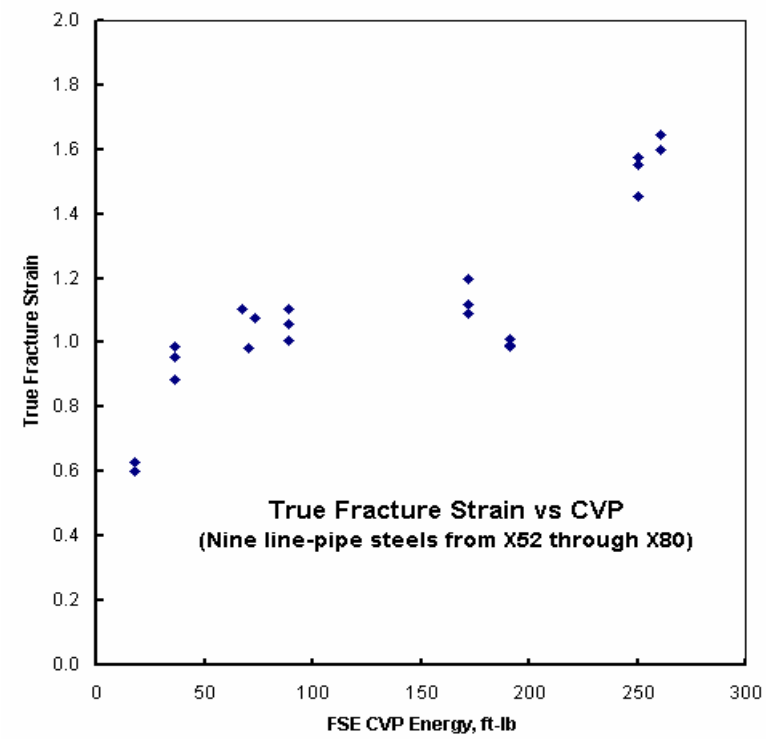

Figure 26. Relationship between the fracture energy from instrumented Charpy impact tests and the true fracture strain from a tensile test.

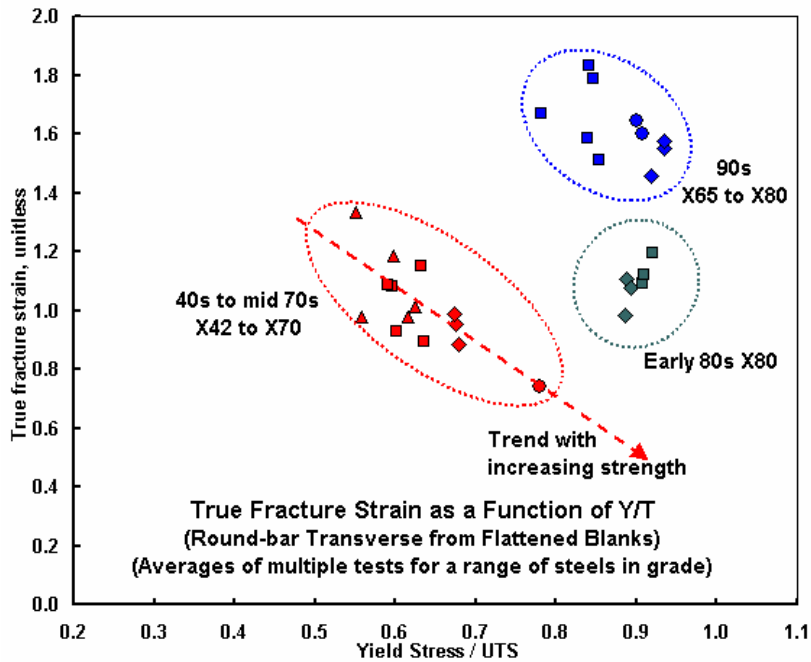

Figure 27. Relationship between the true fracture strain from a tensile test and the ratio of the yield to ultimate stress.

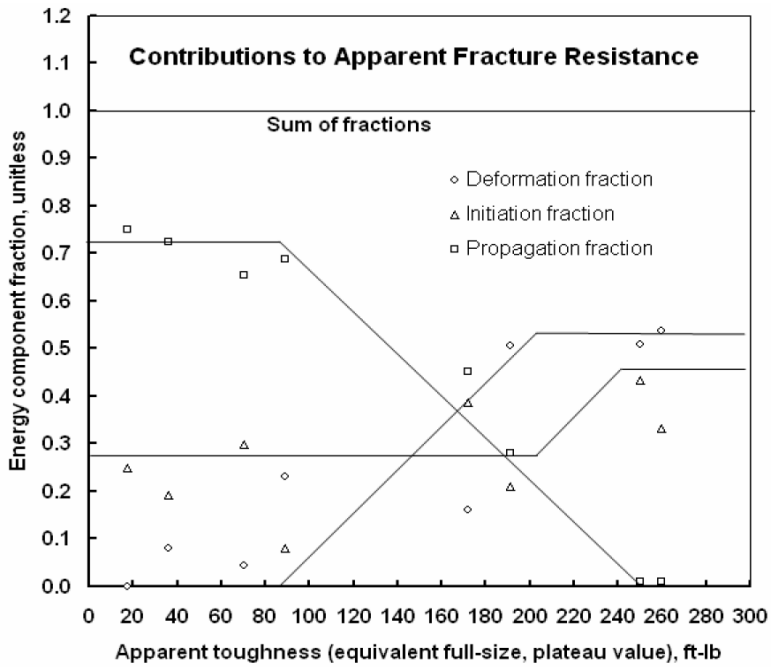

Figure 28. Energy components comprising energy via instrumented CVN testing

ligament. That is, this specimen includes traits considered by Grey as characteristic of full-scale fracture behavior and arrest resistance.

Trending these shifting tendencies relative to the behavior embedded in the fracture curve in the BTCM lead to what has been termed the Leis Correction factor, which has the form:

$$C_v' = C_v + 0.00269\, C_v^{2.04} - 21.18, \quad C_v \geq 70 \text{ ft-lb (94 J)} \tag{13}$$

where:

C_v' = Corrected FSE CVP, ft-lbs

C_v = FSE CVP calculated with the BTCM, ft-lbs

As can be seen from equation, because this correction was developed in reference to the BTCM and its formulation for grades with toughness typically less than 70 ft-lb (~94 J), this correction applies only to toughness levels beyond this lower bound. This correction addresses similitude lost in the response of the CVN specimen for the 1970s steels in contrast to those developed since. As this increase in toughness resulted in a decrease in propagation resistance, which predominated the behavior of these earlier steels, this correction drives the BTCM predicted CVP value up to account for this change. This equation develops from the trends in Figure 28, and so is specific to the fracture response of the CVN specimen and the change in the mix energy dissipation in this specimen as toughness increases beyond about 70 ft-lb (94 J).

If the breakdown in similitude in the fracture response of the CVN specimen as toughness is increased is one factor that underlies the errors evident in the BTCM predictions shown in Figures 22 and 23. The extent to which this breakdown is responsible for such errors has been evaluated specifically in regard to the Battelle simplified equation for arrest toughness for single-

phase decompression. Predictions with this model in conjunction with the correction shown in Equation 13 are shown in Figure 29[3]. The axes in this figure are the same as used in Figures 22 and 23, with the results considered in this figure covering the same database evaluated earlier in Figure 22.

In the format of Figure 29, predicted arrests are indicated by the solid symbols, which should lie anywhere below the one-to-one line, but are conservative even when evident above this line. In contrast, predicted propagations are indicated by the open symbols, which should lie anywhere above the one-to-one line, but are non-conservative when they fall below this line. The dashed trends either side of the one-to-one line indicate the bounds on CVP determined earlier in the uncertainty analysis associated with roughly one-standard deviation in CVP. It is apparent from this figure that the "bend-over" evident in Figure 22 is effectively gone, and that discrimination between solid and open symbols representing arrest and propagate is improved – with the quality of the predictions above and below ~100 J more or less comparable. As such, the breakdown in similitude for CVN specimens circa the era of the BTCM and the more recent steels is largely responsible for problems in the use of the BTCM through the mid to late 1990s.

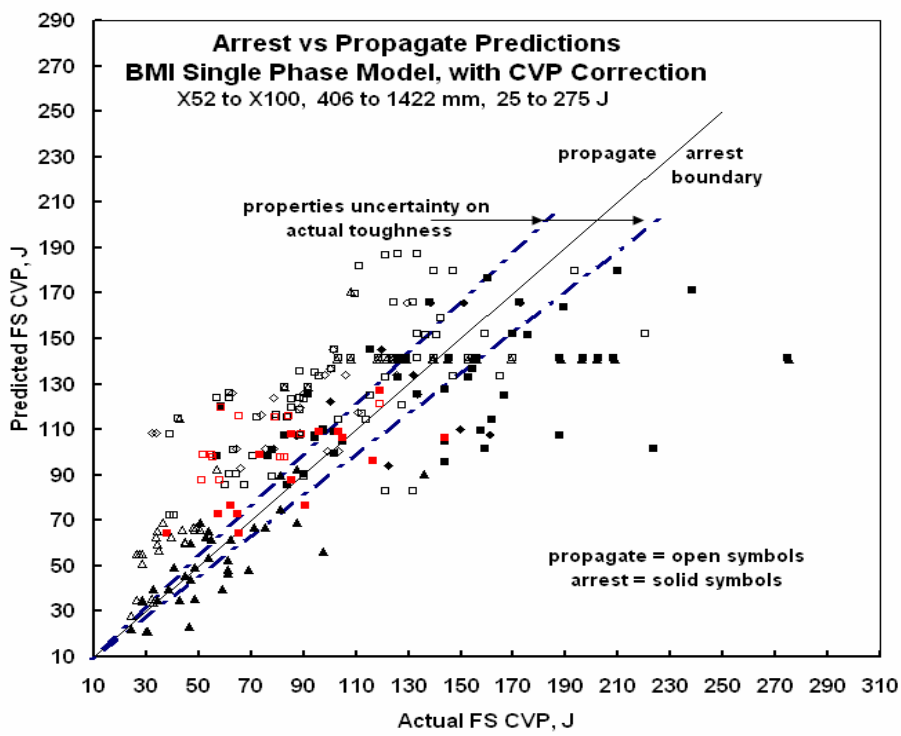

Figure 29. Evaluation of the simplified BTCM in conjunction with Equation 13

[3] While this discussion is specific to the Battelle simplified equation, the similitude correction represented by Equation 13 is relevant to the CVN specimen, such that it should be equally effective for other predictions of arrest toughness for single-phase decompression. Te many empirical schemes advanced for this purpose are elaborated in detail in Reference 5, which includes some background and references to their original publication.

Similitude and Arrest Pressure – Flow Properties

The arrest pressure used in the BTCM as defined in Equation 12 is the second element of the fracture curve where a significant breakdown in similitude is plausible – as the grades of steel of interest today have roughly doubled their strength in comparison to the X52 that dominated construction into the 1970s. Parameters in Equation 12 that can contribute to this breakdown include flow stress, resistance to fracture, and effective crack length, with the bulging factor also a function of the effective crack length. These parameters all are empirically derived, or develop through the CVN specimen that underlies the just discussed similitude concerns.

The extent of changes in the underlying empirical basis of Equation 12 can be illustrated in reference to Equation 8, which indicates the value of *R* in Equation 12 is proportional to the true fracture strain. In reference to this proportionality, Figure 26 indicates that transition to the chemistries and processing practices for these more recent steels has roughly doubled the true fracture ductility available from some of these steels. But, as evident in this figure, this transition has also affected an increase in the ratio of yield stress to ultimate tensile stress (Y/T). The processing of the modern grades has also affected significant anisotropy in the mechanical properties, including the true fracture ductility. One aspect of this transition is illustrated in comparing the tensile properties of vintage X52 versus Grade X100, which respectively are shown in Figures 30 and 31.

Figure 30 shows the stress-strain response typical of 1960s vintage X-52 steel, for both the hoop (transverse) and axial (longitudinal) orientations. These full-range engineering stress-strain curves indicate the engineering fracture strains were about 0.35 and show the tensile response is similar for both orientations. At the scale needed to show these full-range curves, the elastic response is difficult to separate from the vertical axis, and so at strains approaching fracture is trivial compared to the plastic strain.

Figure 31[61] shows the corresponding results for a recently produced X100 steel on true-stress – true-strain coordinates. For purposes of this figure the transverse stress-strain curves have been shifted to the right, to positions such that their continued plastic flow response is more or less coincident. If the transverse response had the same characteristics exhibited by the axial response, this shift would imply the transverse response reflects an initial strain equal to the amount of the shift. In regard to Specimen 8823 for example, the response for the axial direction runs from Point 1 to Point 4. For the hoop response shifted as just discussed, this trend implies a pre-strain of about 1.2-percent associated with the straining from Point 1 to Point 2 that after unloading tracks to Point 3 – the origin of the hoop stress-strain response. Absent some prior pre-strain, most metals exhibit the gradual transition into plastic flow evident for the X52 and the axial X100 results. In contrast, prior plastic or inelastic flow leads to the abrupt transition evident for the X100 grade in the transverse (hoop) orientation. It follows that this X100 steel shows anisotropic response in terms of yield stress, and its initial strain hardening. Close comparison of these curves also indicates quite strong anisotropic response in terms of the true fracture strain. A final observation for the X100 in Figure 31 as compared to the X52 in Figure 34 is the significant reduction on the strain to failure for the higher-strength grade. It follows that in contrast to the X52 this steel will exhibit much less stretch laterally as well as in front of the crack. This implies the arrest response for such steels will involve less dissipation due to initiation and deformation as compared to other steels of similar toughness. In spite of this, the BTCM miss-predicts rather badly, as was apparent in Figure 23.

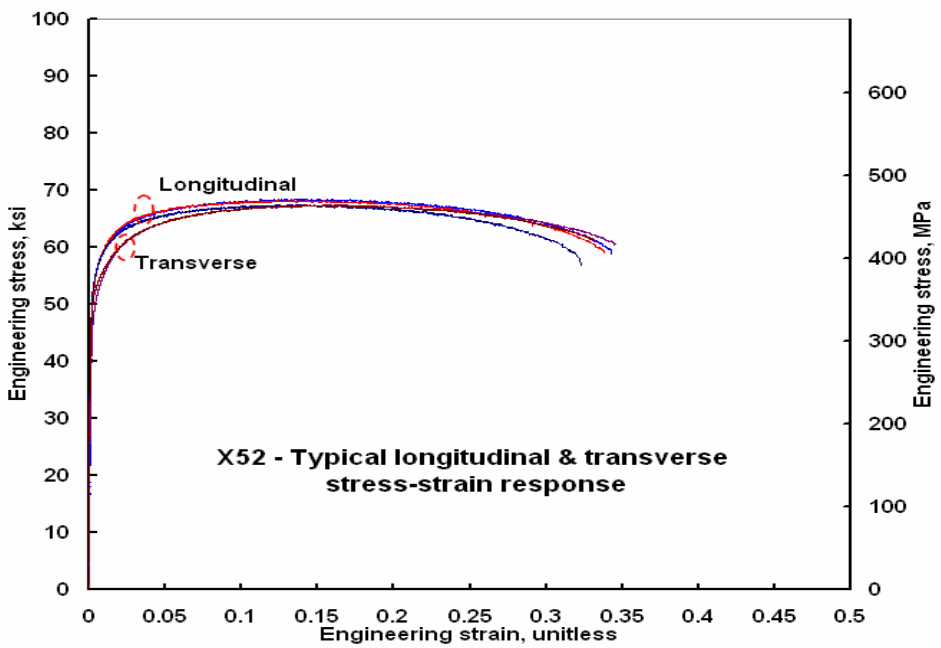

Figure 30. Stress-strain response for X-52 steel for axial and hoop orientations.

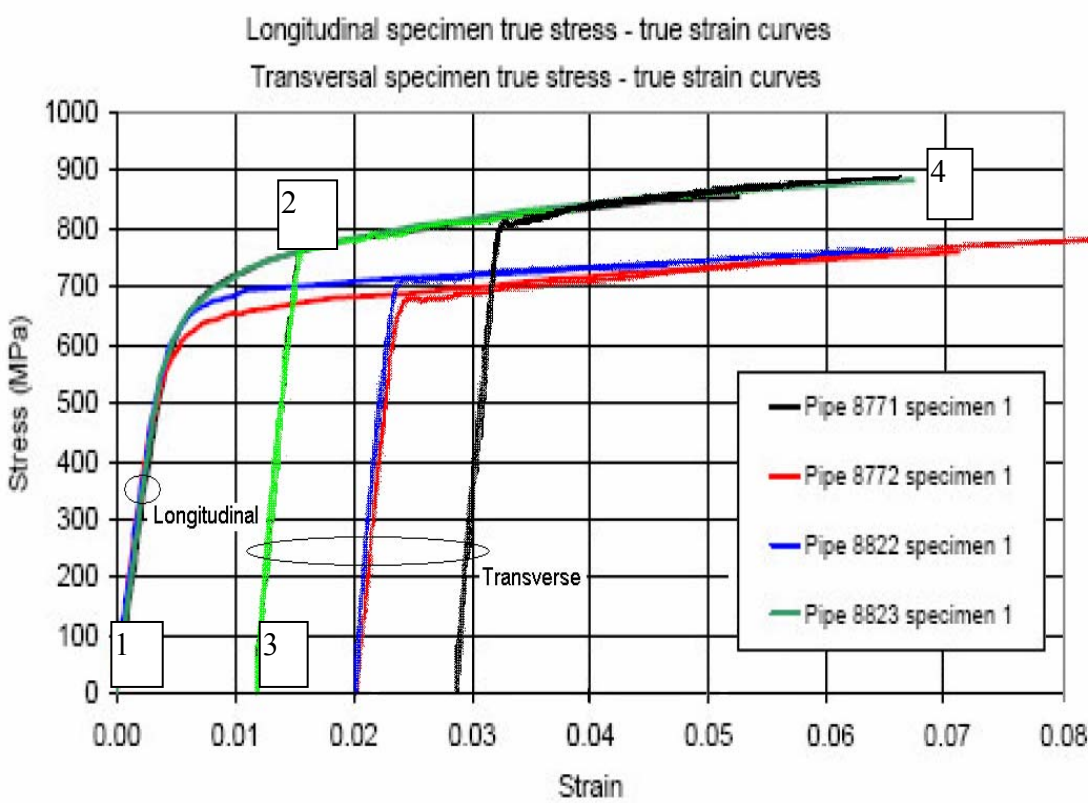

Figure 31. Stress-strain response for recent X-100 steel: axial and hoop orientations

Similitude and Arrest Pressure – Definition of P_a

The above results indicate the inferred dependence of the quality of BTCM predictions evident in Figure 23, while due in part to a breakdown in similitude involving the CVN specimen, also could reflect a breakdown in similitude associated with arrest pressure developed through use of Equation 13. This possibility was quantified by comparing predicted quasi-static failure pressure based on Equation 13 with comparable predictions using the pipe axial flaw failure criterion[73] (PAFFC). PAFFC has its roots in the PRCI ductile flaw growth model (DFGM). This DFGM embeds fracture mechanics necessary to characterizes defect response in vintage steels that fail via fracture control and plastic collapse analyses necessary to address modern higher-toughness steels that fail by plastic collapse. It likewise provides for the transition between these scenarios. Thus, PAFFC has the potential to accurately characterize defect failure behavior in vintage steels as well as modern higher-toughness steels.

Because accuracy in prediction of failure pressure is essential if PAFFC is to assess similitude achieved for the earlier steels versus the modern steels, burst-test results have been assembled from References 27, 28, and 85-87 to discriminate this aspect. These burst tests represent line-pipe properties in diameters from 12 to 48 inches, with diameter to thickness ratios ranging from 49 to more than 100 in grades from Gr B through recent X80, with FSE CVP energies from ~20 ft-lb to levels beyond 200 ft-lb. The lower toughness tests serve as the tie back to the lower-toughness data were used to calibrate the BTCM and Equation 13, while the higher-toughness data address the modern steels. As apparent from Figure 32, which summarizes these results, close correspondence develops between predictions via PAFFC and the actual failure response. This is evident through the clustering or the PAFFC predictions around the one-to-one trend, for which the results show PAFFC accurately predicts the quasi-static burst pressure without bias from vintage through modern steels. This observation supports use of PAFFC to assess the breakdown in similitude associated with use of Equation 13 in the fracture curve formulation of the BTCM.

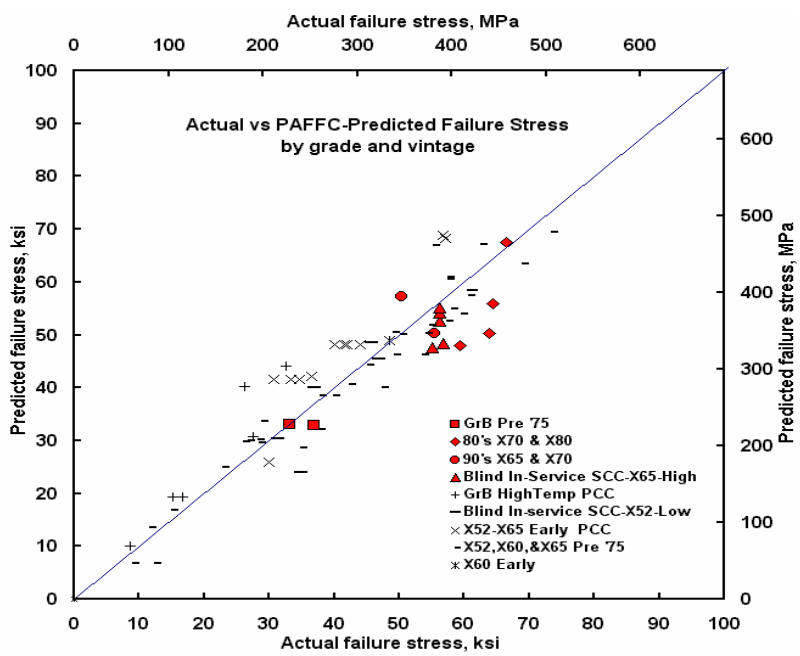

Figure 32. Burst test results validating PAFFC for vintage and modern steels

Figure 33 presents results typical of trends that develop when predictions via PAFFC are compared with those via Equation 13 as it is used in the BTCM. The y-axis of this figure presents predictions via PAFFC normalized by the corresponding predictions via Equation 13, which are plotted as a function of crack length on the x-axis. Differences in such predictions as a function of grade are evident in the contours representing grades from X52 to X90 in this typical

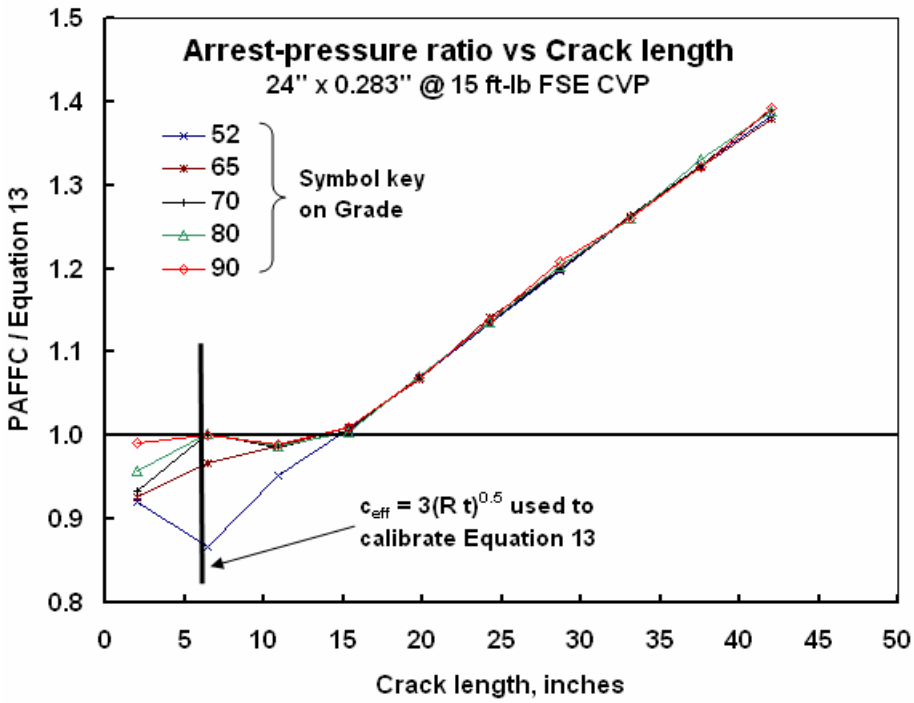

Figure 33. Similitude breakdown associated with arrest pressure in the BTCM (typical)

view of such results. For the specific set of line-pipe properties considered in Figure 33 observe that the trends for all grades converge for crack lengths beyond ~15 inches. On this basis, had $c_{eff} \approx 10(R\ t)^{0.5}$ that more closely approximates the line pipe's diameter been adopted in embedding Equation 13 in the BTCM, similitude would have been ensured for these results. Whether similar trends develop has been broadly assessed as a function of differing line-pipe properties, recognizing that such differences are likely to diminish with the transition to plastic collapse. Because this transition to collapse control begins at CVP equal ~30 ft-lb and finishes in general beyond ~125 ft-lb, conditions that bracket this range have been considered for a range of grades, line pipe geometries, and defect sizes. These results indicate a rather complex dependence on several parameters. Accordingly, PAFFC or its equivalent must be incorporated within a modified two-curve concept to ensure similitude in regard to arrest pressure.

Conclusion

An approach to establish similitude to extend the utility of the BTCM and other such CVN-based arrest models was developed and validated. As this consideration of similitude takes the form of a simple equation (Equation 13), this "correction factor" is transferable and easily implemented. This was done within the BTCM, as well as in the present two-curve adaptation developed herein, which that replaced the fracture-curve of the BTCM with Equation 2 implemented in differential form. The effects of this correction can be significant, increasing the arrest

roughness by more than 30-percent depending on the application. This correction has been validated via blind accurate predictions for full-scale testing.

An approach also was established to address the breakdown in similitude associated with the definition of arrest pressure. This similitude assessment considered both the role of flow properties and the manner arrest pressure was defined, which showed a broad and varied breakdown in similitude that varied with the line pipe's geometric properties, and its mechanical and fracture properties. As this similitude breakdown was not simply trended, the extent of this breakdown could not be simply expressed analytically. Accordingly, this breakdown was offset by embedding a viable approach to correct the current arrest-pressure definition via PAFFC. This quasi-static criterion was embedded into the BTCM, as well as in the present two-curve adaptation developed herein, which has replaced the fracture-curve of the BTCM with Equation 2 implemented in differential form. Comparison of predictions with this revised formulation with the BTCM indicates this correction will selectively drive a small increase in arrest toughness.

Finally, significant differences in the flow response of modern grades were identified in contrast to the steels commercially available and in broad use well into the 1970s. These differences involved both the strain-hardening response and the true fracture strain. As the rate of strain hardening was strongly reduced, as was the true fracture strain, both trends point to potentially unique fracture propagation response for this X100 steel, and other steels with similar traits. Such could be a factor in understanding the trends in Figure 23 wherein the BTCM was shown to err badly in its predictions for this grade, and other modern higher-strength grades.

Backfill Constant and its Empirical Definition

As alluded to in reference to Equation 11, an empirical coefficient that is the leading term in this equation has been referred to as the backfill constant. This constant is the bridge between the two curves in the BTCM. This section considers factors influenced by the backfill as a function of stress, toughness, and parameters that characterize the geometry of the line pipe and the properties of the transported gas or fluid.

Effect of Backfill and its Empirical Role in the BTCM

Early full-scale fracture propagation tests were done above ground, as it was easier and afforded access to measure and directly observe the process. As time passed consideration was given to the more complex full-scale condition, which simulated the effect of cover through backfill, and addressed the earth-anchored state of many buried pipelines by use of anchor blocks at the end of the test-section reservoirs. Recognizing that the earth-anchored state was a worst-case scenario, use of anchor blocks became the usual approach. Accordingly, most of the full-scale tests that provided the empirical definition for the BTCM involved backfilled and earth-anchored test sections. As earth-anchors effectively lock the test section against axial restraint and so are not a consideration with backfill, this subsection is specific to Backfill.

When backfill was used, the backfill materials included what was referred to as "soil" and "sand", although work also has been done for "frozen" backfill and various "shallow water" backfill scenarios[88-91]. Absent details, it can be assumed that the backfill was placed using common pipeline construction techniques, but beyond this little other information available about the "backfill". For example, there is no data that characterizes the mechanical or physical

properties of the backfill or the surrounding native soil. Even simple metrics like moisture content or density are not provided.

Backfill depth typically ranged from 18 to 40 inches. In some cases, the width of the side-fill was recorded as well, which ranged from 18 to 60 inches. Referenced to tests for which measurements were available to establish position-velocity data pairs, the most prevalent test conditions involve natural gas with 40 inches of "soil" backfill. These "soil tests" involve sites such as Battelle's Athens test site, and the British Gas Spadeadam site, and involve depths of cover as shallow as 30-inches. About half as many data pairs were available for testing using pressurized with air, where the test section was covered by 30 inches of "sand" or a sandy-gravel backfill, which involve sites such as the Sardinia facility of CSM. Finally, about half again as many data pairs were available for tests with air / no backfill, which often were among the first full-scale running fracture tests done.

The BTCM crack velocity relationship given as Equation 11 fits the experimental data using two empirically fitted parameters, namely C and m. The BTCM represented by Equation 14 restates Equation 11 but with inclusion of $m = 1/6$:

while C was taken as a units-dependent backfill constant whose value was specific to the nature of the backfill, as follows:

1. $C = 0.47$ for soil backfill
   0.40 for "shallow" water backfill, and
   0.648 for air testing / no backfill (above ground pipelines).

The multiplier C has been termed the backfill constant because its value was considered to depend only on the type and amount of the backfill in formulating the BTCM. In contrast, the exponent m was considered to be independent of the backfill. Significantly, the air tests used to characterize this backfill state were done without axial restraint, while the soil tests used this restraint. These significantly different scenarios contribute to what historically has been viewed as a backfill-only effect that in this context obviously embeds quite different circumstances. As this is likely to be a significant issue, it ultimately needs to be addressed – uncoupling the effect of backfill from the effect of axial restraint.

Similitude and Definition of the Backfill Constant

Figure 34 presents the experimental data that were trended to define the backfill constant noted

$$V_c = C\frac{\overline{\sigma}}{\sqrt{R}}\left[\frac{P_d}{P_a} - 1\right]^{1/6} \tag{14}$$

for either 30-inch-deep soil backfill or no backfill situations, which are shown by the symbols, along with the historical trends used to represent these data. The y-axis in this figure is P_d/P_a, whereas the x-axis addresses the remaining terms from Equation 14. While Equation 14 includes the constant exponent $m = 1/6$, the empirical trends plotted as the BTCM clearly reflect different exponents.

Figure 34 also presents trends that reflect linear regression curve fits through these data made during the course of this work. While a linear regression "best-fit" virtually overlays the empirical trend used in the BTCM to represent the "30-inch backfill" trend, the regression trend and the empirical trend used in the BTCM to represent the "no backfill" results differ significantly. Consistent with the observation that trends for these differing backfill conditions involve differing exponents, the regression determines the exponent for the backfill trend is close to 1/6, whereas that for "no backfill" was almost double – at a value near 0.28. Nonlinear least-square regression done to test the viability of these differing exponents, recognizing it better accounts for statistical uncertainty by considering its coincident occurrence in both the velocity and the pressure measurements does not alter this conclusion – as little difference was found with this method. Thus, the linear least squares curves shown in Figure 34 are viable.

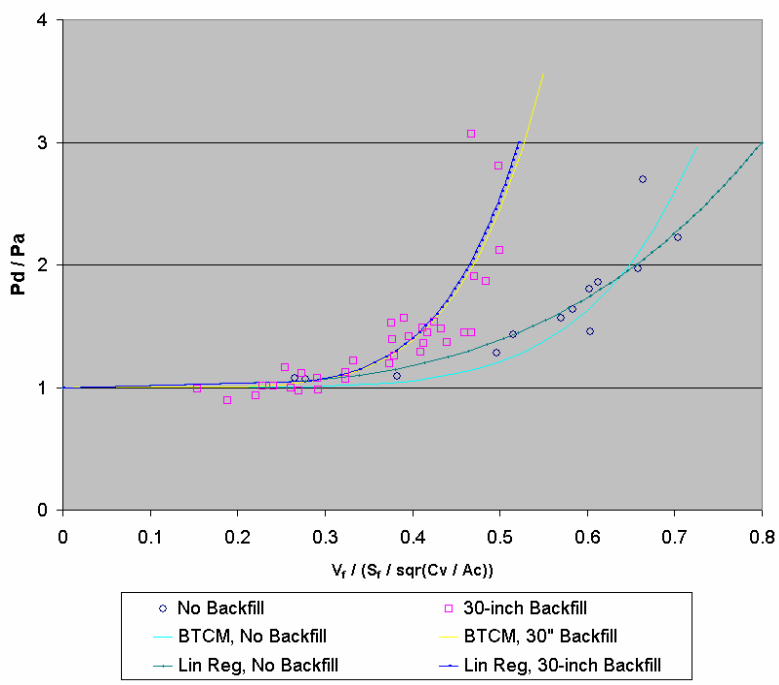

Figure 34. Experimental data used to estimate the backfill constant in the BTCM

It follows from Figure 34 that the effect of backfill evident in the full-scale testing cannot be simple embedded in the leading coefficient of Equation 14 – but that the exponent also must be considered to depend on the backfill.

The variability in results shown in Figure 34 suggests there is a need to more broadly understand the role of both *m* and *C* within the BTCM, along with sources for the uncertainty. The need to consider sources of uncertainty is underscored by the significant scatter evident for "air" backfill, as this is the simplest backfill scenario and yet shows great scatter. For such work to add value other than a few more data points, the testing needs to be well designed, target more than the relative effect of another backfill scenario, and the circumstances of the testing must be openly documented. The reason for this statement becomes evident from Figure 35, which has the same format as that of Figure 34 but considers more recent propagation data.

The data in Figure 35 have been culled to focus on single-phase decompression to remove this possible complication as a driver for scatter – with only results for testing with air considered here. Other than the pipe material and size, the primary test parameters that underlie this figure were the test pressure, which ranged from 648 to 2,625 psi, and the pipe temperature, which ranged from 56 to 80 degrees Fahrenheit. Solid symbols in the plot correspond to test pipes where arrest occurred, while the open symbols denote cases where propagation occurred. Beyond this level of discrimination, the blue diamond symbols represent soil backfill, the mauve triangles represent sand backfill, whereas the mauve squares represent no backfill. This range of backfill conditions covers the broadest extent possible for which data are widely available – representing ~38-percent swing referenced to the soil-backfill scenario.

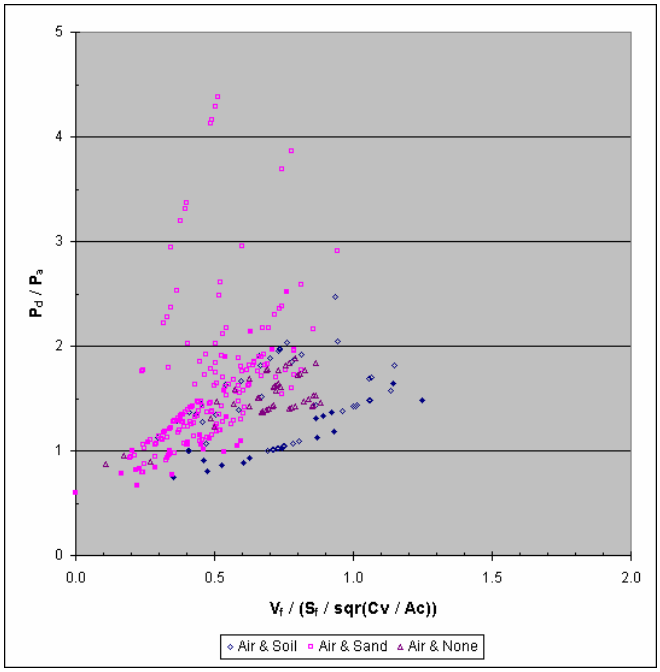

Figure 35. Full-scale results for soil, sand and without backfill and pressurized with air

Inspection of the results in Figure 35 indicate that the observed response tracks the gas decompression curve as has been observed in a broad range of full-scale propagating fracture testing where numerous pressure transducers where installed along the test pipe[(e.g., 57)]. However, while desirable there is no separation between propagate and arrest trends. Moreover, in spite of this significant difference in the backfill constant for the three backfill scenarios dealt with, the predictions in Figure 35 broadly commingle. Some banding of the results is apparent with the soil-backfill results banding toward the bottom of this cluster of propagation velocities, with the sand and air backfill results banding but intermixed lying above the soil scenarios. These trends indicate it would be difficult to define a single crack velocity curve that will be applicable to all of the tests represented in this figure, as is implied by Equation 14. As expected, the same result is generated for the full-scale tests pressurized by natural gas regardless of the gas composition or backfill condition.

The relative impact of the backfill constant free of the significant variability evident in Figure 35 can be identified by comparing the results in Figure 36 for the above-ground air backfill scenario that parallels the soil backfill case addressed earlier in Figures 14 and 15. Consistent with Figure 35 this figure shows that the backfill constant entered into the BCTM or equally the

present adaptation of the two-curve concept can have a significant effect on the predicted propagation velocity. In comparison to the trends in Figures 14 and 15, this figure shows that variability in the backfill constant at the same normalized level considered therein has an effect comparable to that of CVP energy. Variation in propagation velocity due to ±24-percent uncertainty in the backfill constant – which corresponds to ~±one standard deviation in strain hardening exponent for some datasets covering one grade of steel – also indicate that significant variability in fracture velocity can occur within the length of one test pipe, or along the length of the test section – due only to uncertainty in the strain-hardening exponent. It is because of the mathematical form of Equation 14, the lumping of *n* into the backfill constant, and the strong shift in *n* as grade increased that Battelle suggested use of the "Leis-correction factor" be restricted to Grade X70 and less[92].

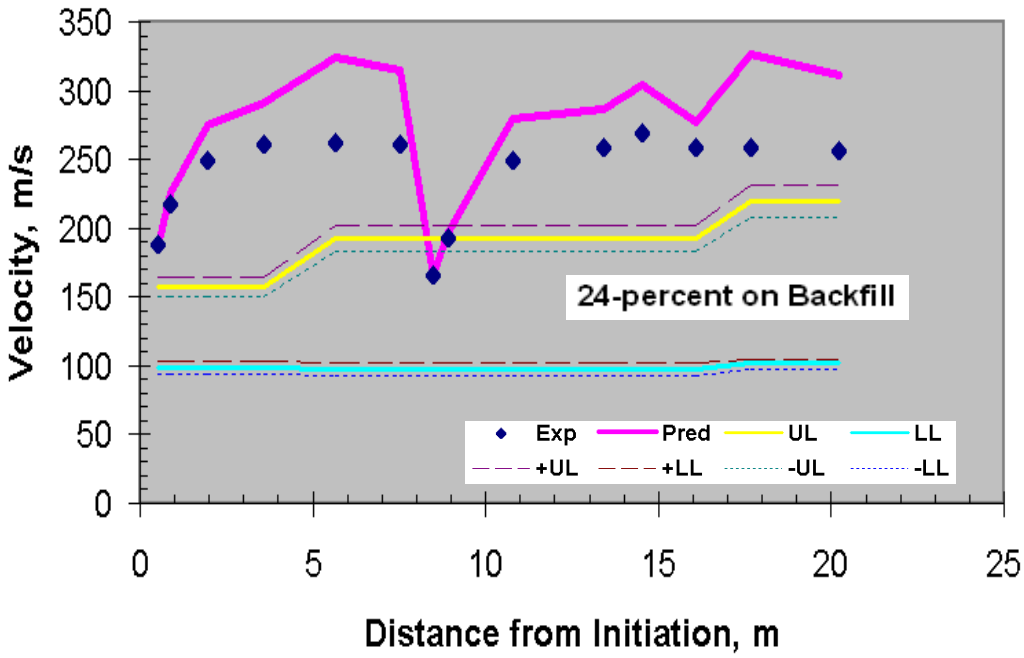

Figure 36. Experimental data and the effect of variation in the backfill constant

In reference to the experimental data presented in Figures 34 through 36 it follows that factors other than the backfill have a significant impact on the role of "backfill" as it has been characterized in the BTCM. Thus, there is a clear need to understand the role of both *m* and *C* within the BTCM, and to more broadly understand the general role of backfill in fracture propagation and arrest. While doing more testing of different backfill types can be instructive, the value of such work could be diminished absent this more general understanding – which becomes obvious in the next subsection.

Similitude and the Plausible Role of Flow Properties Embedded in the Backfill Constant

In regard to the commingled trends shown in Figure 35 remember that the transition from Equation 9 to Equation 10 embedded both the strain-hardening exponent, *n*, and density, ρ, for the line-pipe steel into the backfill constant defined in Equation 14. While the density is constant for present purposes, the strain hardening exponent can vary significantly. On this basis the backfill constant embeds the role of both the backfill and the line-pipe steel.

The plausible contribution of the strain hardening exponent to the commingled effects of backfill evident in Figure 35 depends on the absolute variation in the strain-hardening exponent and its effect relative to that of the backfill calibration shown with Equation 14. The extent of the absolute variation in backfill coefficient can be inferred by comparing the trends in Figures 30 and 31. A more quantitative indication of the extent of this variation can be established by comparing the views that present true stress versus plastic strain for Grade X42 versus an early X70 in Figure 24. The slopes shown in those figures, which are by definition the strain-hardening exponent, are 0.156 and 0.086, respectively for the X42 and the X70, which implies the lumped variation of n in C could be a significant factor in explaining the variability in both Figure 34 and 35.

A more general view of the potential role of the variation of n in explaining the apparent variation in the backfill constant follows from Figure 37, which presents results for line-pipe steels derived from Battelle's archives. Figure 37a plots the strain-hardening exponent as a function of the actual yield stress for grades that cover the range of interest. One measure of the extent of this variation within a grade can be found from the cluster of data for several modern X70 steels, results for which are shown as blue squares toward the lower bound of this band of data. These results indicate more than 50-percent variation can occur in n within one grade. Further insight into the possible variation of n within one grade can be seen in Figure 37b, which presents data derived from Battelle's archives for X52. These results cover a selection of earlier steels such as those considered in the full scale testing done into the later 1970s, along with more recent steels of this grade. The results in Figure 37b are presented as a cumulative distribution function such that population parameters could be inferred.

It is apparent from the data presented in Figure 37 that the value of n can vary by a factor of two within a grade, and can vary by a factor of five across the range of steels covered in full-scale fracture propagation databases. Realizing that the value of n is considered a constant and lumped into the backfill constant in the BTCM, this uncertainty can cause variability in the backfill constant the order of ~45-percent within one grade. If the range of grades is broadened to cover the steels historically evaluated in fracture propagation testing, the variability in the backfill constant increases beyond 200-percent. On this basis much of the variation evident in Figures 34 and 36 might be traced to differences in the flow response of the steels through its impact on the extent of plastic flow and equally the energy dissipated throughout the stretch-zone at the tip of the propagating crack.

It follows from the above discussion that the "backfill constant" is not constant – or even close to constant – even within one grade of steel for a narrow cluster of testing done at one full-scale test site. It is equally clear that the exponent m in Equation 14 previously considered to be

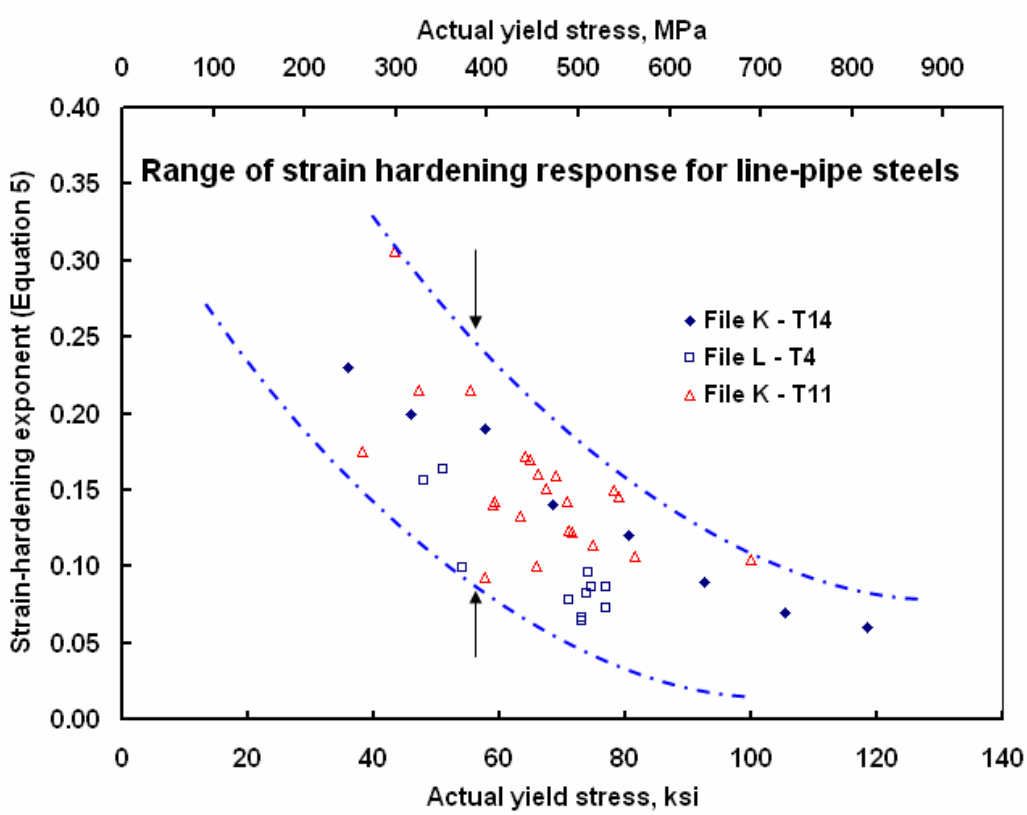

a) variation across a range of line-pipe steels

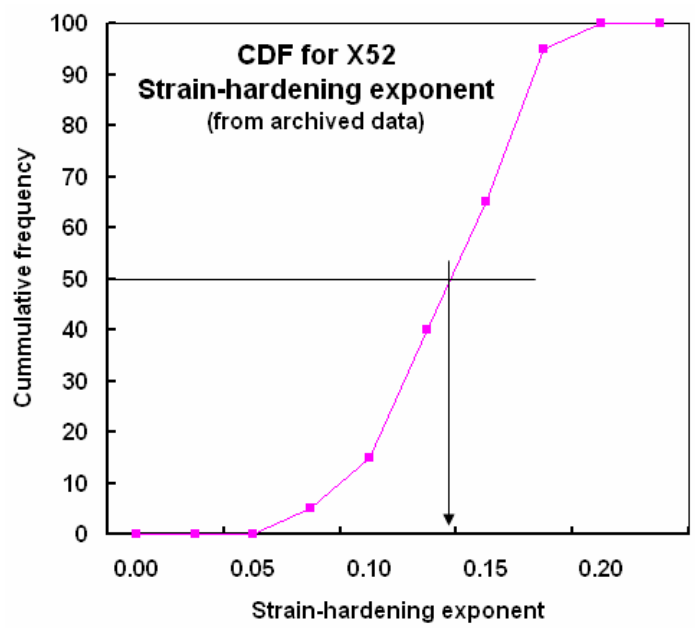

b) variation within a grade as a CDF

Figure 37. Variation in strain-hardening exponent

independent of the backfill apparently can differ by about a factor of two. Finally it is apparent that work is necessary to reformulate this aspect of the BTCM via creative analyses and experiments that target "backfill effects", to uncouple factors currently lumped into this constant and to more generally understand and characterize the role of backfill versus strain-hardening exponent and the related dissipation in the stretch-zone at the crack tip. However, this will require testing and practices other than have historically been used to evaluate backfill effects.

The transition from Equation 9 to Equation 10 also embeds use of the flow stress as a surrogate for the true fracture stress, and so assumes flow stress and the true fracture stress are correlated and linearly related. Figure 38 presents both true fracture stress and flow stress as a function of the UTS, which serves as a common parameter between the datasets shown, based on results derived from Battelle's archives. It is apparent from this figure that the flow stress and the true fracture stress correlate with the UTS, although there is some scatter. While their magnitudes are not comparable, because the difference is almost a constant multiplier this would not cause a related breakdown in similitude due to differences in the steels used in calibrating the backfill constant and those recently introduced. Thus, this specific expedient to facilitate use of the BTCM should not adversely affect predictions of propagation velocity or crack arrest.

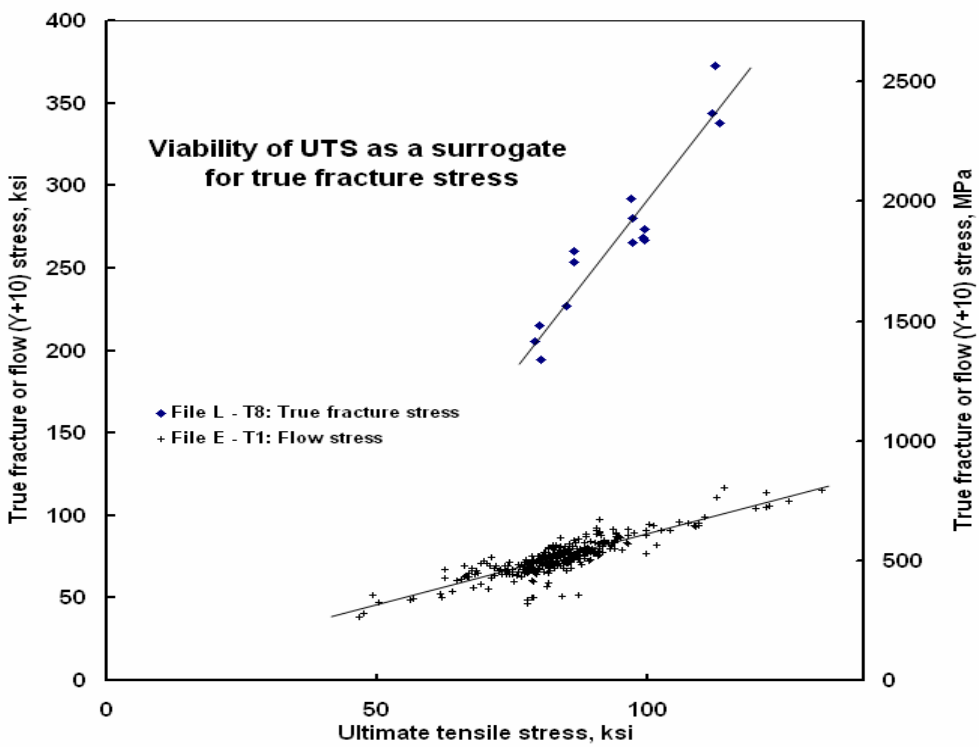

Figure 38. Flow stress as a surrogate for true fracture stress

Conclusion

While considered and termed a "constant" in developing the BTCM, the transition from Equation 9 to Equation 10 as presented herein has demonstrated this parameter to be neither constant nor related only to the backfill. Likewise, the exponent m in Equation 14, previously considered independent of the backfill was found to vary significantly with the backfill. It was determined that lumping the strain-hardening exponent into the backfill constant can drive errors

from 45-percent to in excess of 200-percent in this backfill constant. On this basis much of the variation evident in Figures 34 and 35 might be traced to differences in the flow response of the steels through its impact on the extent of plastic flow and equally the energy dissipated throughout the stretch-zone at the tip of the propagating crack. It was also found that the backfill effect coupled the effects of backfill with the effects of axial restraint – which should be uncoupled if the effects of backfill are to be understood and characterized.

Results that clearly showed that the "backfill constant" is not constant – or even close to constant – even within one grade of steel for a narrow cluster of testing done at one full-scale test site bring into question the trends evident in Figure 34, and their related scatter. Unfortunately, because it was difficult to determine plausible values of strain-hardening response for the historical database, it has been difficult to resolve this aspect within the scope of this project. However, as this single factor can bring sense to both fracture velocity and arrest behavior beyond that identified for toughness in regard to Equation 13, and such understanding is essential to address both existing pipelines and new designs, further resolution of this aspect must be a priority – particularly where possible pressure increases such as that via waiver are a possibility. Work is necessary to address this gap in any two-curve approach to fracture propagation and arrest via creative analyses and experiments, which should be formulated to bridge this gap more generally all formulations. This is a near-term need.

Reformulate the Propagation Velocity and Arrest Model Addressing Similitude

This section summarizes the approaches outlined in the prior section to address the breakdown of similitude as the BTCM was applied to increasing stronger and tougher steels. As has been detailed, this involved similitude lost in association with the CVN specimen, the arrest pressure, and the backfill constant.

Similitude Issues and Gaps

A range of similitude issues were identified and addressed, as follows.

An approach to establish similitude to extend the utility of the BTCM and other CVN-based arrest models was developed and validated. As it takes the form of a simple equation, presented as Equation 13, this "correction factor" is transferable and easily implemented. This was done within the BTCM, as well as in the present two-curve adaptation developed herein, which that replaced the fracture-curve of the BTCM with Equation 2 implemented in differential form. The effects of this correction can be significant, increasing the arrest roughness by more than 30-percent depending on the application. This correction has been validated via blind accurate predictions for full-scale testing.

An approach also was established to address the breakdown in similitude associated with the definition of arrest pressure. This similitude assessment considered both the role of flow properties and the manner arrest pressure was defined, which showed a broad and varied breakdown in similitude that varied with the line pipe's geometric properties, and its mechanical and fracture properties. As this similitude breakdown was not simply trended, the extent of this breakdown could not be simply expressed analytically. Accordingly, this breakdown was offset by embedding a viable approach to correct the current arrest-pressure definition via PAFFC. This quasi-static criterion was embedded into the BTCM, as well as in the present two-curve adaptation developed herein, which has replaced the fracture-curve

of the BTCM with Equation 2 implemented in differential form. Comparison of predictions with this revised formulation with the BTCM indicates this correction will selectively drive a small increase in arrest toughness.

Perhaps the greatest breakdown in similitude was related to what was termed the backfill constant in developing the BTCM – but was found to be neither constant nor related only to the backfill. Likewise, the exponent m in Equation 14, previously considered independent of the backfill was found to vary significantly with the backfill. It was determined that lumping the strongly varied strain-hardening exponent into the backfill constant underlies a breakdown in similitude that can drive errors from 45-percent to in excess of 200-percent in this backfill constant. On this basis much of the variation evident in Figures 34 and 35 might be traced to differences in the flow response of the steels through its impact on the extent of plastic flow and equally the energy dissipated throughout the stretch-zone at the tip of the propagating crack. It was also found that the backfill effect coupled the effects of backfill with the effects of axial restraint – which should be uncoupled.

The results clearly showed that the "backfill constant" is not constant – or even close to constant – even within one grade of steel for a narrow cluster of testing done at one full-scale test site. Unfortunately, because it was difficult to determine plausible values of strain-hardening response for the historical database, it has been difficult to resolve this aspect within the scope of this project. However, as this single factor can bring sense to both fracture velocity and arrest behavior beyond that identified for toughness in regard to Equation 13, and such understanding is essential to address both existing pipelines and new designs, further resolution of this aspect must be a priority – particularly where possible pressure increases such as that via waiver are a possibility. Work is necessary to address this gap in any two-curve approach to fracture propagation and arrest via creative analyses and experiments, which should be formulated to bridge this gap more generally all formulations. This is a near-term need.

Summary: Reformulation and Resolution of Similitude Issues and Gaps

It follows that several aspects of the BTCM were identified as failing to ensure similitude if this model was used much beyond the empirical basis for its calibration. These similitude gaps developed in association with three aspects of Battelle's two curve approach:

1. the CVN specimen used to measure fracture resistance,
2. the arrest pressure prediction, and
3. the definition of the backfill constant C and m.

The first two issues were fully resolved. However, while causes for the breakdown of similitude were identified in regard to the third similitude issue and a plan for resolution identified, gaps remain as implementing this plan was beyond the work-scope of this project.

Significantly, the "two-curve concept" that underlies this 1970s formulation for fracture propagation and arrest was however not associated with any similitude issue. Potential issues associated with the BTCM approach to implement the two-curve concept were recognized in formulating the proposed work plan for this task. Consequently, related issues were addressed in reformulating the fracture curve as outlined in Equation 2, and gaps bridged through the implementation of this equation in differential form. This approach determines fracture

propagation and arrest by numerical integration along the pipeline until the arrest conditions are satisfied.

The ensuing sections of this report present:

- perspective for other potentially important factors,
- a stopgap model for fracture propagation and arrest, and its validation, and
- a first-principles look at dissipation leading to arrest, closing with reflection on the role of dissipation due to the creation of crack surface as the basis for analysis of fracture arrest.

The Plausible Role of Elastic Response

This section of the report considers the stress-strain response of the pipe material and the significance of the elastic response relative to the plastic response.

Background

Consideration of the trends in Figures 30 and 31 respectively show the differences in the stress-strain response typical of X-52 steel into the 1970s as compared to recent X100, covering both the hoop (transverse) and axial (longitudinal) orientations. This comparison shows that the X52 response is isotropic, and exhibits significant strain hardening in route to the UTS along with significant post-yield and post-collapse plastic flow under displacement control conditions. In contrast, the X100 is anisotropic, and exhibits very limited strain hardening with no post-collapse flow response under the same control conditions. Accordingly, the X100 steel shows rather limited capacity for plastic deformation in contrast to X52, and so has a reduced capacity to blunt a running crack. Likewise, the X100 steel has reduced capacity to spread plastic deformation in the zone ahead of this crack or in the lateral stretch-zone at its flanks as tearing occurs leading to crack advance.

Whether or not similitude is adversely affected by the reduced role of plastic deformation for the higher-strength grades as compared to the scenario of the mid-1970s depends first on whether the trends in Figure 30 and 31 are respectively characteristic of the flow properties embedded in the BTCM versus those for more recent higher-strength grades. Figure 39 provides perspective for the changes that have occurred in moving from X52 in the timeframe of the BTCM toward the X100 and beyond circa recent developments. While several experimental steels are included in this archives-based plot, including a quench and temper (Q&T) based EX100 in the 1969s, such strength levels were impractical based on Q&T processing when used in seam-welded line pipe that in a pipeline would be subject to cathodic protection.

Analysis

Steels for use in pipelines must balance strength with ductility, toughness, weldability, and show limited susceptibility to hydrogen effects that might develop in association with the cathodic protection (CP) system used to limit corrosion on pipelines. History indicates the late 1960s into the mid 1970s opened the door to commercially produced line pipe made of high-strength low-alloy (HSLA) steels that satisfied these requirements. Significant changes in steel-making also emerged, particularly in regard to continuous casting. As the HSLA class of steels and their related processing became strength-limited, steel makers followed this class of steels by a class of commercially produced line pipe processed via thermal-mechanical accelerated-cooled and controlled-roll schemes with chemistries matched to these practices. This transition saw the shift from ferrite-pearlite microstructures into bainitic microstructures for grades upward of X100,

with the transition to X120 coming via a shift toward a martensitic-like microstructure. Given these transitions, the traits evident for the X52 can be viewed as common for grades the order of X60 and X65, and possible some early higher-strength grades with the realization that Y/T increased as strength increased. In general, the transition toward bainitic microstructures starts the trend toward the traits of Figure 31, with even less ductility logically evident for martensite-like structures.

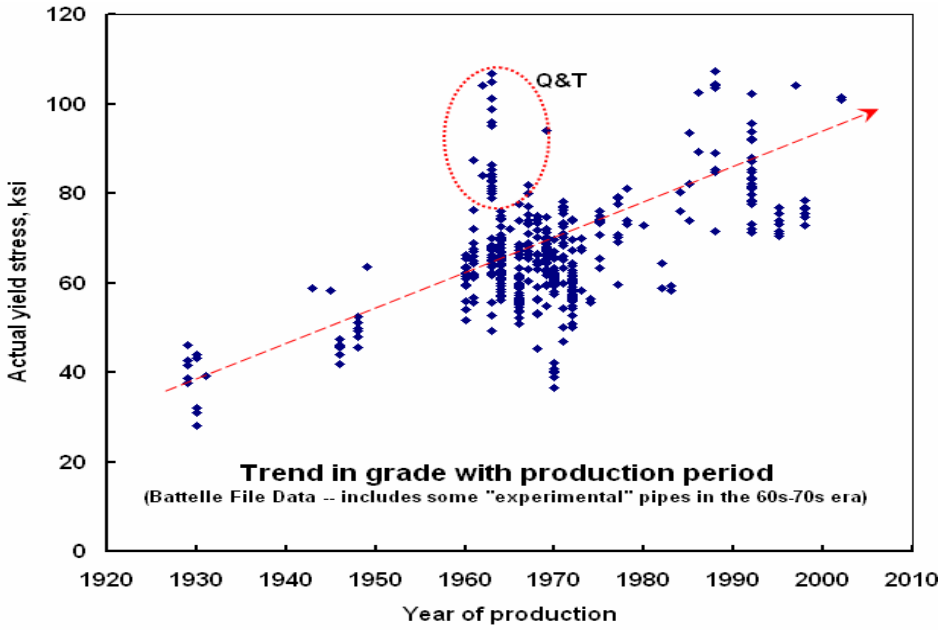

Figure 39. Trend as strength evolved in terms of actual yield stress

It follows that whether or not similitude is adversely affected by the reduced role of plastic deformation for the higher-strength grades as compared to the scenario of the mid-1970s can be assessed in general relative to the trends in Figure 30 and 31.

Regardless of whether strain hardening underlies causes the anisotropy for the X-100 steel, it is clear that the elastic response is a relatively large fraction of the total strain to failure for this grade as compared to that for the X52. As elastic strain energy stored in the pipeline steel creates the driving force for fracture, and this increases as the capacity of the grade to deform elastically increases, this factor might contribute to a breakdown in similitude between the 1970s BTCM and the behavior of more recent higher-strength grades. Such a breakdown in similitude could underlie the shortfall of the BTCM predictions of arrest toughness discussed in regard to Figure 23. However, pressure-induced wall stress is directly embedded in both the BTCM and the modified two-curve concept pursued in this reporting. Moreover, the velocities of propagating fractures in X100 are not high in regard to those observed for the X52, which would be anticipated if the driving force for propagation was uniquely responsive to the increased elastic strain energy. Finally, as was evident in the part of Figure 6 that dealt with the highest-strength grades and the X100 results available when this scenario was evaluated, which is shown here on expanded scales as Figure 40, the propagation response of at least this result is well characterized by the present implementation of the two-curve concept. In reference to Figure 40 it is clear the current implementation of the two-curve concept both predicts trends in propagation velocity and can identify when the arrest conditions are satisfied.

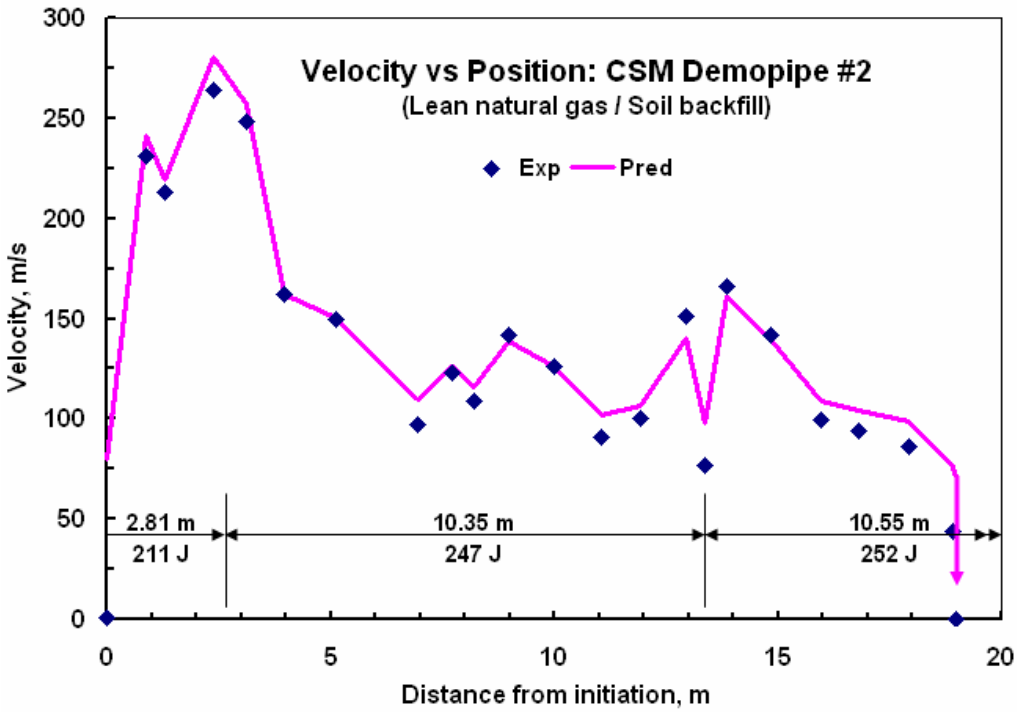

Figure 40. Predicted versus observed propagation response for one X100 test section

Conclusion

Accordingly, one can conclude that differences in stored elastic-strain energy, and other aspects unique between the flow response for Grade X52 versus X100 (i.e., between Figures 30 and 31) are not a factor – aside from the issues already identified in light of the backfill constants *C* and *m*.

The Role of Flow-Induced Dissipation

This section considers the relative significance of flow-induced dissipation local to the crack as the tip blunts prior to tearing as well as throughout the plastic stretch zone in advance of the crack front and lateral to it.

Background

The significance of flow-induced dissipation has been considered as a metric for fracture propagation and arrest since the mid 1970s. This early work primarily at the laboratory of US Steel[(e.g., 93,94)] measured the permanent deformation ahead of and on the flanks of propagating cracks and sought correlations with fracture velocity. Such work showed scattered correlations with fracture velocity, and addressed plausible correlations with various definitions of strain, including consideration of the forming-limit diagram, as well as displacement-based stretch zones. Gray continued this line of thinking, developing expansive datasets illustrating strain distributions in advance of the crack and through its lateral stretch-zone. Again, scattered correlations developed, but for much broader datasets that covered some higher-toughness steels in grades through X75. Lateral stretch zones in some tests were indicated to span the order of 20-percent of the circumference, although the intense flow associated with the cracking was more localized. It follows that significant energy was being dissipated due to this plastic deformation. What was not clear from this work was the differential response along the test

section as the cracking propagated, or within the arresting joint in the vicinity of arrest. On this basis it is difficult to uniquely associate this flow-induced dissipation with the decay in fracture velocity or with the conditions that trigger the abrupt change in velocity evident at the onset of arrest, as was illustrated in Figures 20 and 21.

Analysis

Comprehensive analysis of energy dissipation during running fracture has been considered since the early 1970s, initially for the evaluation of running brittle fracture[95]. Apparent success in that work led to analysis of dissipation contributing to crack arrest of running ductile fracture shortly thereafter[54,96]. Since that time Reference 55 provides perhaps the most comprehensive assessment of the many components of dissipation that can contribute to arrest. The conclusion of that work indicated these were dominated by "stretch energy", which embeds the parameters noted in the background to this section.

Early work proposing CTOA as the means to assess the fracture propagation response of a pipeline likewise considered plastic dissipation local to the crack tip[e.g., 97]. Mapped onto laboratory specimens, such analyses showed dissipation due to plastic flow well in excess of that associated with the creation of new crack surface, the extent to which increased as toughness increased. It is apparent in this context that the trends introduced earlier in Figure 28 for the CVN specimen were paralleled in other laboratory specimens, although the balance between the energy components was shifted slightly. As briefly discussed earlier in regard to Figure 28, the evolution in steel-making that lead to increased fracture toughness drives a shift to increased dissipation due to plastic flow. In turn the relative mix of flow-induced dissipation increases at the crack-tip and the adjacent stretch-zone as blunting develops leading to tearing whereas the fraction of dissipation due to continued tearing diminishes. In contrast, for lower-toughness steels flow-induced dissipation is near zero.

While at the scale of milliseconds, the time required to achieve the true fracture strain local to the crack tip facilitates the spread of the stretch zone, with this time increasing as toughness increases given the rather strong dependence of true fracture strain on toughness shown earlier in Figure 26.. As this blunting must continue to occur as the crack-tip advances, the effect of flow-induced dissipation must increase as the toughness increases – with this dissipation slowing the crack. As the toughness necessary for arrest is approached, the extent of flow-induced deformation becomes more expansive, with larger-scale blunting leading to more dissipation over a still longer time interval. It follows that flow-induced dissipation becomes autocatalytic with the onset of arrest, which points to arrest occurring over very short distances even though the toughness is constant over this distance. Moreover, because it is autocatalytic flow-induced dissipation affects arrest in even shorter distances as the toughness available for arrest becomes large compared to that necessary for arrest.

While flow-induced dissipation is autocatalytic as just discussed, propagation response tending to arrest associated with "dissipation per increment of crack advance" remains constant a slow steady process. The coupled effects of flow-induced dissipation and dissipation per unit-area of crack advance are embedded in the fracture curve of Equation 2. Their effects are evident as typically shown in Figure 41, which plots crack velocity as a function of position along a typical full-scale test pipe. The zero-length for this figure is the transition into a pipe joint with incrementally larger toughness. It is apparent from this figure that there is sharp initial drop in propagation velocity that is followed by a steady decay with distance traveled toward the end of

this test pipe. Analyses indicates the sharp initial drop in crack velocity reflects the flow-induced dissipation due to the slightly increased toughness experienced by the crack as it enters this pipe joint. Beyond this rapid drop in velocity, a slow continued decay in velocity is evident that reflects the dissipation due to the creation of new crack surface – for otherwise the same toughness that caused the sharp initial drop. While overall the effects of these two sources of dissipation are comparable, the trends in Figure 41 indicate flow-induced dissipation has orders of magnitude greater effect per unit length propagated than does the dissipation associated with creating new crack surface.

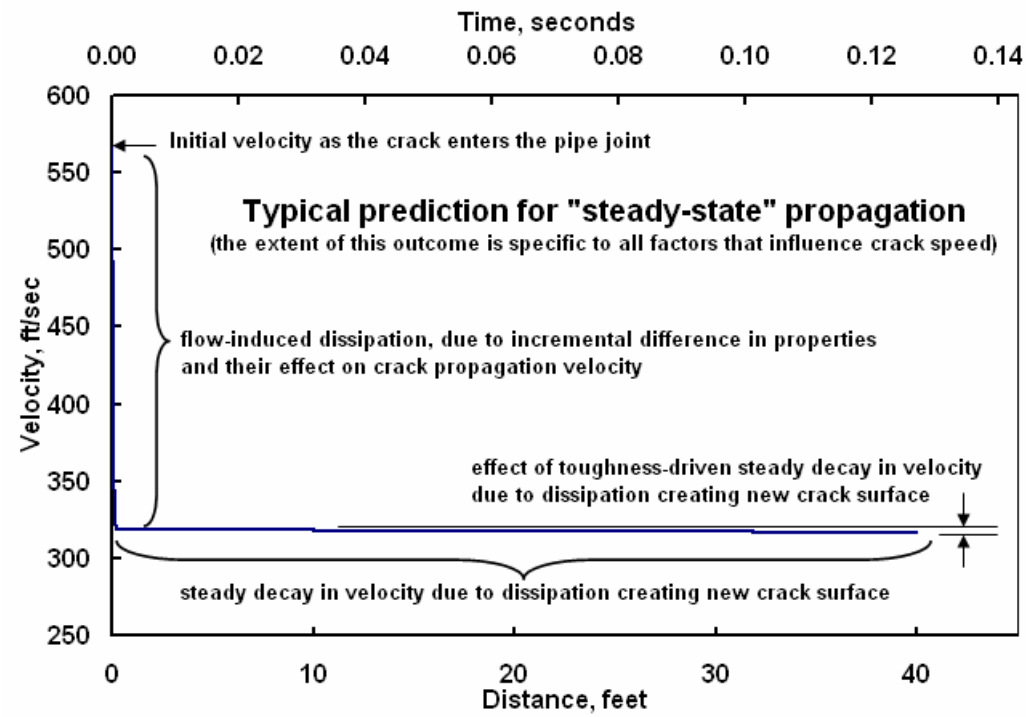

Figure 41. Typical illustration of simulated crack-velocity response within a test pipe

Conclusion

It follows that flow-induced dissipation has orders of magnitude greater effect per unit length propagated than does the dissipation associated with creating new crack surface. Further, it follows that the autocatalytic nature of flow-induced dissipation following the onset of arrest triggers arrest over a very short distance. Finally, it follows that because it is autocatalytic this flow-induced dissipation can affect arrest in even shorter distances as the toughness available for arrest becomes large compared to that necessary for arrest. In contrast, while flow-induced dissipation is autocatalytic, dissipation per increment of crack advance is not – leaving its effect to be rather a slow steady process.

Stopgap Fracture Arrest Model

The Stopgap Formulation

Thus far, a newly defined "fracture curve" and the now-proven robust "gas curve" of the BTCM have been implemented within the two-curve concept in concert with approaches developed to address the similitude concerns that existed for the BTCM. The fracture curve characterizes the

crack velocity in terms of the dynamic gas pressure while the gas curve models the pressure versus velocity response of the gas as it decompresses due to the propagating fracture. This new two-curve formulation has been validated thus far primarily in terms of correct predictions of propagation velocity, although consideration also was given to select arrest predictions. While definition of the "backfill constant" remains an issue that complicates developing future control plans for advanced design pipelines and the design of fracture arrestors, it is much less a factor for the present approach in predicting fracture behavior in full-scale testing. Applications of the model in that context have proven it quite reliable, as was illustrated for the second CSM X100 "Demopipe" test in Figure 40. Not only were the trends in propagation velocity faithfully predicted, arrest likewise was correctly predicted – which can be done within meters of the actual location. It follows that a viable approach has been formulated to predict fracture propagation and arrest, which also has been recast for the design of integral arrestors.

This section continues validation of the new two-curve formulation, focusing on predictions of arrest versus propagation. The validity of the model is presented graphically, and expressed in terms of the arrest/propagate outcomes versus actual test results. Implications of this section for fracture propagation and the distance required for arrest in regard to the existing pipeline system are discussed in the next section.

Approach

As mentioned previously, typical full-scale pipe tests being used to evaluate the viability of the model as developed consist of a series of pipe segments organized in a test section to simulate the response of a pipeline. A running crack is initiated centrally with propagation running in opposite directions, with crack position measured versus time using trip-wires placed at known locations along the test section. These data were used to estimate the velocity of the crack as functions of the pipe geometry and material, the backfill, and the type of gas used to pressurize the pipeline. A small cross-section of such data was used to train the fracture curve of Equation 2 expressed in differential form, which then couples with the gas curve and the other analytical aspects to simulate the fracture response as a function of time or position along each pipe joint or the pipeline. This formulation is fully general in terms of line-pipe properties (wall thickness, pipe diameter yield, ultimate, toughness, and their distribution along the pipeline), operation and upsets in terms of the transported fluid properties (temperature, composition, pressure), and the backfill conditions. The same technology has been used to design arrestors, although its implementation is somewhat different.

Steady State Propagation versus Reality

As indicated above and discussed earlier, Figure 40 was introduced to demonstrate that the two-step concept as implemented with a new fracture curve and consideration of similitude can predict the propagation velocity and arrest for X100 in contrast to the trends for the BTCM that showed significant miss-predictions for arrest versus propagate. In contrast, the Figures 19 and 41 illustrate the fracture velocity as characterized as a "steady-state" process wherein the toughness-dependent effect of dissipation due to the creation of new crack surface causes a gradual decay in crack velocity. As detailed in reference to Figure 3X, the effect of the flow-induced dissipation is much more profound, as it can in alter the crack velocity orders of magnitude faster that can dissipation due to creation of new crack surface. Significantly, the observed crack velocity for the early lower-toughness steels follows trends like that in Figures 19 and 41. This observation is consistent with Figure 28 and the related discussion which indicates

that arrest in such lower-toughness steels in dominated by the toughness-dependent effect of dissipation due to the creation of new crack surface – that as the velocity data tends to track a more gradual decay in crack velocity. The gradual decay in velocity associated with such steels is toughness dependent, which as the toughness decreases increasingly focuses the dissipation at the crack tip. In the limit, as toughness diminishes the crack simply continues to propagate until an arrest joint is encountered – which gave rise to the term "steady-state" propagation. This term continues to be applied to fracture propagation in pipeline scenarios – even though as Figure 40 shows the process is anything but steady.

It follows that the trends for X100 shown in Figure 40 must be viewed as "non-steady-state" propagation. As the propagation process becomes increasingly non-steady – similitude between the steady-state models and the reality is increasingly eroded. The critical problem is that a steady decay with periodic steeper reductions in velocity due to incremental changes in toughness moving from one pipe joint to the next – as occurs in steady-state models cannot capture the periodic instabilities that include spike increases in velocity. That is, consideration of the trends in Figure 40 as a steady-state process cannot account for the periodic instability in cracking and the related spike increases in crack velocity.

The spike increases in crack velocity keep the crack propagating until the arrest conditions are satisfied. Because the crack continues to propagate further along into the full-scale test section until the arrest conditions are satisfied, predictions of this arrest occurring earlier in the test-section based on a steady process always underestimate the required arrest toughness. This is exactly the trend evident earlier in Figure 28. Significantly, while toughness is a factor driving no-steady propagation, the data indicate that other factors also contribute to this process. The analytical aspects of this formulation likewise indicate other factors are involved, such as variability in the strain-hardening exponent, which enters through its impact on the local extent of crack-tip blunting and the adjacent lateral stretch-zone. While the strain-hardening parameter has been addressed in the present formulation, its effect must be more explicitly addressed, along with the reformatting of what has been addressed via the "backfill" constant.

Further illustration of the extent of non-steady behavior that can develop in X100 is illustrated in Figure 42, which has the same format as Figure 40 and presents results for the first CSM "Demopipe" experiment. Trends for this full-scale propagation test are not unlike those seen in Figure 40. Each of the transitions between pipe joints beyond initiation is evident as a spike in velocity. The expected overall increase in cracking velocity as toughness is decreased is evident, and correctly predicted, as are the other major swings in crack velocity. Whereas the two-curve concept as implemented in this work correctly predicted "arrest" for the scenario in Figure 40, it also correctly predicts propagate for this test – although the conditions for arrest are being approached.

It follows from evaluation of these X100 full-scale propagation tests that successful prediction of crack propagation velocity requires a non-steady formulation, and consideration of flow-induced dissipation as well as crack-surface-related dissipation.

Model Validation in terms of Arrest versus Propagate

The validity of the new two-curve non-steady-state formulation was evaluated by comparing the results from full-scale tests with predictions made using this formulation. Two databases can be used for this comparison. One is not broadly published, which deals with a compilation of full-scale test results in terms of propagation velocity as a function of position within a pipe joint or

along the test section subject to the testing parameters. This database considers all the pipe joints used in a full-scale test other than those used for initiation. Even after ignoring the initiation pipe, the dataset contains more than one thousand crack velocity versus crack location data-pairs, all of which have been considered in this subsection to assess / validate the new two-curve formulation. The second database is more broadly available. It presents arrest versus propagate results again in terms of the full-scale testing parameters, but tends to focus on the terminal pipe in each test section. As such, it is somewhat smaller in size, roughly in proportion to the ratio of test pipes to terminal pipes in each full-scale test. While there is some overlap among the test conditions evaluated, there are many cases for which this overlap does not occur. This second database of "arrest versus propagate" results has been compiled and is available in Appendix E of Reference 5.

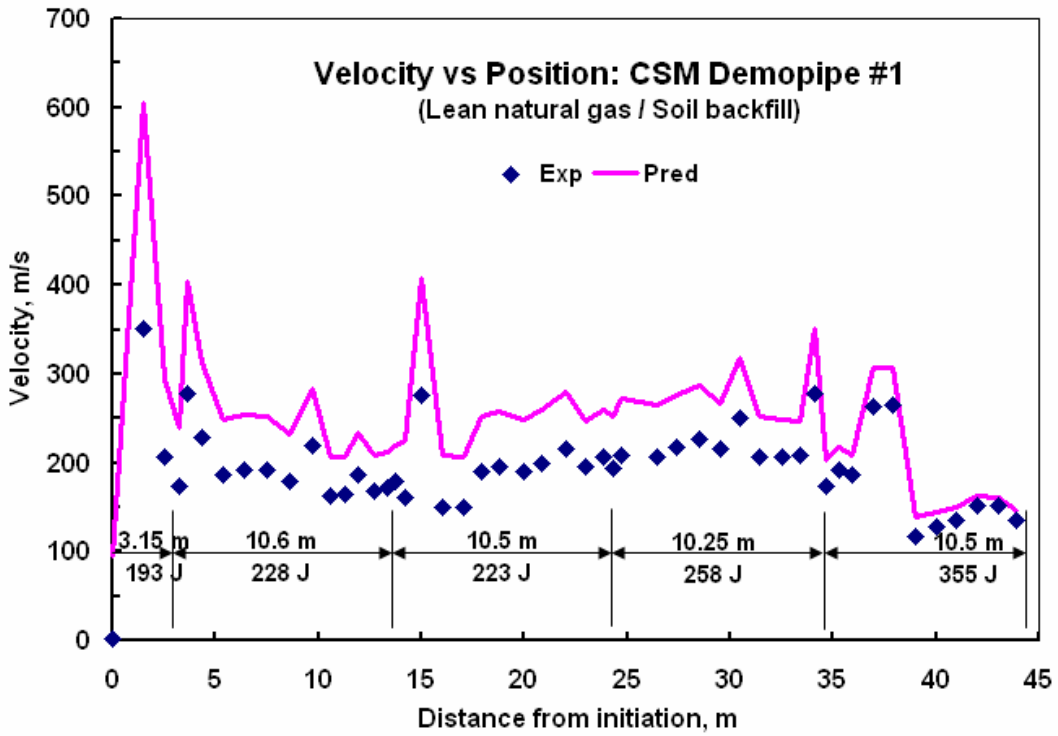

Figure 42. Predicted versus observed propagation response for another X100 test section

The quality of the model was assessed via a comparison of the experimental observations to the model predictions. The results of this comparison are presented for the first database in tabular format, as summarized in Table 2, whereas Figure 43 is used to present the results for the second database.

Table 2a presents the raw comparison where as Table 2b presents the results as a percentage. This tabulation represents rich gas two-phase decompression along with single-phase cases for grades through X100 and toughness in excess of 250 J. The full-scale results that caused problems for the 1970s BTCM in regard to Figures 22 and 23 were targeted for inclusion in this database. For purposes of this tabular reporting the predictions were divided into four categories depending on whether a prediction was correct or incorrect (i.e., good or bad) and whether it was an arrest or propagate prediction. "Good-a" indicates an accurate prediction of an observed arrest. "Bad-p" indicates an incorrect prediction of an observed propagation, and so on. It

should be noted that "Bad-p", an incorrect prediction of a propagating crack is a conservative prediction error. Whereas an incorrect prediction of an arrest when the crack was observed to propagate was a non-conservative prediction, as such "Bad-a" outcomes were the primary concern and the "Bad-p" outcomes were a significant but lesser concern.

The tabulation indicates the new two-curve formulation leads to non-conservative predictions in only ~15-percent of the cases. This level is roughly comparable to that historically achieved by the BTCM – but prior to the advent of tougher higher-strength steels and the similitude issues evident in Figure 22 and higher-strength in Figure 23. If those scenarios were included for the BTCM its success rate falls sharply with the order of 80 percent being non-conservative.

While not apparent from the tabulation, the modest number of non-conservative predictions was achieved without bias to grade or toughness. These tabulated results show acceptable predictions were made for ~85 percent of the cases – in spite of inclusion of grades through X100 and toughness in excess of 250 J. Given the level of success of this new approach is comparable to the best achieved historically by the BTCM – prior to the advent of higher-toughness higher-strength steels, one can conclude this success rate reflects a significant improvement through the technology evolved through this project.

Table 2. Comparison of model predictions versus observed test outcomes.

a) as number of test observations

Good-p	Good-a	Bad-p	Bad-a	Total
788	86	69	158	1,101

b) as percent of total test observations.

Good-p	Good-a	Bad-p	Bad-a	Total
71.6	7.8	6.3	14.4	100

Figure 43 presents results of arrest versus propagate predictions for the database compiled in Appendix E of Reference 5. As for the tabulated evaluation, this database includes rich gas two-phase decompression results along with single-phase cases and covers grades through X100 and toughness in excess of 250 J. The y-axis in this figure represents the energy predicted for crack arrest, while the y-axis represents the energy observed for arrest. Depending on the design of the test, actual arrest values can fall anywhere below the one-to-one line that indicates exact predictions. Predicted arrest results that fall below this line are accurate predictions or Good-a in the language of the tabulations, while arrest predictions above the line were noted in the table as Bad-a, which because more toughness was predicted as compared to required are conservative and so an acceptable outcome. Predicted propagate results that fall above the one-to-one line are accurate predictions, labeled Good-p in the language of the tabulations. Propagate predictions that fall below the line reflect inadequate toughness and so would be non-conservative, being labeled Bad-p for purposes of the tabulation.

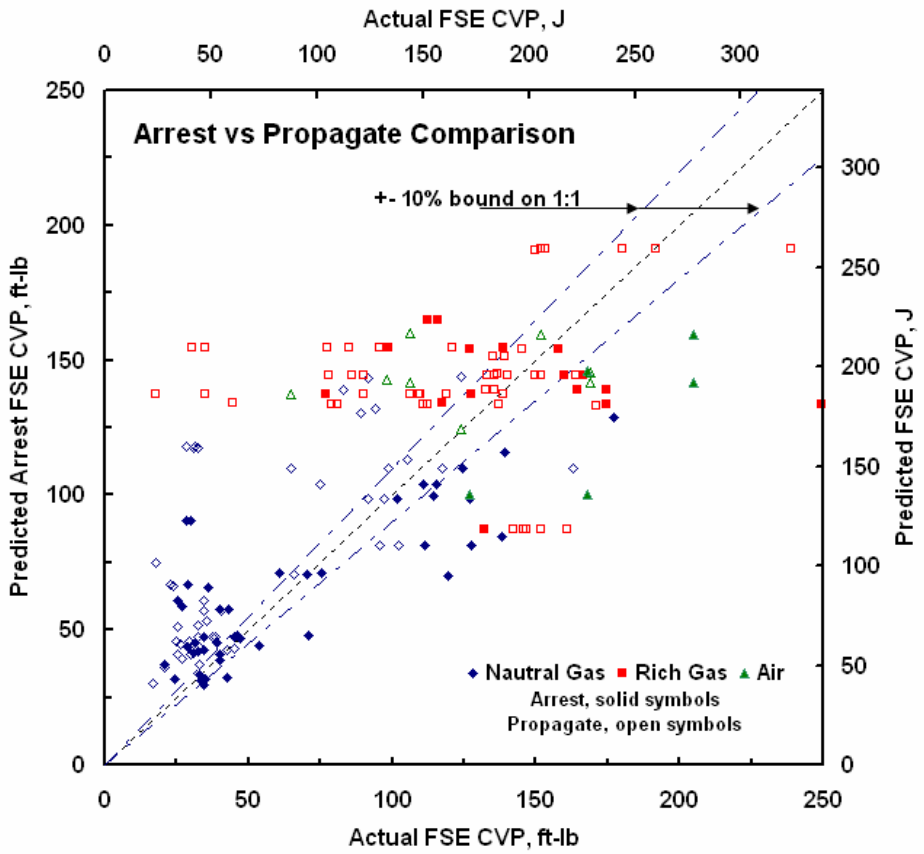

Figure 43. Arrest versus propagate comparison for terminal pipe joint

As is apparent from the figure the results for this database are comparable to that in the tabulation. There are crossover cases, with a roughly comparable balance of acceptable versus non-conservative results. Again, as for the table there is no consistent bias with any of the parameters considered to drive or arrest fracture propagation.

While no bias was found for either database in regard factors typically considered as drivers or metrics for resistance to fracture propagation or arrest, a still large fraction of the predictions was found to be non-conservative. Part of the reason for this lies in the observation that the form of the backfill constant and its role in the two-curve concept makes tracking its influence difficult. Yet, as Figure 36 emphasizes the backfill constant can drive significant scatter and so is capable of causing rather large errors. As was discussed in the section that considered backfill and the definition of the related constants, what has been termed the backfill constant reflects both the backfill and the line-pipe steel, and is anything but constant. Moreover, the exponent in Equation 14, which has been considered constant and independent of the backfill is neither. Its value in regard to Figure 34 differed by almost a factor of two depending on whether the backfill was soil or "air". It is critical to fully understand the many facets of this backfill situation if the potential of and benefits from this stopgap model are to be realized.

Conclusion

The section evaluated the validity of the new two-curve non-steady-state formulation by comparing results from full-scale tests with its predictions. Two databases were used – one that is broadly published that presents arrest versus propagate results for the terminal pipe in the test sections of full-scale tests – and a second compiled for present purposes in terms of propagation velocity as a function of position within a pipe joint or along the test section subject to the testing parameters. These databases include rich gas two-phase decompression along with single-phase cases for grades through X100 and toughness in excess of 250 J. The second database compiled for present purposes targeted full-scale results that caused problems for the 1970s BTCM in regard to Figures 22 and 23.

The results of this comparison demonstrated the validity of the new two-curve formulation in terms of accurate predictions of fracture propagation behavior and comparisons of arrest versus propagation. The results showed acceptable predictions were made for ~85 percent of the cases – in spite of inclusion of grades through X100 and toughness in excess of 250 J. This success level is comparable to the best achieved historically by the BTCM – prior to the advent of higher-toughness higher-strength steels. When such scenarios are included, the success rate for the BTCM falls sharply with the order of 80 percent being non-conservative.

It was shown that the fracture propagation behavior of pipelines can vary from "steady-state" through "non-steady-state" conditions, depending on the line-pipe steel involved, and related factors. It was noted that steady-state models cannot capture the periodic instabilities that include spike increases in velocity under non-steady conditions. Because these spike increases keep the crack propagating longer than considered by steady-state models predict, such models will always underestimate the required arrest toughness.

The stopgap model represented by two-curve concept as implemented in this project correctly predicted "arrest" as well as "propagate" by tracking the fracture propagation velocity throughout the test sections of full-scale tests. These successful predictions validate this model and demonstrate that prediction of crack propagation velocity requires a non-steady formulation, and consideration of flow-induced dissipation in addition to less important crack-surface-related dissipation. Given the success achieved relative to the historic success of the BTCM one can conclude a significant improvement results through the technology evolved through this project. In spite of this it is critical to fully understand the many facets of this backfill situation if the potential of and benefits from this stopgap model are to be realized.

Energy-Based Framework for Dissipation

Over the years analysis of energy dissipation has provided insight into factors that drive running fracture. This section considers possible sources of energy dissipation in running ductile fracture in light of the new "fracture curve" as implemented within the two-curve concept. At a high level, within the pipeline dissipation can occur via deformation, crack initiation, and crack propagation, whereas for the "system" containing the pipeline the anchoring of the pipeline and the backfill are considerations.

Background

Comparable to the situation discussed in the Approach and Deliverables section for CTOA, papers have been written for decades that seek to quantify the energy available to drive

propagation in contrast to that sources of dissipation that contribute to arrest for system parameters where propagation is more or less "steady".

The use of energy as a means to understand fracture traces back to the 1920s and the now classic work of Griffith. Griffith noted that when a crack is introduced to a stressed plate (or shell) of elastic material, a balance must develop between the decrease in potential energy and the increase in surface energy due to the presence of the crack. Equally, an existing crack would grow by some increment if the necessary increment in surface energy was supplied to the system in balance. In analogy to Griffith, in the late 1960s Irwin and Corten established this balance for the brittle fracture arrest stress that in turn relates to pressure in the form[100]:

$$\sigma_{a\,B} = \frac{P_a\ R}{t} = \sqrt{\frac{R_F\ E}{\pi\ R}} \qquad 15$$

where in addition to the previously defined symbols:

R_F = the CVN energy at S_F, the associated shear-area fraction, in-lbs/in^2 or J/mm^2,

SF= is the expected ductile or shear fraction for the fracture surface, and

$\sigma_{a\,B}$ = the brittle-fracture-arrest stress, in ksi or MPa.

The underlying derivation assumes that strain energy in the pipe wall is equal to the energy required to create new crack surface during steady-state propagation and LEFM conditions.

Equation 15 indicates that the arrest pressure or hoop stress is proportional to the square root of toughness (fracture resistance R_F, as defined above). Toughness and shear area drop rapidly below the transition temperature. Therefore, fracture arrest generally requires a substantial drop in pressure to avoid long-running brittle fractures. At temperatures much more than 40ºF (22ºC) below the fracture propagation transition temperature it becomes difficult to accurately predict the brittle fracture appearance such that this formulation is not likely to be accurate. Likewise as there is considerable scatter in the prediction of the shear area over the DBTT region, caution is essential in implementing the results of Equation 15.

Since the work of Irwin and Corten, several have tried to parallel their LEFM formulation by considering the many processes that contribute to fracture propagation in pipelines[(e.g., 52-56, 95-97)]. Energy-based schemes are central to engineering mechanics – consequently such methods are broadly employed, including other applications to pipelines wherein energy methods have been applied to assess the severity of mechanical damage.

For propagating fracture the system energy balance that must be addressed in this context is very complex. As was discussed in the Approach and Deliverables section, characterizing fracture propagation and its arrest couples three complex processes that involve:

9. the mechanics and dynamics of the soil-structure interaction,
10. the gas dynamics during decompression, and
11. the dynamic fracture process in the pipe.

Each of these processes is nonlinear and so taken alone are very complex. On this basis the interaction of two much less three of these processes is even more complex. Thus an approach was adopted that sought to exploit value of past investments in full-scale testing and related technology development with a view to identify and assess plausible paths forward. This section

begins this identify and assess cycle with analysis of each of these complex processes relative to the two-curve concept as it has been implemented thus far.

Analysis

The two-curve concept directly addresses Items Two and Three on the above list, considering each as independent processes that are coupled through the backfill constant, which addresses Item One in this list. As such, the two-curve concept facilitates isolation of each process to the extent possible. However, as it has been implemented thus far – in the BTCM and here as well – consideration of Item One has commingled facets of at least Item Three with those of the soil-structure interaction in the way the backfill constant was defined and calibrated. As the earlier similitude consideration indicated the gas-dynamics process of Item Two can be well represented by "GASDECOM"[4] embedded in the BTCM, and Item Three in spite of its coupling to the backfill constant now can be reasonably characterized, the remaining work must focus on the backfill constant and the uncoupling it currently embeds. Thus, there is a path forward that facilitates an engineering approach to fracture propagation. Consistent with the Approach and Deliverables section this path forward is based on the premise that fracture arrest occurs through dissipation mechanisms in addition to crack-propagation resistance – and the premise that arrest as toughness increases as a process that transitions from a propagating crack to a running tensile instability. While these views differ substantially from the historical view that RDF can be characterized simply in terms of dissipation through the creation of new surface leading to crack propagation, they were found through this work to be consistent with propagating fracture behavior across the range of line-pipe scenarios – past and present. More critically, these views are compatible with future scenarios as the scope of past and present embeds a mix of fracture and deformation behavior that ranges in combinations for both deformation and fracture from brittle to ductile. It is more likely in this context that GASDECOM will become limited as new higher-pressure pipelines are anticipated, or transported product compositions shift.

Recognizing that an apparently viable framework has evolved herein to address the "fracture curve", aspects of this framework are explored to gain further insight into and certainty for the path forward. As the above comments in the context of the two-curve concept are applicable in general, the comments that follow while specific to this two-curve concept are equally viable for analytical, numerical, or other schemes to address and couple the above-noted three processes that underlie fracture propagation and its arrest.

As discussed previously in reference to Equation 2, at a high-level dissipation[5] within a pipeline is associated with deformation, crack initiation, and crack propagation, while the "system" containing the pipeline includes considerations such as the anchoring of the pipeline and backfill. This subsection evaluates plausible sources of energy dissipation in running ductile fracture in light of the new "fracture curve" as implemented within the two-curve concept.

---

[4] While the basic formulation circa the mid-1970s was sound, the numerical representation of this formulation to address current computation power and other aspects must be addressed – this update began at Battelle in the mid-1990s motivated by work with the transportation of specific HCLs and the ultra-rich gas scenario of the Alliance Pipeline.

[5] The focus here is dissipation, which is but one aspect of what that must be tracked in a general energy-based approach to assess fracture propagation. The purpose here is to evaluate aspects of dissipation rather than discuss a comprehensive energy-based formulation.

Sources of dissipation within the pipeline – deformation, crack initiation, and crack propagation – have been quantified earlier in Figure 28 in terms of their relative contribution to the total energy dissipated. This specific illustration made use of instrumented Charpy testing, and covers only a select group of steels. Clearly there is benefit in broadening the scope of this response to better understand historic versus current versus emerging steels.

The active sources of energy dissipation diminish the energy stored in the compressed gas and the strain energy stored in the pipe, in addition to other facets of propagation such as flap formation, and flow-induced deformation in advance of the crack tip and the adjacent lateral stretch zone. Initially, these sources of stored energy are in equilibrium and due to regulations on the maximum allowable operating pressure of a gas pipeline, the strain energy remains within the elastic range of the pipe material. During running fracture, the effects of this strain energy are focused ahead of the crack propagation path and the stress concentration due to the crack tip. If sufficient energy is dissipated within the pipe subject to its interaction with the surrounding soil or backfill state, the crack will arrest. This full-scale fracture propagation scenario embeds the trends of Figure 28, but modifies the mix of these components subject to the line-pipe's properties, the transported fluid's properties, and the viability of the definition of the backfill constant and its applicability, which can vary case by case.

Table 2 and in Figures 40, 42, and 43 indicate the "fracture curve" characterized by Equation 2 and implemented in differential form is a valid measure of the fracture propagation and arrest behavior. While Figure 35 make clear that similitude issues with the backfill constant remain, this validation of the present two-curve adaptation indicates Equation 2 as implemented is a viable tool to assess the energy dissipated during crack propagation. As such, the differential form of Equation 2 will be used to represent the coupled effects of dynamic pressure and stress acting at the moving crack tip as a function of the properties of the line pipe and pressurizing media over the distance traveled by the crack. More precisely, the decrease in crack velocity will be examined as the crack propagates to estimate the energy dissipated as the crack propagates within and between pipe joints.

Equation 2 written as a total differential has the form:

$$dV = \frac{\partial V}{\partial S_d} dS_d + \frac{\partial V}{\partial S_f} dS_f + \frac{\partial V}{\partial (Cv / A_c)} d(Cv / A_c) + \frac{\partial V}{\partial x} dx \qquad (16)$$

The partial derivative of the velocity with respect to the distance traveled is shown in Figure 44 covering a practical range of toughness in part a) and flow stress in part b). The relative effect of flow stress versus toughness evident between the two parts of this figure is as expected in light of the trends discussed earlier in Figures 14 and 15.

The shallow decrease in crack velocity as the crack travels along a pipe segment is consistent with the observations that relatively little energy is dissipated by propagation in the instrumented Charpy impact tests discussed in regard to Figure 28. The decrease in velocity as the crack propagates form one segment into the next can be estimated by setting the differentials equal to the difference in flow stress and toughness defined as the respective value for the segment the crack is about to enter minus the value for the segment the crack is about to leave.

To determine the effect of dissipation due to distance traveled within the transition region between the adjacent segments, the transition can be visualized as the width of the girth weld and heat affected zones. In its present form, the two-curve formulation embedding Equation 16 does

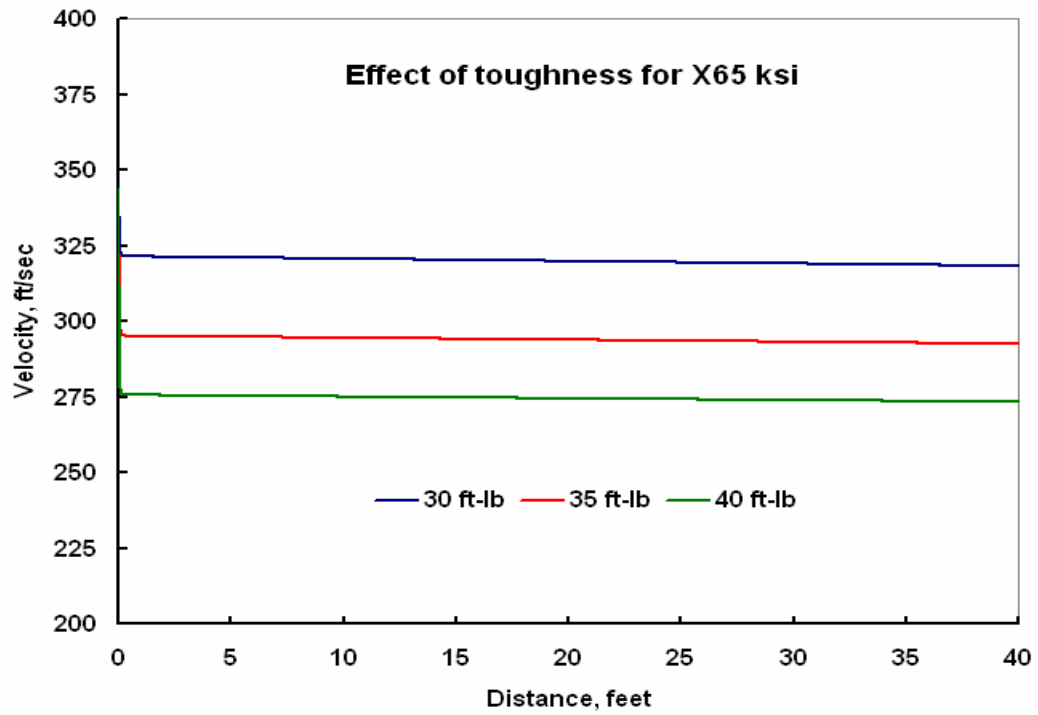

a) relative effect of toughness

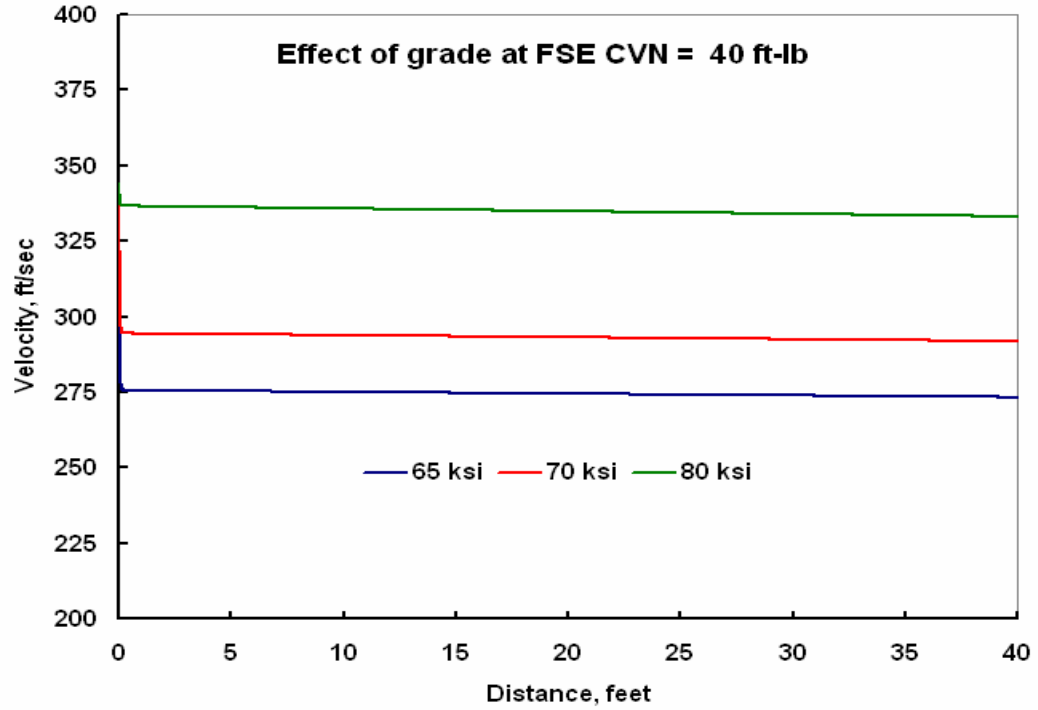

b) relative effect of flow stress

Figure 44. Illustration of dissipation as characterized by Equation 16

not include a transition "segment". For present purposes the differential of the distance traveled, dx was taken to be the width of the transition region and the value for the distance traveled, x at the time the crack enters a new segment was set to the nominal length of a pipe joint. On this basis, the decrease in velocity due to the distance traveled to reach the girth weld (transition region) dictates that the energy dissipated when the crack crosses the weld region. The computed numerical value of the energy dissipated as the crack propagates across the transition region is small due to the exponential form of that term and the relatively large value of x.

For the nominal variations in flow stress and Charpy impact energy discussed earlier for a typical pipeline, namely 4-percent for flow stress and 10-percent for toughness, reductions in velocity between segments determined with Equation 16 are computed to be on the order of only a few percent of the velocity at which the crack enters the transition region. However, these modest decreases (or possible increases) in crack velocity influence the dynamic stress via the gas curve, and therefore in the incremental solution framework used to compute the velocity of the crack at successive time steps, each reduction in velocity precipitates a reduction in the dynamic stress. Referring to regression coefficients in Equation 3, the power on the dynamic stress term, $a1$ causes this term to become the dominant term of the total differential of the velocity. Depending on the actual values of material parameters of the pipeline, the reduction in crack velocity due to the reduction in the dynamic stress is on the order 20-percent.

One final observation concerning dissipation develops in regard to the use of the dynamic stress in Equation 2 and its differential form shown above as Equation 16. Access to the value of the dynamic stress reflects the manner that this "fracture curve" is coupled to the "gas curve", which reflects approach used to deploy the two-curve concept. The present formulation makes use of Equation 14, which had its roots in Equations 1 through 12, to determine the dynamic stress through the coincident velocity that exits between the fracture and gas curves at arrest. Recall in this context that the plastic wave velocity was used as a surrogate for the crack propagation velocity. The derivation of the plastic wave velocity made use of the area under the stress-strain curve and the CVN energy, which can be expressed as the area under the force-displacement curve for the CVN test. These areas were used to transform the tangent modulus into commonly available properties for line pipe steels, which meant true stress and strain were replaced by engineering stress and engineering strain, and the corresponding area under the stress-strain curve. Later in this process the area under the CVN force-displacement curve was portioned to infer the relative contributions of energy dissipation split between initiation, propagation, and deformation. Of concern is the observation that this inference is as yet unproven – that is similitude has not been tested. Whether these sources of dissipation are active in the same proportion up to and through crack initiation and propagation of the necked region of a tensile test remains unknown – and likely will as it is difficult to measure. In contrast it is relatively easy to determine when the crack initiates in a Charpy test by conducting the test with suitable instrumentation.

Conclusions

From the above considerations, the dominant sources of dissipation responsible for arresting a running ductile fracture include the change in deformation properties as the crack crosses from one pipe joint into another, and to a lesser extend the dissipation of energy due to crack propagation as the crack propagates within a segment.

Practical Cases where Dissipation via Creation of Crack-Surface Can Dominate

Figure 28 indicates that the balance between dissipation due to plastic flow at and ahead of the crack tip and in the adjacent lateral stretch-zone and the creation of new surface in advancing the crack depends on toughness, which is likely a surrogate for true fracture ductility or true fracture toughness. Figures 20 and 21 clearly show the merit of tougher steel in quickly arresting fracture. Figure 41 has demonstrated that the effect of flow-induced dissipation can be orders of magnitude greater that that due to the creation of new crack surface. These observations are significant as they suggest potentially significant differences in the length of fracture propagation as a function of toughness. This section considers changes in fracture properties and related correlations to mechanical properties to identify plausible practical service scenarios within the pipeline infrastructure that might be susceptible longer ductile fracture propagation by virtue of changes in service as compared to prior usage, or because of possible in-service degradation.

Background

A number of running brittle fractures in the late 1950s provided the impetus to study this phenomenon. These RBFs ran in some cases for many miles (kms), but as they occurred in cross-country pipelines they posed a business risk more than a public or environmental concern. Resolution to RBF, which opened to door to RDF, came via understanding of this mode of fracture. This understanding prompted controls on steel chemistry and changes in processing to reduce the ductile-to-brittle transition temperature (DBTT) while not adversely reducing the available fracture resistance. Problems with RBF occurred coincidentally at a time of significant change in the steel industry targeting properties matched to the needs of modern civil and mechanical engineering demands for stronger, tougher, weldable steels, which for line-pipe applications had to be insensitive to the effects of hydrogen. These changes were elaborated in regard to Figure 39 and so are not repeated here.

Analysis

Figure 45 shows one measure of the historical evolution in toughness as steels evolved to meet the needs of pipeline design and construction – which parallels trends in strength shown earlier in Figure 39. The DBTT likewise has changed appreciably over this interval, showing an inverse trend with DBTT, decreasing as the quality of the steel and its design to produce properties essential to the pipeline evolved. For steels from the 1940s the DBTT could be the order of 125ºF (~50ºC) or higher. In contrast, line-pipe steels are commercially available today without price penalty with transition temperatures well below typical design needs, even under upset conditions.

If the trend in Figure 45 and that noted for DBTT reflect the US pipeline transmission system, then these results when coupled with results for period of construction[(78)] indicate that much of the US system is characterized by lower-toughness response, with possibly high transition temperature. The trends in Figure 45 coupled with those in Figure 28 indicate that if ductile fracture initiated in this portion of the infrastructure its growth would be dominated by crack propagation resistance rater than by flow-induced dissipation. Figure 41 implies that arrest occurs much more slowly for such cases, which depending on the distribution of the toughness and the strain-hardening exponent along the pipeline opens the door to longer-running fractures.

In regard to Figure 45, construction prior to the middle 1970s is more prone to this situation. This scenario embraces roughly two-thirds of the US transmission pipeline infrastructure[78,98].

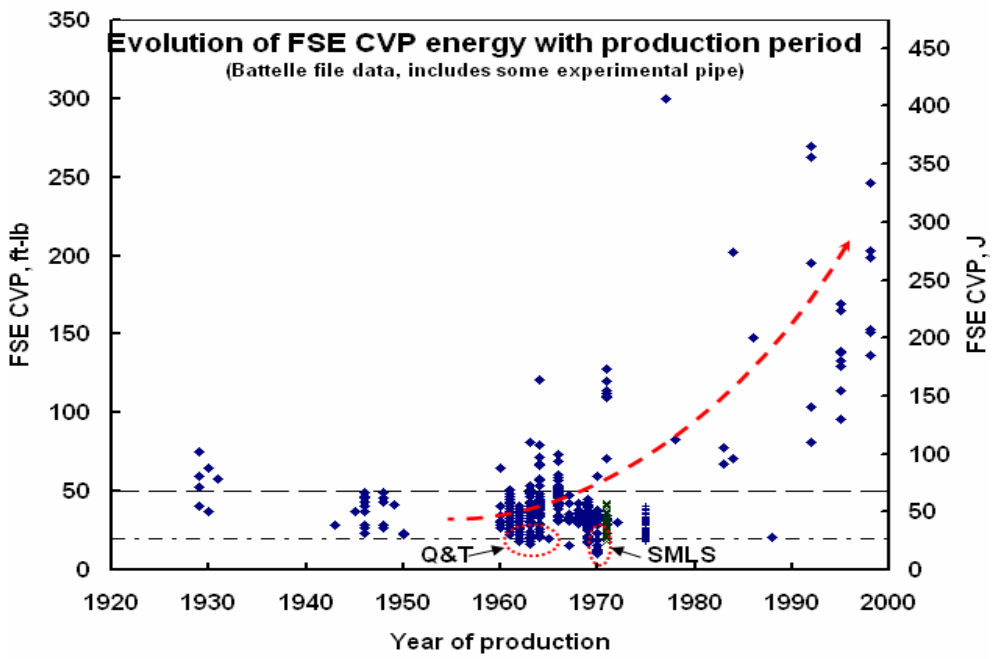

Figure 45. Trend as strength evolved in terms of toughness measured as CVP

For fracture propagation to be a threat to this infrastructure, fracture initiation must occur. For fracture propagation to be a greater threat in the future as compared to past experience, there must be a change in it's the pipeline's service or its typical operational scenario. Taken together, these two concurrent requirements help define what portion of the above-noted 70-percent of the existing pipeline infrastructure is potentially prone to an increased threat of longer-propagating running ductile fracture.

Consider first circumstances and/or changes over time that could prompt fracture initiation. For fracture initiation to occur a crack-like defect must exist or form in service. Hydrotest and incident experience indicate crack-like defects can be present from pipe-making or pipeline construction. However, such defects sufficiently large to grow in-service typically do so rather quickly and so are largely removed from the defect population early in the life – typically well before 30 or 40 years pass.

It follows that pre-existing crack-like defects due to steel/pipe making and construction are less likely to initiate fracture and open the door to its propagation in contrast to in-service degradation that leads to critically sized crack-like defects over time. For pipelines this can occur via fatigue from a pre-existing defect, which would be more common for service with frequent larger pressure cycling, which tends to occur more often in liquid service than it does in gas service. Stress-corrosion cracking (SCC) also can prompt fracture initiation, as could selective seam corrosion, or corrosion that by circumstance favors an axial orientation. Analysis of company records, like-similar analysis, and benchmark analysis as part of developing integrity management plans should help target susceptible segments. Such segments that also traverse a high-consequence area (HCA) should be given particular attention.

Fracture initiation also can be motivated by a change in service driven by increasing demand or the return to full service after a pressure reduction done for rehabilitation, or to manage the risks associated with construction near or over the pipeline. This last scenario – while well motivated and innocent in concept – was responsible for Europe's worst natural-gas transmission pipeline failure[99], with the loss of 18 immediately and more than 40 others injured. As encroachment was a factor in this context, again pipelines traversing HCAs should be given particular attention – as should any scenario where the pressure is to be increased.

As for fracture initiation occurs, fracture propagation beyond initiation becomes a greater threat as compared to past experience through changes in it's the pipeline's service or its typical operational scenario. As above, pressure increases can be motivated by increasing demand or by the return to full service after a pressure reduction done for rehabilitation, or to manage the risks associated with construction near or over the pipeline. While the Ghislenghien rupture of 2004 was a disaster, the fact remains it could have been much worse had the rupture propagated with a fireball in its wake. Instead, because the toughness of that X70 steel was high, there was no propagation beyond the initiating crater. Otherwise the loss of life could have been even more staggering. Again, where encroachment can be a factor in this context, or the pipeline traverses one or more HCAs, particular attention should be given to cases where the pressure could be increased.

Three aspects involving changes in service relative to historic conditions also merit comment. One develops in response to FERC Order 636. This order unbundled the pipeline system and so made pipelines common-carriers, and has uniquely affected some gas transmission systems, as follows. One aspect of this action made price a stronger driver for the source of gas being shipped. Thus, pipelines fed from formations with currently less expensive gas tend to push to full capacity, and are likely to experience "pack and draft" service. Such cyclic pressures open the door to fatigue where it had not been an issue. The second aspect derives from the observation that enforcing minimum gas quality standards in common-carrier service – targeting heating value as well as deleterious content – can be difficult because closed-loop sensor and control technology tends not to be in place. This has often been pragmatically rationalized – because transported gas is commingled between several injection sites such that a problem source due for example to an upstream process upset is diminished by mixing – so it is not a practical concern. While apparently viable over the recent past, the advent of LNG derived gas undermines this concept specifically for pipelines with LNG as a single or primary source – which leads to the third aspect involving changes in service. The concern is these systems will transition to operation at much reduced temperatures whereas historic operation involved the heat of compression that increased the gas temperature. Because gas that can be transported via the usual infrastructure is obtained by expansion from a very low shipping temperature of -162ºC for some applications the gas will remain quite cold.

Lower temperatures due to shipping LNG opens the door to both RBF and RDF in pipelines with higher DBTT or lower CVN at the service temperature thus – because the toughness at this temperature can be much below the CVP as the fracture mode swing from ductile to brittle. This scenario is made worse by the presence of heavy ends (HCLs) in the LNG obtained from several sources worldwide. For the illustration in Figures 20 and 21 the presence of HCLs demanded roughly 50-percent more toughness to ensure arrest. As the length of fracture propagation depends on the statistical likelihood that a joint of pipe with sufficient toughness will be

encountered[6], an increase in required arrest toughness of this order opens the door to long running ductile fracture, with RBF also possible.

One RDF due to a scenario where HCLs entered a pipeline due to an upstream processing upset is documented in Battelle's files. This 1980s RDF ran for ~one-half mile (~1 km) before its arrest at one end in heavy wall pipe at a road crossing, with a sufficiently tough joint stopping it at the other end. Other scenarios are documented in the files where a long sequence of pipe joints fails via RDF in association with fracture initiation events such as SCC, or selective seam corrosion. Such initiation events would be prone to much longer running fractures if the pipeline ran slightly colder or contained even a small fraction of HCLs.

It follows that scenarios where fracture initiation from crack-like origins is possible care should be taken to evaluate the operations and other susceptibility factors to limit exposure to ductile (or brittle) propagating fracture. Aspects involving operations factors include the possibility of upstream processing upsets, the transport of LNG or other products that differ from typical usage, and the use of pack and draft operations. The transported product and line-pipe properties also affect susceptibility to RDF or RBF. Based on transported product, pipelines moving natural gas, rich natural gas, and certain hazardous liquid lines transporting CO_2, propane, and other like HCLs that exhibit two-phase decompression are susceptible. In regard to line-pipe properties, systems constructed using steels with lower CVN values at the service or upset temperature are most susceptible, which is made worse if coupled with higher DBTT values. In this last regard, a potentially significant portion of the vintage pipeline system is susceptible.

Implications for Vintage Pipelines

A previous section demonstrated the validity of a stopgap formulation to predict the fracture propagation response of pipelines. This stopgap formulation – while useful to develop fracture control plans for modern advance-design pipelines or the design of fracture arrestors – is equally viable for applications involving existing pipelines. More than 70-percent of the infrastructure currently qualifies as "vintage" in view of Figure 45. Recognizing that natural-gas transmission pipelines are susceptible, combining 70-percent and gas transmission pipelines indicates the order of 200,000 miles (~320,000 km) of potentially susceptible pipelines within the US. While susceptible, there is no concern for RDF (or RBF) without fracture initiation. This fact implies that care must be taken to preclude exposure to fracture initiation – which is most effectively dealt with by avoiding conditions that promote its occurrence – particularly for pipelines that traverse HCAs. Use of "traverse HCAs" here in lieu of "in HCAs" follows from the observation that propagating fractures can move from a remote location into an HCA. Thus propagation distance is the critical consideration. The improved technology demonstrated valid a few sections earlier will help to better determine this exposure. However, the scatter in Figure 35 and the as yet unresolved role of the backfill factor remain issues in quantifying that exposure. As nothing can be done to enhance the fracture resistance of existing pipelines save for expensive retrofits such as fracture arrestors, better guidance to focus such investments is essential where changes are anticipated that increase exposure to propagating fractures through operations and susceptibility factors.

---

[6] See Appendices A and B of Reference 5 for details.

Conclusion

This section interpreted how a pipeline's operation coupled with its fracture properties help to identify practical service scenarios with likely increased exposure to fracture propagation, and susceptibility to longer propagation.

Factors affecting susceptibility were grouped into operations factors and line-pipe properties. Operations factors included the possibility of upstream processing upsets, the transport of LNG or other products that differ from typical usage, the use of pack and draft operations, and the nature of the transported product. Susceptible pipelines in this context include those transporting natural gas, rich natural gas, and hazardous liquid lines transporting HCLs that exhibit two-phase decompression (e.g., CO_2, propane, etc). Susceptibility based on line-pipe properties involves consideration of steels with lower CVN values at the service or upset temperature, which is made worse when coupled with higher DBTT values. Such characteristics indicate that much of the vintage pipeline system is susceptible.

It follows that scenarios where fracture initiation from crack-like origins is possible care should be taken to evaluate susceptibility to RDF (or RBF) to limit exposure to propagating fracture. The upside is that fracture propagation is not a threat to this infrastructure unless fracture initiation occurs – which requires the presence of a defect, with crack-like defects being more commonly a problem than blunt defects. Fatigue, SCC, selective seam corrosion, long axial corrosion, and other such defects thus are precursors to fracture initiation. Susceptibility to fracture initiation and propagation also was tied to changes in service driven by increasing demand, or the return to full service after a pressure reduction done for rehabilitation, or to manage the risks associated with construction near or over the pipeline. Finally, susceptibility was indicated in regard to "pack and draft" service and/or transport of LNG for which a reduced service temperature opens the door to both RBF and RDF. This scenario was found to be potentially much worse if the LNG contains heavy ends (HCLs).

Where fracture initiation is plausible from crack-like origins in the vintage pipeline system care should be taken to evaluate operations factors and susceptibility to RDF (or RBF). The stopgap formulation shown valid in predict fracture propagation in previous sections can be used for such purposes. Because the inherent resistance of the line pipe cannot be changed for the existing vintage system, fracture control can be achieved only by limiting exposure to fracture initiation. Where this is difficult and other factors drive continued exposure, risk must be managed by retrofitting the pipeline using fracture arrestors. As risk is typically greatest in HCAs, pipelines that traverse HCAs should be addressed – with the realization that fracture propagation can bring exposure from a remote location into an HCA. For this reason propagation distance was cited as the critical consideration. While the improved technology demonstrated valid a few sections earlier will help to better determine this exposure, scatter and the as yet unresolved role of the backfill factor remain issues in quantifying that exposure. As nothing can be done to enhance the fracture resistance of existing pipelines except for expensive retrofits, better guidance to focus such investments is essential where changes are anticipated that increase exposure to propagating fractures through operations and susceptibility factors.

Summary and Conclusions

The Pipeline and Hazardous Materials Safety Administration (PHMSA) supports a wide range of technical research programs to ensure the safety of the nation's pipeline infrastructure. This report addresses one key element of the complex but related issues that impact pipeline integrity, namely catastrophic rupture and unstable fracture propagation along the pipeline. Such running fracture can occur in ruptures of gas pipelines, and can occur in hazardous liquid lines that transport products like propane or CO_2 that can under go a liquid-to-gas phase change during decompression. The distance that the running fractures can travel away for either side of a rupture can dramatically influence the consequences of a failure. This report develops an approach to running fracture designed to help operators design pipelines to avoid this threat and determine the extent of this threat to minimize its consequences if a rupture occurs.

Technology available for engineering analysis of running fracture reflects work done in the early 1970s by Battelle. The primary result of this technology was the Battelle Two-Curve Model, typically written as BTCM, which facilitated prediction of whether a running fracture would arrest or propagate. The model derives its name because it discriminates between arrest and propagation via the point of tangency between two curves – one being the crack velocity curve and the gas decompression velocity curve. This model is applicable to pipelines transporting gas or liquids that can under go a phase change upon decompression. The fracture velocity curve is based on considerations of the plastic wave velocity and an empirically calibrated fracture mechanics estimate of the arrest pressure. The gas curve represents that pressure of the escaping gas at the tip of the crack. This pressure is responsible for the circumferential stress that drives the crack. It has been derived from thermodynamic consideration of a fluid exiting an open-ended cylinder. The BTCM includes an empirically derived backfill constant. Separate full-scale tests conducted on pipe that was buried in soil, aboveground or submerged in water were used to determine backfill constants for each of these conditions.

Through its formulation this model discriminated arrest versus propagation but did not track the propagation process as it ran along the pipeline. Accordingly, where concern existed for the length of propagation – to assess the possible exposure to the consequences of running fracture – a purely statistical construct was used to evaluate the distribution of properties along the pipeline to determine the arrest length. Likewise, as the BTCM relied on empirical calibration, its use has become limited as similitude broke-down in successive aspects of its formulation largely due to changes in the toughness and strength of the line pipe. Finally, by virtue of its formulation to simply discriminate between arrest and propagation the BTCM lacked utility in understanding the factors controlling fracture propagation behavior. This confounded understanding of the means to measure propagation resistance using simple laboratory tests and specimens, and limited understanding of how changes in service directly affected susceptibility to running fracture.

This project formulated an alternative fracture curve and the reassessed approach used to deploy the two-curve concept that underlies the BTCM to develop a model for fracture propagation and arrest that tracks the fracture process along the pipeline. This facilitates assessing the response as the crack-tip encounters differing circumstances in its travel along the pipeline or full-scale test section. Further, it facilitates identifying first-order factors that must be addressed and helps to understand the breakdown of similitude between the model and the reality of the full-scale test or operating pipeline.

This project's objectives in implementing the just-noted approach were to:

12. assess the viability of the premise that fracture arrest is due to energy dissipated in the creation of new crack surface, to better understand the ideal laboratory specimen and test practice to characterize propagating fracture resistance,
13. develop insight into 1) the mechanics and dynamics of the soil-structure interaction, 2) the gas dynamics during decompression, and, 3) the dynamic fracture process in the pipe by exploiting existing analytical formulations and semi-analytical schemes, as the basis to maximize productivity,
14. assess the premise that fracture arrest occurs through dissipation mechanisms in addition to crack-propagation resistance – and the premise that arrest as toughness increases as a process that transitions from a propagating crack to a running tensile instability, as the basis to understand the essential aspects of fracture propagation and arrest, and as appropriate,
15. develop an engineering model for fracture propagation and arrest by exploiting existing analytical formulations and semi-analytical schemes like the BTCM.

Important conclusions from this work were presented in the conclusions subsection to each major aspect of this report. Readers interested in the details should consult each section. Suffice it here to list the critical conclusions. Critical conclusions regarding the first objective on the list above include:

- an engineering model was formulated based on the two-curve concept and shown valid by its application to the propagation behavior over the course of such full-scale testing, as well as for its discrimination between arrest and propagation – the validation considered grades through X100 and toughness levels up to ~250 ft-lb (340 J) for both single-phase and two-phase decompression,
- a fracture-arrestor design model was developed based on this validated technology, and formatted for use in Windows-based software,
- an alternative "fracture curve" was formulated for use in the two-curve concept that reflects the dissipative effects of both the flow and fracture properties,
- the results indicate that energy dissipated in the creation of new crack surface is second-order in comparison to the effects of flow-induced dissipation,
- the ideal laboratory specimen and test practice to characterize propagating fracture resistance should embed dissipative traits that contribute to flow and fracture – in a balance dictated by further analysis.

Critical conclusions regarding the second objective on the list above include:

- the mechanics and dynamics of the soil-structure interaction is poorly characterized in the prior deployment of the two-curve concept, which carried over to the present formulation as data characterizing this topic tend to be available only in the framework of the BTCM,
- the gas dynamics response during decompression is well characterized at least for the present – as time passes limitations might develop, and
- the dynamic fracture process was better as a consequence of this work as was noted above for the first objective – however, as this was the first-cut at reformulation there is very likely potential for improvement,

- much value was derived by exploiting existing analytical formulations and semi-analytical schemes – which as this mining only scratched the surface opens the door to further improvement with great potential return for the effort.

Critical conclusions regarding the third objective on the list above include:

- the premise that fracture arrest occurs through dissipation mechanisms in addition to crack-propagation resistance was demonstrated viable in contrast to historical views that held the creation of new crack surface was the key,
- the premise that arrest as toughness increases as a process that transitions from a propagating crack to a running tensile instability likewise was demonstrated,
- other opportunities to improve engineering prediction of fracture propagation might exist through a broader view of the fundamental aspects of this problem,
- engineering models should be formulated on the premise that fracture arrest occurs through dissipation mechanisms in addition to crack-propagation resistance – with opportunities to broaden these models under the premise that arrest as toughness increases as a process that transitions from a propagating crack to a running tensile instability.

Critical conclusions regarding the fourth objective on the list above include:

- an engineering model for fracture propagation and arrest was successfully formulated by exploiting existing analytical formulations and semi-analytical schemes like the BTCM.

Recommendations

A number of more subtle improvements are identified in the conclusions subsection to each major aspect of this report. Readers interested in that level of detail should consult the conclusions noted for each section. Suffice it here to list recommendations that have high-level significant impact, as follows:

16. Backfill and axial restraint have a significant impact on the propagation velocity and so the arrest conditions, but as yet these effects have been commingled with the effects of the strain-hardening exponent and considered a "backfill constant" – during the course of this work the historical archives for most of Battelle's full-scale tests were fortuitously located, including extensive and generally unpublished data on "backfill effects".

    There is great potential value in mining this data and in its analysis and incorporation in the two-curve formulation developed in this project, which avoids the cost of the testing and so has great value-added.

    There is equally great value-added by developing and evaluating alternative formulations for the "backfill constant", to uncouple backfill and the line pipe properties, which should consider the as yet untapped value of the recent work considering the plastic wave velocity.

    Much of what is attributed to backfill effects could develop via the effects of axial restraint, which act to limit the size of the plastic zone ahead of the crack, thereby leading to higher cracking velocity – again much added value can arise by uncoupling what is attributed to backfill but is more likely due to axial restraint.

17. The initial design of the full-scale tests spaced crack-detection wires a meter apart such that at the transition between pipe joints the spacing is typically two meters. This practice has persisted, which is unfortunate as it precludes identifying the true effect of the change in toughness and flow properties on the propagation velocity.

    The present work implies countering effects of these parameters, and local complexity due to the effects of momentum. More detailed analysis of this scenario is possible by mining the literature, and by further simulation – again with great value-added.

18. The alternative "fracture curve" was formulated for use in the two-curve concept focusing both the flow and fracture properties, but with limited insight into the concern addressed in Point 2 above.

    Following consideration of Point 2, care should be taken to incorporate the findings into the fracture curve – otherwise the added value is lost.

19. The results indicate that ideal laboratory specimen and test practice to characterize propagating fracture resistance should embed dissipative traits that contribute to flow and fracture – in a balance dictated by further analysis. As this is a significant departure from current directions, consideration should be given to alternative test practices.

    The insight provided by Equation2 implemented in the form of Equation 16 should be utilized as a guide to identify the appropriate test to characterize running fracture resistance – with great potential value but only for targeted applications.

20. The premise that arrest as toughness increases as a process that transitions from a propagating crack to a running tensile instability has great utility in understanding the fracture response of modern-design pipelines.

    Consideration should be given to the further development of this concept to ensure the safe serviceable operation of pending pipeline designs.

21. The engineering model as currently formatted and packaged in software can be used in the design of fracture arrestors, but in this form cannot applied to characterize fracture propagation or discriminate between propagation and arrest.

    Consideration should given to packaging the engineering model for use in software much like DYNAFRAC packages the BTCM. This would help to capture the value of this project.

22. Changes in the possible use of the pipeline infrastructure point to the use of the current system to transport LNG, or where waivers are granted to experience higher pressures.

    Consideration should be given to an evaluation of such impacts in regard to the potential for fracture propagation, as guidance to avoid future related problems.

23. A validated engineering model for the design of fracture arrestors was developed and packaged as software to facilitate the design of integral fracture propagation arrestors.

    As this technology is fully general and could be generalized for similar use with external arrestors, consideration should be given to such applications – with great potential value added given the platform already exists for integral arrestors.

References

1. anon., Code of Federal Regulations, Title 49 -Transportation, Part 195.
2. anon., Code of Federal Regulations, Title 49 -Transportation, Part 192.
3. anon., "Managing System Integrity for Hazardous Liquid Lines", 1st Ed., API Standard 1160-2001, November 2001.
4. B31.8S Anon., ASME Code Supplement on Integrity Management for Pressure Piping, B31.8S, Revision 1, 2002.
5. Eiber, R. J., and Leis, B. N., "Fracture Control Technology for Natural Gas Pipelines – Circa 2000", PRCI Catalog No. L51846, Pipeline Research Council International, 2002.
6. Duffy, A. R., Paper 43, Symposium on Line Pipe Research, A.G.A., Cat. No. L30000, 1965.
7. various authors and papers in A.G.A. NG-18 Symposia on Line Pipe Research, 1969, 1974, 1979, 1986, 1993, and, 1996.
8. Eiber, R. J., Carlson, L., and Leis, B. N., "Full-Scale Tests Confirm Pipe Toughness," Oil & Gas Journal, Nov. 8, 1999, pp. 48-54
9. Maxey, W. A., Paper J, 5th Symposium on Line Pipe Research, American Gas Association, Catalog No. L30174, 1974.
10. Eiber, R. J. and Maxey, W. A., "Full-Scale Experimental Investigation of Ductile Fracture Behavior in Simulated Arctic Pipeline," ASME Grey Rocks Symposium, 1976: see also Eiber, R. J. and Maxey, W.A., "CAGSL Crack Arrest Experiments 1 and 2," Battelle Report to Northern Engineering Service Co. Ltd., January 3, 1975, and related Battelle–CAGSL Burst Test Report, Submitted to the National Energy Board of Canada, 1976
11. Sugie, E., Matsuoka, M., Akiyama, T., Tanaka, T., and Tsukamoto, M., Paper 1, A.G.A. Line Pipe Research Committee - Japanese High-Pressure Line Pipe Committee Joint Symposium, Columbus, 1984.
12. Final Report on The Test Program at the Northern Alberta Burst Test Facility, August 10, 1981, No. 18031, Filed in the Foothills Hearing with the National Energy Board of Canada.
13. anon., ASTM Standard E23, Part 10, ASTM, Philadelphia, PA.
14. Maxey, W. A., Kiefner, J. F., and Eiber, R. J., A.G.A. Catalog No. L32176, 1975.
15. anon., "Running Shear Fractures in Line Pipe," Subcommittee of Large Diameter Line Pipe Producers, AISI Technical Report, 1974.
16. Fearnehough, G. D. and Jones, D. G., "Toughness Specification for Shear Fracture Arrest in Pipelines," I. Conf. on Analytical and Exp. Fracture Mech., Rome, 1980.
17. Vogt., G. H.,and Wiedenhoff, W.W., "Toughness for Crack Arrest in Gas Pipelines," EPRG Report, 3R International, Vol. 22, 1983, pp. 98-105 and pp 247-250.
18. Bonomo, F., Bramante, G. A., Bozzo, E, A., "A Survey and Tentative Revision of the Ductile Fracture Arrest Criterion in Pipelines for Gas Transmission," International Conference on Analytical and Experimental Fracture Mechanics, June 23-27, Roma, 1980.
19. Sugie, E., Matsuoka, M., Akiyama, T., and Mimura, H., "A Study of Shear Crack Propagation in Gas Pressurized Pipelines. ASME Annual Meeting 1982, Paper 82-WA/PUP-11.
20. 83 eprg paper showing non-conservative predictions

21. Leis, B. N., Carlson, L., Eiber, R. J., and Gilroy-Scott, A., "Relationship Between Apparent Charpy Vee-Notch Toughness and the Corresponding Dynamic Crack-Propagation Resistance," International Pipeline Conference, ASME, Volume 2, pp. 723-731, 1998.
22. Pelleni, W. S., Principles of Structural Integrity, Office of Naval Research, 1976.
23. Tiara, T., Takehara, J., and Aoyagi, K., Paper 19, A.G.A. Pipeline Research Committee - Japanese High-Pressure Line Pipe Committee Joint Symposium, Columbus, 1984.
24. Leis, B. N., "Relationship between Apparent Charpy Vee-Notch Toughness and the Corresponding Dynamic Crack-Propagation Resistance", 1997, Report to R J. Eiber, Consultant, Inc. in support of the Alliance Pipeline fracture control plan: see Evidence filed with Canadian National Energy Board, GH-3-97, V 45, 1997.
25. Eiber, R. J., Carlson, L. E., and Leis, B. N., "Fracture Control For the Alliance Pipeline", International Pipeline Conference, Proceedings Paper IPC 00-103, ASME, Calgary, pp. 267-277, 2000
26. Eiber, R. J., Carlson, L., and Leis, B. N., "Fracture Control Requirements for Gas Transmission Pipelines," 3rd Pipeline Technology Conference, Brugge, 2000, pp. 437-453.
27. Maxey, W. A., Kiefner, J. F., Eiber, R. J., and Duffy, A. R., "Ductile Fracture Initiation, Propagation and Arrest in Cylindrical Vessels," ASTM STP 514, American Society for Testing and Materials, Philadelphia, 1972, pp. 70-81.
28. Kiefner, J. F., Maxey, W. A., Eiber, R. J., and Duffy, A. R., "The Failure Stress Levels of Flaws in Pressurized Cylinders," ASTM STP 536, 1973, pp 461-481.
29. Wilkowski, G. M., Maxey, W. A., and Eiber, R. J., "What Does the Charpy Test Really Tell Us," American Society for Metals, 1978, pp 201-225.
30. Fearnehough, G. P., Dickson, D. T., and Jones, D. G., Volume 1, Dynamic Fracture Toughness Conference, London, Welding Institute/ASM, 1976.
31. Wilkowski, G. M., Maxey, W. A., and Eiber, R. J., Can Met Quart, V 19, pp. 59-77, 1980.
32. Venzi, S. et al, Proc. Int. Conf. on Anal. and Exp. Fracture Mechanics, Noordhoff, 1981
33. Martinelli, A., and Venzi, S., Engr. Fract. Mech., Vol. 53, No. 2, pp. 263-277, 1996.
34. Kanninen, M. F. et al, Proc. Pipeline Technology Conf, Oostende, 1990, Part B, pp 16.1-13
35. Demofonti, G. and Hadley, I., "Review of Fracture Parameters for laboratory Measurement of Resistance to Ductile Crack Propagation in Line Pipe Steels," CANMET Pipeline Conference, Calgary, 1992.
36. Demofonti, G., Venzi, S., and Kanninen, M., "Step by Step Procedure for the Two Specimen CTOA Test," 9th EPRG/PRCI Symposium, 1995, pp. 18-1 through 18-10.
37. Wilkowski, G. M., Wang, Y. Y., and Rudland, D., Advances in Welding and Pipeline Technology, EWI, Galveston Texas, October, 1999.
38. Salvini P., Fonzo A., and Mannucci G., "Identification of CTOA and Fracture Process Parameters by Drop Weight Test and Finite Element Simulation," Engineering Fracture Mechanics, 70/3-4, 553-566, 2003
39. Hashimi, S. H., et al, "A Specimen for Studying the Resistance to Ductile Crack Propagation in Pipes," 5th Int. Pipeline Conference, IPC04-0610, Calgary, 2004.
40. Shterenlikht, A., Hashemi, S. H., Howard, I. C., Yates, J. R. and Andrews, R. M., "A Specimen for Studying the Resistance to Ductile Crack Propagation in Pipes," Eng. Frac. Mech., Vol. 71, pp. 1997-2013, 2004.

41. Buzzichelli, G., Nicolazzo, F., Demofonti, G., Re, G., Venzi, S. Kanninen, M. F., Cardinal, J. W., Polch, E. Z., Morrow, T. B., Green, S. T., and Popelar, C. H., "Second Annual Report on the Development of A Ductile Pipe Fracture Model," Southwest Research Institute report to Pipeline Research Committee, AGA Contract No. PR 182-527 and PR 15-527, May 29, 1987.
42. Buzzichelli, G., Demofonti, G., Rizzi, L., Venzi, S., Kanninen, M. F., Cardinal, J. W., O'Donoghue, P. E., and Morrow, T. B., "The Development of a Ductile Pipe Fracture Model," NG-18 Interim Report, AGA Contract No. PR 182-526 and PR 15-527, January 31, 1989
43. Kanninen, M. F., "Report on the Completion of the Development and Validation of a Ductile Fracture Analysis Model," Southwest Research Institute presentation for AGA Contract No. PR-182-9210, May 17, 1994.
44. Kanninen, M. F., O'Donoghue, P. E., Cardinal, J. W., Leung, C. P., Morrow, T. B., Green, S. T., Popelar, C. F., Buzzichelli, G., Demofonti, G., Rizzi, L., and Venzi, S., "Dynamic Fracture Mechanics Analysis and Experimentation for the Arrest of Ductile Fracture Propagation in Gas Transmission Pipelines," Internal Conference on Pipeline Technology, Belgium, October 15-17, 1990.
45. Demofonti, G., Buzzichelli, G., Venzi, S., and Kanninen, M. F., Proc 2nd Conf. on Pipeline Technology, Vol. II, pp. 503- , Elsevier, 1995.
46. Mannucci, G., Buzzichelli, G., Salvini, P., Eiber, R. and Carlson, L., "Ductile Fracture Arrest Assessment in a Gas Transmission Pipeline using CTOA," Third International Pipeline Conference (IPC 2000), Calgary, Alberta, Canada, Vol. 1, pp. 315-320, 2000.
47. Berardo, G., Salvini, P., Mannucci, G. and Demofonti, G., "On Longitudinal Propagation of a Ductile Fracture in a Buried Gas Pipeline: Numerical and Experimental Analysis," In Proceedings of the 2000 International Pipeline Conference, Vol. 1, New York: The American Society of Mechanical Engineers, 2000, pp. 287 –294.
48. Demofonti, G. et al, Pipeline Technology Conf., Vol. 1, Scientific Surveys, 2004, pp467-482
49. anon., "CTOA for Fracture Arrest in Alliance Pipeline", Written private communication to E. L. (Tiny) von Rosenburg, formerly of Exxon, from C. W. (Cliff) Peterson (then of Exxon), providing a SwRI Report predicting the CTOA for propagation arrest for the Alliance Pipeline, March 1998.
50. Rudland, D. L, and Leis, B. N., "Dynamic Fracture Testing Program for the Alliance Pipeline," 1999, Report to R J. Eiber, Consultant, Inc. in support of the Alliance Pipeline fracture control plan and pipeline certification(Canadian National Energy Board, Hearing GH-3-97.
51. Leis, B. N., "Evolution of Line-Pipe Steel and its Implications for Transmission Pipeline Design", International Pipeline Conference, Proceedings Paper IPC 02-27015, ASME, Calgary, 2002.
52. van Elst, H. C., "Criteria for Steady State Crack Extension in Gas Pipelines," International Conference on Prospects of Fracture Mechanics, Netherlands, pp. 299 – 318, June 24-28, 1974.
53. McGuire, P. A., Sampath, S. G., Popelar, C., and Kanninen, M. F., "A Theoretical Model for Crack Propagation and Arrest in Pressurized Pipelines," American Gas Association, Catalogue No. L00033, November 1978.

54. Poynton, W. A., "A Theoretical Analysis of Shear Fracture Propagation in Backfilled Gas Pipelines," Crack Propagation I Pipelines, Paper No. 14, published by the Institute of Gas Engineers, Newcastle upon Tyne, England, March 1974.
55. Abbassian, F., "Long-Running Ductile Fracture of High Pressure Gas Pipelines," dissertation for PhD, University of Cambridge, November 1985.
56. Fruend, L. B. and Parks, D. M., "Analytical Interpretation of Running Ductile Fracture Experiments in Gas-Pressurized Linepipe," *Crack Arrest Methodology and Applications,* ASTM STP 711, G. T. Hahn and M. F. Kanninen, Eds., pp. 359-378, 1980.
57. Generic JTMeeting ref & years – including Vogt., G., Re, G., Pistone, V., Demofonti, G., and Jones, D.G., "EPRG Recommendation for Crack Arrest Toughness for Hight Strength Line Pipe Steels, PRC/EPRG Ninth Biennial Joint Technical Meeting, May 1993. -- Re, G., "An EPRG Full Scale Test at Very High Hoop Stress," Paper 15, Seventh Biennial NG-18/EPRG Joint Technical Meeting, Calgary, 1988, Paper 15. -- Mannucci, and G, Demofonti, G., Structural Integrity of API 5L X70-X80 Steel Grade Pipeline for High Pressure Long Distance Transmission Gas Lines, Paper 13, 12th Bien. Jt. EPRG-PRCI Tech. Meeting, Groningen, 1999 -- Mannucci, M., Landi, M., and Demofonti, G., "State of The Art on Mechanical Crack Arrest Devices for Large Diameter Pipelines," 12th Biennial Joint Technical Meeting on Pipeline Research, EPRG/PRCI, Netherlands, May 1999, pp 14-1 through 14-6.
58. anon., "EPRG Data Bank, Full Scale Tests at Hoop Stress Higher than 350 MPa,".
59. Sugie, E., Matsuoka, M, Akiyama, T., Tanqaka, K, and Kawaguchi, Y., "Notch Ductility Requirements of Line Pipes for Arresting Propagating Shear Fracture", Trans. ASME, Vol. 109, Nov. 1987, pp. 428-434.
60. Maxey, W, .A., , Kiefner, J.F., Eiber, R.J., and Duffy, A.R., Experimental Investigation of Ductile Fractures in Piping, 12th World Gas Conference, Nice 73, IGU/C 34-73.
61. Demofonti, G., "X100 Girth Welding and Defect Tolerance Assessment", X100 Forum – CSM, Pula (Sardinia, Italy), 6 / 7 April 2006.
62. IPC fracture test - BG
63. ditto - Ital
64. Sanderson, N., "Access to Portions of BP X100 database," April, 2006
65. X120 paper PTC 04
66. X120 papers / symposium ISOPE 05
67. leis – arrestor paper / Berlin
68. DOT corrosion report
69. corrosion on seams -- PRCI
70. Leis, B. N. and Stephens, D. R., "An Alternative Approach to Assess the Integrity of Corroded Line Pipe – Part One: Current Status and Part Two: Alternative Criterion", 7th International Conference on Offshore Pipelines and Polar Engineering, Vol. 3, pp 624 – 634 and pp 635 – 641, 1997.LPC1
71. Leis, B. N., Brust, F. W., and Scott, P. M., "Development and Validation of a Ductile Flaw Growth Analysis for Gas Transmission Line Pipe", American Gas Association Catalog No. L51643, June 1991.

72. Leis, B.N. and Ghadiali, N., “Pipe Axial Flaw Failure Criteria-PAFFC, Version 1.0 User's Manual and Software”, NG-18 Report 211. Release 1.0, May 1994, through Release 4.0, January 2001.
73. Kolsky plastic speed page
74. Hutch’s paper on wave speed
75. Gray’s PRCI report on variability
76. toughness variability paper
77. Clark, E. B., Leis, B. N., and Eiber, R. J., “Integrity Characteristics of Vintage Pipelines,” Battelle Report to the INGAA Foundation, October, 2004.
78. BG-Stoner Decompression Report
79. Leis, B. N. and Kilinski, T. J., “Mechanical and Fracture Properties Essential in Integrity Management of Steel Transmission Pipelines”, Final Report, PRCI Report PR-3-9606/9737, December, 2000.
80. Leis, B. N., “Hydrostatic Testing Of Transmission Pipelines: When It Is Beneficial and Alternatives When It Is Not”, PRCI Report PR-3-9523, Pipeline Research Council International, 2001.
81. rate dependence of yield stress
82. Gray – stretch zone report 1984
83. Leis, B. N., “Using Laboratory-Scale Practices Characterizing Dynamic Crack-Resistance Of Pipelines,” International Pipeline Conference - 2000, ASME, Calgary, pp. 295 - 306, October, 2000: see also Leis, B. N., “Contrasting Fracture Behavior Characterized Using Charpy Vee-Notch and Dynamic-Tear Test Methods,” 3rd Pipeline Technology Conference, Brugge, May 2000, Volume 1, pp. pp. 343-358.
84. Williams, D. N., and Maxey, W. A., “Evaluation of an X70 Low Carbon Bainitic-Steel Pipe,” NG-18 Report No 145, February, 1985; “Evaluation of an X70 Pipe Fabricated From an Accelerated Cooled C-Mn-V-Cb Steel,” NG-18 Report No 157, May, 1986; “Evaluation of an X70 Pipe Fabricated from an Accelerated-Cooled Boron-Containing Steel,” NG-18 Report No 161, August, 1986; “Evaluation of a Heat-Treated X80 Grade Pipe,” NG-18 Report No 163, April, 1987; “Evaluation of an X80 Pipe Fabricated from a Controlled-Rolled Steel,” NG-18 Report No 169, November, 1987; “Evaluation of an X80 Pipe Fabricated from a Plate Processed Using On-Line Accelerated Cooling,” NG-18 Report No 178, August, 1988. (not available for distribution outside the PRCI)
85. anon., “Stress-Corrosion Cracking on Canadian Oil and Gas Pipelines,” National Energy Board (of Canada), Report of Inquiry MH-2-95, 1996, p. 137.
86. Olson, R. J., Narendran, V. K., Leis, B. N. Kilinski, T. J., Scott, P. M., and Gertler, R. C., “Appendix A7 – Full-Scale Testing to Validate PAFFC and Develop Data to Assist Evaluating the Benefits of Hydrotesting”, Appendix Seven to Reference 81
87. Maxey TM#17
88. Maxey quarry test
89. Wilkowski, G., Scott P., and Maxey, W., “Design and Optimization of Mechanical Crack Arrestors for Pipelines,” AGA Report NG-18 No. 134, July 26, 1983.
90. Wilkowski -- BAA
91. leis IPC 04 fracture paper

92. Smith, J. H. and Shoemaker, A. K., "Use of Pipe Wall Ductility to Characterize Fracture in line Pipe," U. S. Steel Report 12-C-002 (018-4), March 31, 1975
93. Shoemaker, A. K. and McCartney, R. F., "Displacement Considerations for a Ductle Propagating Fracture in Line Pipe," U. S. Steel Research Laboratory Report 12-C-002 (018-1), January 31, 1974
94. Fearnehough, G. D., et al, "The Arrest of Brittle Fracture in Pipelines," I. Mech. Engr., 1971
95. Poynton, W. A. and Fearnehough, G. D., "The Analysis of Shear Fracture Propagation in Pipelines," Proceedings of the International Conference on Dynamic Crack Propagation, Lehigh University, 1972
96. Venzi, S., Re, G., Buzzichelli, G., Demofonti, G., Nicolazzo, F., and DeVito, A., "Modeling of Ductile Crack Propagation in Relation to Plastic Deformation of the Pipe," Paper 18, 5th EPRG-AGA Joint Technical Meeting, San Frisco, September, 1983
97. Kiefner, J. F. and Trench, C. J., "Oil Pipeline Characteristics and Risk Factors: Illustrations from the Decade of Construction," American Petroleum Institute, December 2001.
98. anon., Ghislenghien Rupture, Communiqué de presse, 30 juillet 2004, Fluxys SA, www.fluxys.net
99. Irwin, G. R. and Corten, H., "Evaluating the Feasibility of Basing Pipeline Operating Pressure On In-Place Hydrostatic Test Procedure", Final Report to El Paso and Northern Natural Gas Company, November, 1968.
100. Orynyak, I.V. and Borodii, M.V., "A Ductile Fracture Model for a Pipe with an Axial Surface Crack," Eng. Fract. Mech. 49, N2. 287 – 294 (1994): see also Orynyak, I.V., Torop, V.M., and Borodii, M.V., "Ductile Fracture of a Pipe with a Part-Through Slot," Int. J. Pres. Ves. & Piping. 65, N2, 171-180 (1996)

Appendix A – Crack Arrestor Concepts and Designs

References cited in the body of the report are numerous, with many new references appearing in this appendix. For this reason it is convenient to use a numbering system here that is independent of the body of the report. Where figures, footnotes, and tables are used they are likewise numbered independently from the body of the report.

Crack Arrestor Concepts and Designs

Background – Running Ductile Fracture and its Arrest

As noted in the body of the report, because of the compressibility of certain transported fluids, fracture initiation leading to a rupture creates the possibility that the energy stored in some high-pressure transmission pipelines might sustain axial propagation of that rupture. However, if the decompression front propagates from the fracture origin at a speed greater than the fracture, this front outpaces the fracture and the fracture arrests when the pressure decays to a level that no longer supports propagation. In contrast, where sufficient dissipation does not slow the fracture, continued axial propagation is possible, leading to loss of service, and the need to replace potentially significant lengths of pipeline. More importantly, running fracture for some products and pipeline locations lead to exposure to the public and environment whose consequences are unacceptable, requiring that if initiated such fractures can be arrested within quite short distances.

While historically a concern, running "brittle" fracture (RBF) – which involved propagation with limited dissipation in terms of deformation and cracking – is no longer a threat as modern steels are available with transition temperatures well less than typical design requirements. However, running "ductile" fracture (RDF), where propagation occurs with significant plastic deformation and cracking mechanisms associated with locally ductile stretching remains a concern as design requirements and other drivers demand more fracture resistance than available. This appendix considers fracture arrestor concepts as the means to supplement available fracture resistance, or offset the demand for it when faced by possible RDF.

As RDF propagates axially along a pipe, the fracture tends to open and the pipe flattens in the wake of the propagating crack. The size of the flaps and their opening reflects the energy driving the passage of the crack and the dynamic response of the pipeline as the energy stored is released by the crack's passage. Flap formation and the extent of their opening develop longitudinal and circumferential stresses ahead of the crack. These stresses cause thinning of the wall thickness and can induce significant ovality of the pipe's cross-section. RDF crack concepts in some cases address constraint of flap formation, on the presumption that the stresses due to the flaps and the related dynamics contribute to the crack's advance. RDF arrestor concepts in other cases address dissipation of the fracture energy, or enhancing the apparent fracture resistance.

Approaches to characterize driving force and inherent fracture resistance can be found elsewhere in terms of fracture mechanics, gas dynamics, and thermodynamics, as discussed in the body of the report. Suffice it to note here that crack arrestor concepts manage arrest by directly tipping the balance between driving force and fracture resistance toward arrest, or by redirecting axial propagation from along the pipe until the crack driving force subsides (i.e., the decompression front runs past the crack tip).

Background – History and Usage

The historic development and use of crack arrestors can be seen in consideration of the references compiled at the end of this appendix. This discussion reflects dialog with knowledgeable pipeline personnel and operators, supplemented by Battelle's files and the authors' knowledge, subject of course to proprietary constraints. As the history of RDF traces approximately to the early 1970s, the earliest plausible use of an arrestor traces to this period.

This appendix begins with discussion of concepts for RDF crack arrestors and thereafter outlines generic implementation schemes for such arrestors and considers their practical deployment, with this appendix closing with discussion of desirable attributes.

Generic Arrestor Concepts

Concepts for fracture arrest logically target the mechanics of fracture propagation and arrest. As noted in the introduction, fracture arrest occurs when either the driving force for propagation drops below the available resistance to propagation, which when arrestors are used is coupled with the arrestors' ability to counter that driving force or retard axial advance until the driving force subsides. Accordingly, arrest can be achieved directly – by tipping the balance between driving force and fracture resistance toward arrest by locally reducing the driving force or by locally increasing the resistance. Arrest can occur by reducing the fracture's speed as compared to that in the pipeline until the pressure decreases to a level that will not support fracture. Arrest also can be indirectly affected by redirecting axial propagation from along the pipe, or by dissipating focused cracking, until the crack driving force subsides, which occurs when the decompression front runs well past the crack tip.

Against this background, arrestor concepts for RDF fall into one of four generic categories:

1. increase fracture resistance,
2. decrease the apparent driving force,
3. restrict flap opening and its effects, and
4. ring-off or otherwise dissipate cracking.

Categories 1 and 2 directly manage the balance between driving force and fracture resistance. Category 3 indirectly manages this balance by removing kinetic energy due to flap formation, and its role in sustaining the apparent driving force. Finally, Category 4 indirectly targets this balance by redirecting propagation onto a path or paths that slow its axial speed, which allows the pressure to decay thereby reducing the local crack driving force.

RDF has been observed to run at axial speeds from ~150 to ~1200 f/s (~45 to ~370 m/s). As arrest requires the axial passage of the decompression front well beyond the crack tip to avoid possible re-initiation, the concept used to arrest RDF must remain fully effective throughout the arrest event. This leads to concern for the time interval for arrest, which typically is manifest in terms of the length of the crack arrestor and/or consideration of parameters that characterize distance or time.

Generic Implementation Schemes

There are two generic implementation schemes for RDF arrestors – ***integral*** to the pipeline or ***external*** to the pipeline. Integral arrestors are built into the pipeline during its construction or during its rehabilitation. In contrast, external arrestors are overlaid and/or wrapped or wound onto and/or around the pipeline, and so could be installed during construction or rehabilitation, with the benefit for the latter of not taking the pipeline out of service[7]. This section presents and

[7] While this consideration favors external concepts over integral concepts, there are other considerations that work in reverse. Further details follow later in the section that addresses all such considerations.

discusses implementation schemes categorized in this manner. Examples of some of these schemes are presented later, along with consideration of desirable attributes and some current applications and a summary of approaches for arrestor design and/or analysis.

Integral implementation schemes can be accomplished by one or more of the following approaches:

- increase fracture resistance – lengths of higher toughness line pipe, or with rolling direction for spiral roll or circumferential roll, or their combinations,
- decrease relative driving force – lengths of heavier wall pipe or reduced relative stress pipe, and their combinations,
- induce ring-off – lengths with weaker spiral-seam weld or with brittle/low ductility girth weld,
- novel multilayer dissipation/redirection concepts – layered pipe lengths with helical mid-layer slits or notches to dissipate energy, break the crack's continuity, and redirect its path,
- novel but less proven or less practical concepts – group of short-length girth-welded lengths with alternating brittle and high-toughness segments, to divide the propagation energy by developing multiple cracks that "shatter" the brittle pipe length, which individually lack the axial orientation and energy to reinitiate in the high-toughness segments.

Integral arrestors are best used in new construction or retrofits where the line is out of service, the latter requiring tie-in welds. Integral arrestors can be designed as transitions with matched inside diameter (ID) to facilitate in-line inspection (ILI) and limit potential restrictions. Integral arrestors also can be designed with outside diameter (OD) and ID matched to the run pipe, which makes it easy to coat them and protect the pipe from corrosion and environmental cracking.

Overlays and/or ***wraps*** or ***windings*** comprising ***external*** arrestors can be implemented by one or more of the following schemes:

- cylindrical (steel) sleeve external to the pipe, installed loose or tight, with or without grout, all of which are largely stress-free unless needed for arrest,
- welded cylindrical (steel) sleeve external to the pipe, installed loose or tight, with or without grout, which bears some load at least near the welds, some of which permit preload (e.g., Petrosleeve),
- type B (fillet-welded) sleeve breaching a gap between otherwise uncoupled pipe joints, breaking continuity of the crack path,
- channels, rings, or bands, installed loose or tight, which when feasible might be grouted, with installation through bolts, welding, and other schemes some of which permit preload,
- filament(s) or wire(s) over-wound either loose or tight, some of which through counter winding develop compressive preload, with some available for "over-the-ditch" installation,

- fiberglass sleeves/wraps loosely overlaid or tightly wound onto pipe which could be end-capped for fabrication and drawn down to create local compression in service, or onto full composite joints,
- novel, but less proven or less practical concepts, to restrain flap-opening by high density backfill or matt, or other elements set in the ditch with the same intent, or redirect the crack via asymmetrically stiffening of the run-pipe to "ring-off" the crack.

As time passes and the need gives rise to appropriate equipment, some developing overlays and wraps might be conveniently installed onto a completed pipeline. Currently schemes like Clock Spring can be used in a retrofit mode, whereas other schemes that involve more complex reverse helical weaves are being factory installed onto line pipe and shipped to the spread to be installed in the same manner used for integral arrestors. When installed in this way, the potential benefit of external arrestors for retrofit applications is lost.

External arrestors by definition add to the cross-section of the pipeline. Additions to the cross-section create the possibility for crevice corrosion. Some historically considered wrap concepts also used steels that required long-term corrosion protection to avoid their susceptibility to environmentally assisted cracking. Each such consideration must be addressed in design and construction that for some external arrestor concepts opens the door to longer-term maintenance requirements.

Desirable Attributes

Desirable attributes of crack arrestor concepts and their implementation include:

- sufficient to arrest unsteady fracture, according to design requirements, including origins near or adjacent the arrestor and those that initiate remote to the arrestor,
- consistent with the pipeline in respect to function, maintenance, detection, inspection, etc., which can often be best satisfied by integral designs, but can be accommodated by wraps or other types of overlay, particularly avoiding undesirable stresses in the pipe that could lead to crack initiation, buckles, or other in-service problems,
- form and construction consistent with pipeline's overall stiffness, flexible enough to limit stress-concentration at its end-transitions and to accommodate construction-induced loadings, and in-service deformations and loadings other than pressure, particularly avoiding functional concerns and aspects that complicate future inspection,
- corrosion and stress-corrosion resistant, particularly avoiding maintenance concerns, or problems related to corrosion through cathodic shielding or other effects, and any chance for environmental cracking,
- ensures soft arrest (contains the fracture such that it cannot reinitiate RDF nor eject pipe from the ditch), which appears feasible for only certain arrestor concepts or designs within those concepts.

This list provides guidance in the selection of an arrestor concept and the manner it is deployed. In some applications, one attribute might have greater value than another, while in still other cases other attributes become important. Discussion relevant to these topics follows next.

Soft Arrest

Soft arrest is achieved by designs that abrupt termination of the propagating fracture (hard arrest), which typically involves a complete ring-off around the pipe circumference. Soft arrest prevents longitudinal separation of the pipeline and pipe-whip or ejection from the ditch due to the jetting gas stream. In addition to limiting consequential damage, soft arrest also precludes potential fracture re-initiation continued and a continued running fracture.

Any abrupt increase in apparent fracture resistance, as can occur at fillet-welded steel sleeves or abrupt changes in wall thickness, has the potential to arrest cracks by ring-off or circumferential separation of the pipe leading to a hard arrest. This is not to say that any integral or fillet-welded sleeve arrestor always leads to hard arrest, as this response can be avoided for such concepts by a gradual increase in fracture resistance.

Arrest Running Fracture Remote to its Origin

In this review, high speed fractures that had small crack tip openings were difficult to arrest. The ultimate case of this is a brittle fracture with very little crack opening making it very difficult to arrest with tight sleeves that do not reduce the stress in the pipe. The closer the arrestor is to the origin of a fracture, the higher the fracture speed as the fracture is in a highly transient state. As the fracture propagates, the gas decompresses and the fracture speed slows down to a process that approaches or achieves steady state, which makes fracture arrest more likely and feasible. For scenarios where the risk profile along the pipeline demands it, consideration should be given to arrestor design and spacing relative to both transient and nominally steady-state conditions.

Select the Arrestor Concept Relative to its Function and the Pipeline Scenario

The toughness and strength level of the carrier pipe play a role in the speed of the ductile fracture that is to be arrested. For example, the need to arrest high-speed fractures that involve limited flap opening require an arrestor concept that works other than by flap constraint. Lower speeds involve greater flap opening, which makes their arrest via flap constraint possible.

Avoid Introducing Undesirable Local Stresses or Loads

Sleeves that carry a significant load by virtue of design and appropriate installation practices can introduce undesirable local axial bending stresses at the ends of the sleeve. As the load carried by the sleeve decreases, these bending stresses decrease. Such local bending stresses are stress concentrators for mechanical loadings and also can favor nucleation of corrosion/environmental cracking, or act as sites for buckle initiation if a pipeline is free to move laterally. While this effect can be diminished by design of an end-transition, such details open the door to crevice and/or other corrosion related processes. While structurally less-stiff composite arrestors diminish this concern, the end-transition remains a factor for composite arrestors wound under tension, such that the diameter of the pipe is reduced by the wrap tension. As for the steel sleeves, this could lead to local bending and also problems in future internal inspection.

The end transition for a stiff, tight sleeve is a design consideration in the selection of sleeve and wrap arrestors, but is not a factor for integral arrestors, wherein negatives like hard arrest can be offset by external (or internal) taper transition. Likewise, potential ILI problems with sleeves and wraps are not a factor for integral designs. All such attributes must be weighed when selecting the arrestor concept.

Avoid Maintenance and Corrosion Problems

A steel sleeve on a pipeline shields the pipe from the CP current and potentially creates a situation where crevice corrosion could occur under the arrestor. It could also create problems in maintaining the coating at the edge of the arrestor if the sleeve and pipe can move relative to each other. While these are potential concerns, to date none of these problems has been experienced in service for pipelines using steel sleeve arrestors.

Avoid Internal Inspection Problems

If heavy wall inserts are used, the reduction in internal diameter could pose problems for future internal inspection. This could be avoided by using pipe where the excess wall thickness is placed on the outside of the pipe. This concept could also make it easier to maintain the external corrosion resistance coating.

References to Appendix A

1. Marsili, D. I. and Stevick, G. R., "Reducing the Risk of Ductile Fracture on the Canyon Reef Carrriers CO_2 Pipeline," SPE 65th Annual Technical Conference, Paper 20646, New Orleans, LA, September 23-26, 1990, pp 311-319
2. McCollough, D .E., Lux ,M. D., et al, "FLAGS Offshore Gasline Project," European Petroleum Conference, Soc. Pet. Eng. Ltd. London, 1982.
3. Tise, T. C., "Construction of the Northern Border Pipeline," Pipeline Engr. Symp., Houston, TX, ASME Pet. Div., January 1993.
4. Quarles , W. R., "Willbros Nears Completion on Cortez CO_2 Trunkline," Pipeline Industry, August 1983.
5. Porter ,P. C. and Patrick ,A. J., "Retrofitting Crack Arrestors on a Pipeline Converted from Liquid to Gas Service," ASME, IPC 2002, Calgary, 2002, Paper IPC02-27011.
6. Watts, J., "Sheep Mountain CO_2 Pipeline to Boost West Texas Production," Pipeline Gas Journal, Vol/Issue 210/6, May 1, 1983.
7. Horner, C., "Choctaw Carbon Dioxide Line Laid in Mississippi," Pipeline and Underground Utilities Construction.
8. Hayes, D. J. and Lux, M. D., "Full Scale Crack Arrest Test and Arrestor Device Performance for the Flags Gasline," SPE 8220, AIMME, 1979.
9. Peterson, C.W., Papka, S. D., Stevens, J. H., Macia, M. L., and Fairchild, D. P., "Full-Scale Burst Crack-Arrest Testing Vets X120 Line Pipe," 13th International Offshore and Polar Engineering Conference, Honolulu, May 25-30, 2003.
10. Hillenbrand, H. G., Brauer, H. and Knauf, G., "Crack Arrestors," Pipeline Technology Conference, Ostend, Belgium, 2004.
11. Paton, B. E., Medovar, B. T., Pivovarskii, N. B., Saenko, V. Ya., and Astaf'ev, N. A, "Full Scale Test of Rolled Quasi-Laminated Crack Arrestors in High Pressure Gas Transmission Pipelines," Paton Welding Institute Kiev, Problemy Spetsial'noi Elektrometallurgii Vol. 4, No. 1, 1988, pp. 26-33.
12. Shoemaker, A. K., Melville, T., and Steiner, J .E.; "Fracture Resistance of Wire Wrapped Cylinders," Journal of Engineering for Industry, Transactions of the ASME, February 1973, pp 219-226.